Fourier analysis of non-Blazhko ab-type RR Lyrae stars observed with the Kepler space telescope

J.M. Nemec, R. Smolec, J.M. Benko, P. Moskalik, K. Kolenberg, R. Szabo, D.W. Kurtz, S. Bryson, E. Guggenberger, M. Chadid, et al.

Monthly Notices
of the
ROYAL ASTRONOMICAL SOCIETY

Mon. Not. R. Astron. Soc. **417,** 1022–1053 (2011) doi:10.1111/j.1365-2966.2011.19317.x

Fourier analysis of non-Blazhko ab-type RR Lyrae stars observed with the *Kepler* space telescope

J. M. Nemec,[1,2⋆] R. Smolec,[3] J. M. Benkő,[4] P. Moskalik,[5] K. Kolenberg,[3,6] R. Szabó,[4] D. W. Kurtz,[7] S. Bryson,[8] E. Guggenberger,[3] M. Chadid,[9] Y.-B. Jeon,[10] A. Kunder,[11] A. C. Layden,[12] K. Kinemuchi,[8] L. L. Kiss,[4] E. Poretti,[13] J. Christensen-Dalsgaard,[14] H. Kjeldsen,[14] D. Caldwell,[15] V. Ripepi,[16] A. Derekas,[4] J. Nuspl,[4] F. Mullally,[15] S. E. Thompson[15] and W. J. Borucki[8]

[1]*Department of Physics and Astronomy, Camosun College, Victoria, British Columbia V8P 5J2, Canada*
[2]*International Statistics & Research Corporation, PO Box 39, Brentwood Bay, British Columbia V8M 1R3, Canada*
[3]*Institute for Astronomy, University of Vienna, Türkenschanzstrasse 17, A-1180 Vienna, Austria*
[4]*Konkoly Observatory of the Hungarian Academy of Sciences, Konkoly Thege Miklós út 15-17, H-1121 Budapest, Hungary*
[5]*Copernicus Astronomical Center, ul. Bartycka 18, 00-716 Warsaw, Poland*
[6]*Harvard College Observatory, 60 Garden Street, Cambridge, MA 02138, USA*
[7]*Jeremiah Horrocks Institute of Astrophysics, University of Central Lancashire, Preston PR1 2HE*
[8]*NASA Ames Research Center, MS 244-30, Moffett Field, CA 94035, USA*
[9]*Observatoire de la Côte d'Azur, Université Nice Sophia-Antipolis, UMR 6525, Parc Valrose, 06108 Nice Cedex 02, France*
[10]*Korea Astronomy and Space Science Institute, Daejeon 305-348, Korea*
[11]*Cerro Tololo Inter-American Observatory, Casilla 603, La Serena, Chile*
[12]*Physics & Astronomy Department, Bowling Green State University, Bowling Green, OH 43403, USA*
[13]*Osservatorio Astronomico di Brera, Via E. Bianchi 46, 23807 Merate, Italy*
[14]*Department of Physics and Astronomy, Aarhus University, DK-8000 Aarhus C, Denmark*
[15]*SETI Institute/NASA Ames Research Center, MS 244-30, Moffett Field, CA 94025, USA*
[16]*INAF-Osservatorio Astronomico di Capodimonte, Via Moiariello 16, I-80131 Napoli, Italy*

Accepted 2011 June 24. Received 2011 June 23; in original form 2011 March 28

ABSTRACT

Nineteen of the ∼40 RR Lyr stars in the *Kepler* field have been identified as candidate non-Blazhko (or unmodulated) stars. In this paper we present the results of Fourier decomposition of the time-series photometry of these stars acquired during the first 417 d of operation (Q0–Q5) of the *Kepler* telescope. Fourier parameters based on ∼18 400 long-cadence observations per star (and ∼150 000 short-cadence observations for FN Lyr and for AW Dra) are derived. None of the stars shows the recently discovered 'period-doubling' effect seen in Blazhko variables; however, KIC 7021124 has been found to pulsate simultaneously in the fundamental and second overtone modes with a period ratio $P_2/P_0 \sim 0.593\,05$ and is similar to the double-mode star V350 Lyr. Period change rates are derived from O − C diagrams spanning, in some cases, over 100 years; these are compared with high-precision periods derived from the *Kepler* data alone. Extant Fourier correlations by Kovács, Jurcsik et al. (with minor transformations from the *V* to the *Kp* passband) have been used to derive underlying physical characteristics for all the stars. This procedure seems to be validated through comparisons of the *Kepler* variables with Galactic and Large Magellanic Cloud (LMC) RR Lyr stars. The most metal-poor star in the sample is NR Lyr, with [Fe/H] = −2.3 dex; and the four most metal-rich stars have [Fe/H] ranging from −0.6 to +0.1 dex. Pulsational luminosities and masses are found to be systematically smaller than L and $\mathcal{M}$ values derived from stellar evolution models, and are favoured over the evolutionary values when periods are computed with the Warsaw linear hydrodynamics code. Finally, the Fourier parameters are compared with theoretical values derived using the Warsaw non-linear convective pulsation code.

Key words: surveys – stars: abundances – stars: evolution – stars: fundamental parameters – stars: Population II – stars: variables: RR Lyrae.

⋆E-mail: nemec@camosun.bc.ca

1 INTRODUCTION

The *Kepler* mission is designed to detect (*via* transits) Earth-like planets around solar-type stars (Koch et al. 2010). To achieve this goal the 1.4-m *Kepler* telescope has been monitoring almost continuously the light variations of over 150 000 stars in a field located at $(\mathrm{RA,Dec.})_{J2000} = (19{:}22{:}40, +44{:}30)$ or $(l, b) = (76.3, +13.5)$. The mandate of the Kepler Asteroseismic Science Consortium (KASC) is to use these data to better understand the astrophysics of the stars seen in the *Kepler* field, with Working Group 13 being responsible for the study of the RR Lyr variable stars.

Kolenberg et al. (2010) discussed the initial selection of 28 target RR Lyr stars in the *Kepler* field and presented preliminary results based on the earliest *Kepler* observations for RR Lyr and V783 Cyg, both of which exhibit the Blazhko (1907) effect, and for the 'non-Blazhko' star NR Lyr. An important discovery was the phenomenon of 'period doubling', a cycle-to-cycle amplitude variation that occurs at certain Blazhko phases. The effect has been explained by Szabó et al. (2010) as a 9:2 resonance between the fundamental mode and the ninth-order radial overtone. More recently Kolláth, Molnár & Szabó (2011) showed that the resonance destabilizes the fundamental mode limit cycle leading to period doubling. Among RR Lyr stars period doubling has been observed to date only in the Blazhko variables. Benkő et al. (2010, hereafter B10) studied a sample of 29 modulated and unmodulated RR Lyr stars using *Kepler* Q0–Q2 long-cadence (LC) data, and identified 14 of the 29 stars (48 per cent) as exhibiting the Blazhko effect. Most recently, a more detailed investigation of RR Lyrae itself has been made by Kolenberg et al. (2011), and Smolec et al. (2011) have used non-linear hydrodynamic models to model Blazhko RR Lyr stars.

In the present paper we look more closely at the unmodulated ab-type RR Lyr stars – that is, those stars pulsating in the fundamental mode and believed to exhibit no amplitude or phase modulations and to have the most stable light curves. According to the notation established by Alcock et al. (2000) our sample stars are of type RR0. The analysis is based primarily on the *Kepler* LC (30-min) photometry acquired in quarters Q0–Q5 (over 18 000 measurements per star made over 417 d), and the short-cadence (SC; 1-min) photometry for FN Lyr and AW Dra acquired in Q0 (over 14 000 high-precision brightness measurements per star made over 9.7 d) and Q5 (∼135 000 observations per star made over ∼90 d).[1]

We first discuss the sample selection (Section 2.1) and procedure for transforming the raw fluxes delivered from the *Kepler* Science Office to magnitudes on the *Kp* system (Section 2.2). Before analysing the *Kepler* data a search (Section 3.1) was conducted of available historical data for the stars (e.g. photometry, periods, light curves and times of maximum light). Accurate periods were derived using all the available *Kp* photometry (Section 3.2). Then, from the plotted light curves, total amplitudes and risetimes (RTs) were measured (Section 3.3). Period change rates (dP/dt) and revised periods were calculated from O − C diagrams constructed with the historical data combined with the *Kepler* data (Section 3.4). Fourier analysis of light curves (Section 4.1) was carried out for both the *Kp* data (Section 4.2) and for the extant *V* data (Section 4.4). The long time base and intensive sampling of the *Kepler* data provided an opportunity to examine the light curves for cycle-to-cycle variations. To test for such variations the data were divided into single-cycle blocks, and for each block a separate Fourier analysis was conducted (Section 4.3). For the *Kepler* stars observed correlations among the Fourier parameters (all cycles combined) were examined (Section 5) for both the *Kp* and *V* passbands (Section 5.1). The resulting *V*–*Kp* offsets (Section 5.2) allowed comparisons to be made between the *Kepler* stars and RR Lyr stars in Galactic and Magellanic Cloud globular clusters (GCs; Section 5.3) and field stars in the inner regions of the Large Magellanic Cloud (LMC; Section 5.4). Physical characteristics were also derived from suitably modified extant *V*-band correlations (Section 6). These include iron (or metal) abundance [Fe/H], dereddened colour $(B - V)_0$, effective temperature $T_{\rm eff}$, distance d, absolute magnitude M_V, pulsational and evolutionary luminosities, L(puls) and L(evol), pulsational and evolutionary masses, $\mathcal{M}$(puls) and $\mathcal{M}$(evol), and location in the instability strip (IS). Finally, new non-linear hydrodynamical models (Warsaw code) are presented and compared with the observational data (Section 7), and our results are summarized (Section 8). In Appendix A the newly discovered double-mode star KIC 7021124 is discussed, and in Appendix B the cyclic behaviour of nine non-Blazhko stars in the $(V - I, V)$ diagram [based on All Sky Automated Survey (ASAS-North) data] is discussed.

2 DATA PROCESSING

2.1 Selection of non-Blazhko stars

Approximately 40 RR Lyr stars are presently known in the *Kepler* field, up from the 29 stars discussed by Kolenberg et al. (2010) and B10. Four are multiperiodic c-type RR Lyr stars and are the subject of another paper (Moskalik et al., in preparation), and ∼20 are Blazhko stars, many of which have quite complex modulated light curves (see B10). We are interested here in the unmodulated non-Blazhko ab-type RR Lyr stars with the most stationary light curves. When the Fourier parameters and physical characteristics of these stars are known this information will provide a useful reference for future comparisons with the more complex Blazhko stars (see Jurcsik et al. 2009).

Table 1 of B10 gives coordinates for 16 of the 19 stars considered here, and pulsation periods to five decimal places. Three stars are not in the B10: FN Lyr (KIC 6936115) and AW Dra (KIC 11802860), both of which were observed at SC in Q0 with LC Q1 data and SC Q5 data released later; and KIC 7021124, which was discovered subsequently. The RA and Dec. coordinates (J2000) of these three stars are as follows: FN Lyr (19:10:22.25, +42:27:31.6), AW Dra (19:00:48.00, +50:05:31.3) and KIC 7021124 (19:10:26.69, +42:33:37.0).

Three of the stars included in the present study are special cases: (1) V349 Lyr was identified by B10 as a Blazhko star with a small amplitude modulation and Blazhko-period longer than 127 d. It is one of the faintest RR Lyr stars in the *Kepler* field, at $\langle Kp \rangle = 17.433$ mag. The detrended light curve in fig. 1 of B10 shows the amplitude decreasing slowly throughout the Q1–Q2 epochs. Classification of this star depends on the detrending procedure that is used to transform the raw fluxes to magnitudes (see the next section and Fig. 1). It has been included here as a borderline non-Blazhko star. (2) V350 Lyr was discovered by B10 to be pulsating simultaneously in the fundamental and second overtone modes (i.e. an RR02 star), with a secondary period $P_2 = 0.352\,09$ d and a period ratio $P_2/P_0 = 0.592$. So far, there has been no evidence for the Blazhko effect. With the additional ∼270 d provided by the

[1] Public data are available from the internet website http://archive.stsci.edu/kepler/. It is the policy of the *Kepler* mission to make public all the data mentioned in published research papers. Thus the Q0–Q5 long- and SC data analysed here will become publicly available upon publication of the present paper.

Table 1. Basic data for the 19 *Kepler* non-Blazhko ab-type RR Lyr stars.

KIC	Star name	⟨*Kp*⟩ (mag)	Period (d) (this paper)	Freq. (d^{-1}) (this paper)	t_0 (BJD)	RT (*Kp*) (phase)	*Kp*-range (mag)	A_{tot}(*Kp*) (mag)
(1)	(2)	(3)	(4)	(5)	(6)	(7)	(8)	(9)
3733346	NR Lyr	12.684	0.682 0264(2)	1.466 2189(4)	54964.7381	0.144	12.215–12.982	0.767
3866709	V715 Cyg	16.265	0.470 704 94(4)	2.124 4731(2)	54964.6037	0.136	15.612–16.600	0.988
5299596	V782 Cyg	15.392	0.523 6377(1)	1.909 7173(4)	54964.5059	0.200	15.108–15.631	0.523
6070714	V784 Cyg	15.370	0.534 0941(1)	1.872 3292(4)	54964.8067	0.195	15.036–15.670	0.634
6100702	KIC 6100702	13.458	0.488 1457(2)	2.048 5687(8)	54953.8399	0.200	13.140–13.715	0.575
6763132	NQ Lyr	13.075	0.587 7887(1)	1.701 2916(3)	54954.0702	0.144	12.576–13.387	0.811
6936115	FN Lyr	12.876	0.527 398 471(4)	1.896 099 54(1)	54953.2690	0.118	12.146–13.227	1.081
7021124	KIC 7021124	13.550	0.622 4925(7)	1.606 445(2)	54965.6471	0.139	13.018–13.849	0.831
7030715	KIC 7030715	13.452	0.683 6137(2)	1.462 8145(4)	54953.8434	0.177	13.092–13.739	0.647
7176080	V349 Lyr	17.433	0.507 0740(2)	1.972 0987(8)	54964.9555	0.130	16.780–17.768	0.988
7742534	V368 Lyr	16.002	0.456 4851(1)	2.190 6520(5)	54964.7828	0.134	15.237–16.370	1.133
7988343	V1510 Cyg	14.494	0.581 1436(1)	1.720 7451(3)	54964.6695	0.138	13.868–14.848	0.980
8344381	V346 Lyr	16.421	0.576 8288(1)	1.733 6166(3)	54964.9211	0.141	15.809–16.773	0.964
9508655	V350 Lyr	15.696	0.594 2369(1)	1.682 8305(3)	54964.7795	0.143	15.086–16.059	0.973
9591503	V894 Cyg	13.293	0.571 3866(2)	1.750 1285(6)	54953.5627	0.144	12.579–13.684	1.105
9947026	V2470 Cyg	13.300	0.548 5894(1)	1.822 8569(3)	54953.7808	0.193	12.971–13.570	0.599
10136240	V1107 Cyg	15.648	0.565 7781(1)	1.767 4774(3)	54964.7532	0.151	15.151–15.969	0.818
10789273	V838 Cyg	13.770	0.480 2799(1)	2.082 1192(4)	54964.5731	0.134	13.040–14.138	1.098
11802860	AW Dra	13.053	0.687 2160(2)	1.455 1466(6)	54954.2160	0.165	12.538–13.430	0.892

Q3–Q5 observations this star's behaviour has been confirmed and strengthened. One question of interest concerns the stability of the f_2 frequency – B10 determined that the f_2 amplitude was varying between 0.00 and 0.05 mag. This result is confirmed by the newer data. Recent work to better understand this phenomenon has been presented by Kolláth et al. (2011). (3) KIC 7021124 was found during the course of the present study to be pulsating simultaneously in the fundamental and second-overtone modes, and to be similar to V350 Lyr. The details of its pulsational behaviour are given in Appendix A.

Basic data for the 19 unmodulated *Kepler* RR Lyrae stars are given in Table 1. Column 3 contains the mean *Kp* magnitude given in the *Kepler* Input Catalogue (KIC). Columns 4–5 contain our best estimate of the pulsation period and frequency derived using the *Kp* data (see Table 3 for details). Column 6 contains accurate values for the times of maximum light, and Column 7 lists precise RTs derived from the *Kp* photometry. Columns 8 and 9 contain the *Kp* magnitudes at which the light curve reaches maximum and minimum light, the difference being the total amplitude in the *Kp* passband.

2.2 From raw fluxes to *Kp* magnitudes

The preprocessing phases of the LC *Kepler* data have been described by Jenkins et al. (2010a,b) and B10. Since then three more 'seasons' (or ∼270 d) of LC data (Q3–Q5) have become available for 18 of the 19 stars in our sample. Also available now are Q0 (∼10 d) and Q5 (∼90 d) SC photometry (see Gilliland et al. 2010) for FN Lyr and AW Dra. The procedures used here for transforming the raw fluxes to *Kp* magnitudes are described next.

2.2.1 Long-cadence data

The present analysis of the stars in Table 1 is based on the raw fluxes. 16 of the stars were observed at LC (30 min) in 'seasons' Q1 to Q5, and of these, five were also observed in Q0. KIC 6100702 was not observed in Q5, and KIC 7021124 was observed only in Q1. The Q2–Q4 LC observations of FN Lyr were acquired as part of the *Kepler* Guest Observer Program and Drs K. Mighell and S. Howell kindly shared their observations with us. The original data consisted of raw flux counts as a function of time, with times given as barycentric Julian date (BJD). For convenience all the times were translated by subtracting 54 953 d so that the first Q0 observations occur at time $t = 0.53$ d.

Fig. 1 helps to illustrate the procedures used to convert LC fluxes to *Kp* magnitudes. The left-hand panels show the observed raw fluxes (log10 scale) of V894 Cyg (top) and V349 Lyr (bottom) plotted against time. Both stars were observed every 30 min in 'quarters' Q1 to Q5 and V894 Lyr was also observed in Q0. One sees zero-point differences (sensitivity variations) resulting from quarterly 'rolls' of the *Kepler* telescope causing the light from a given star to fall on different CCD chips and pixels each quarter, and trends (both linear and non-linear, and increasing and decreasing) within a given quarter. The scalloped pattern seen for V894 Cyg (with amplitude larger at maximum than at minimum light) is due to the 30-min interval between the LC observations going in and out of phase with the light cycle determined by the pulsation period of 0.57 d. The time ranges for each LC 'season' were as follows: BJD 54953.53 to 54963.24, corresponding to time 0.53 to 10.24 d (Q0), BJD 54964.51 to 54997.98, or 11.51 to 44.98 d (Q1), BJD 55002.94 to 55091.47, or 49.94 to 138.47 d (Q2), BJD 5093.52 to 55182.50, or 140.22 to 229.50 d (Q3), BJD 55185.38 to 55275.20, or 232.38 to 322.20 d (Q4), and BJD 55275.99 to 55370.66, or 322.99 to 417.66 d (Q5).

The right-hand panels of Fig. 1 show the corresponding detrended and normalized *Kp* apparent magnitudes. The procedure for transforming the raw fluxes into apparent magnitudes was as follows: (1) the data were separated into blocks, usually by 'quarter' but various blocks were tried (see the left-hand panels of Fig. 1); (2) the raw fluxes were converted to apparent magnitudes using 'mag = 33.5–2.5 × log10(Fraw)', where the magnitude zero-point is as yet only approximate but gives mean values roughly in accordance with the KIC mean magnitudes; (3) within a block the magnitudes were

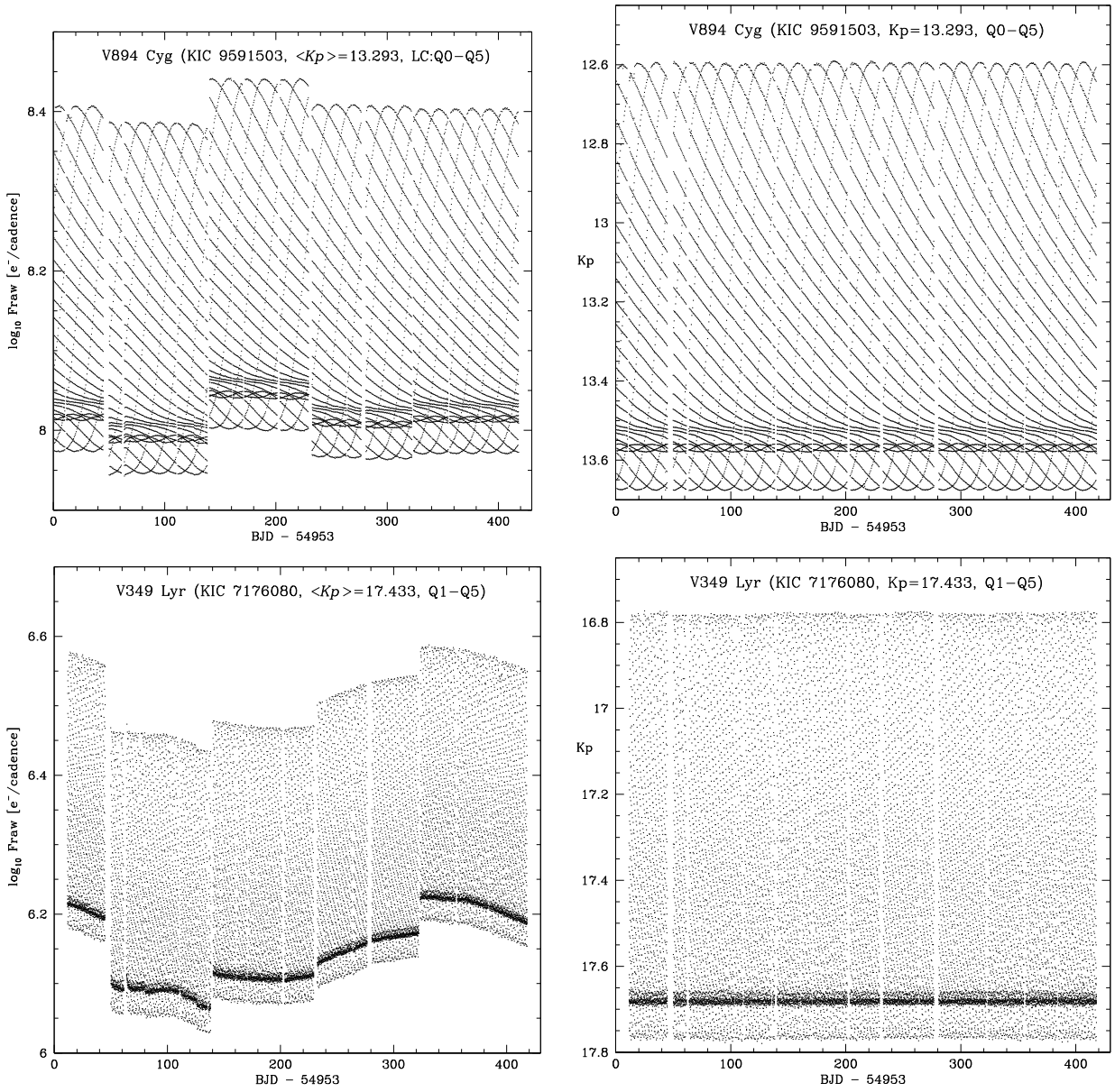

Figure 1. Raw (left) and processed (right) photometry for V894 Cyg (top) and V349 Lyr (bottom). V894 Cyg was observed 18 911 times at LC in quarters Q0–Q5 and is of intermediate brightness with raw flux density $\sim 1.6 \times 10^8$ e$^-$/cadence. V349 Lyr is the faintest RR Lyr star in the *Kepler* field and was observed 18 387 times at LC:Q1–Q5 with raw flux density $\sim 2 \times 10^6$ e$^-$/cadence.

detrended by fitting and subtracting either a linear or polynomial fit; (4) the detrended data for each block were shifted to the *Kp* mean magnitude level given in the KIC; (5) within each block the magnitudes were stretched or compressed by multiplying by an appropriate scalefactor so that the minimum and maximum magnitudes were in agreement with an adopted reference quarter (usually either Q4 or Q5); (6) obvious outliers ($\sigma > 5$) were removed – before this was done the total number of LC observations per 'quarter' was as follows: 476 (Q0), 1639 (Q1), 4354 (Q2), 4370 (Q3), 4397 (Q4) and 4633 (Q5); (7) the resulting light curves were fitted according to their Fourier descriptions and secondary trending (usually at the 1–2 sigma level) was removed.

This method of normalization works well for unmodulated stars but might explain the observed apparent absence of amplitude modulation for V349 Lyr. Owing to its relative faintness (V349 Lyr is the faintest star in our sample), and, if it is a Blazhko star as suggested by B10, its long Blazhko period and low Blazhko amplitude, we may have to wait another year or longer to decide if the variations are intrinsic or due to instrumental effects.

2.2.2 *Short-cadence data*

In addition to the LC observations, FN Lyr and AW Dra were observed at SC (1 min) in Q0 and Q5. The time baseline for the Q0 observations was 9.7 d (0.528 d to 10.254 d), while the Q5 observations were made over 94.7 d (322.98 d to 417.67 d). When combined the total number of data points amounted to ∼150 000 observations per star (14 280 from Q0 and 13 6140 from Q5). Processing of the data required removal of a small number of outliers ($\sigma > 5$) and three spurious dips occurring in Q0 at times centred on 3.298 d, 6.261 d and 8.342 d. The SC data were detrended in the same way as the LC observations.

Table 2. Other periods, amplitudes, RTs and ASAS $\langle V\rangle$-magnitudes and $\langle V-I\rangle$-colours.

Star	P (GEOS) (d)	P (B10) (d)	$A_1(Kp)$ (mag)	RT(V) (phase)	$A_{\rm tot}(V)$ (mag)	$\langle V\rangle$ (mag)	$\langle V-I\rangle$ (mag)
(1)	(2)	(3)	(4)	(5)	(6)	(7)	(8)
NR Lyr	0.682 0287	0.682 04	0.266	0.15	0.68	12.444(08)	0.708(13)
V715 Cyg (VV14)	0.470 672 98(43)	0.470 71	0.340	(0.09)	–	–	–
V782 Cyg (VV22)	0.523 633 83(26)	0.523 64	0.195	(0.18)	–	–	–
V784 Cyg (VV24)	0.534 1026(11)	0.534 10	0.229	(0.19)	–	–	–
KIC 6100702	–	0.488 15	0.206	0.21	0.70	13.641(09)	0.659(22)
NQ Lyr	0.587 7888	0.587 79	0.280	0.14	0.75	13.361(13)	0.576(23)
FN Lyr	0.527 397 16	–	–	0.13	1.27	12.779(09)	0.597(14)
KIC 7030715	–	0.683 62	0.231	0.15	0.81	13.241(14)	0.667(25)
V349 Lyr	–	0.507 08	0.357	–	–	–	–
V368 Lyr	–	0.456 49	0.407	–	–	–	–
V1510 Cyg	–	0.581 15	0.341	–	–	–	–
V346 Lyr	–	0.576 83	0.322	–	–	–	–
V350 Lyr	–	0.594 24	0.339	–	–	–	–
V894 Cyg	–	0.571 39	0.384	0.15	1.07	12.923(11)	0.585(17)
V2470 Cyg	–	0.548 59	0.219	0.19	0.70	13.534(09)	0.605(16)
V1107 Cyg	–	0.565 79	0.270	–	–	–	–
V838 Cyg	0.480 2795	0.480 29	0.390	0.13	1.32	14.246(13)	0.545(23)
AW Dra	0.687 1941	–	–	0.19	1.06	12.851(06)	0.562(11)

3 PERIODS AND LIGHT CURVES

3.1 Previously published periods, risetimes, etc.

All but one of the 19 stars in Table 1 (the exception being KIC 7021124) has been studied previously, either from the ground or using the early *Kepler* photometry. In Table 2 some of this information is summarized.

The GEOS RR Lyr data base (see Le Borgne et al. 2007) at http://rr-lyr.ast.obs-mip.fr/dbrr gives pulsation periods for eight of the 19 stars – these are summarized in Column 2 of Table 2. Much of the historical photometry was derived from photographic plates taken through various filters and on different emulsions, often but not always approximating Johnson V and B magnitudes. The data base also includes HJD times of maximum light, RTs, and visual and CCD observations acquired over many decades.

Two historical studies of particular interest are the impressive 1953 and 1956 photographic investigations by W. J. Miller, S. J. The former study includes an analysis of V715 Cyg (then known as Vatican Variable 14 or VV 14), while the latter includes analyses of V782 Cyg (VV 22) and V784 Cyg (VV 24). Both studies were based on photographic magnitudes ($m_{\rm pg}$) derived from Harvard and Vatican plates taken between 1927 (JD 242 5148) and 1952 (JD 243 4323). The number of individual $m_{\rm pg}$ observations was as follows: 840 for V715 Cyg, 735 for V782 Cyg and 741 for V784 Cyg. Observed times of maximum light are given for V782 Cyg (46 epochs) and V784 Cyg (42 epochs) but not for V715 Cyg. For all three stars the GEOS catalogue adopts the pulsation periods and times of maximum light from Miller's investigations.

For the eight stars with periods given in the GEOS data base agreement with the *Kepler* periods is very good, the average difference amounting to only 0.4×10^{-6}d. The biggest period discrepancies are for V715 Cyg, V784 Cyg and AW Dra. The RT differences are discussed in Section 3.3. Possible slowly changing periods that may not be detectable in the Q0–Q5 *Kepler* data were assessed from O − C diagrams and are discussed in Section 3.4.

Nine of the *Kepler* non-Blazhko stars also were observed during the course of the ASAS-North survey (see Pigulski et al. 2009; Szczygiel et al. 2009, and the ASAS website at ttp://www.astrouw.edu.pl/asas). For the nine stars ∼80 V and a similar number of I CCD photometric measurements were made over ∼500 d in 2006 and 2007. A reanalysis of the online ASAS data was made and RTs and total amplitudes, Fourier-fitted $\langle V\rangle$ magnitudes, and $\langle V-I\rangle$ colours are given in the last four columns of Table 2. If the ASAS-South survey is any indication the ASAS-North RR Lyr light curves will be 'close to the standard V system' (Kovács 2005). The ASAS V data are discussed further in Section 4.5, and the cyclic behaviour of the stars in the Hertzsprung–Russell (HR) diagram is discussed in Appendix B.

Most recently, pulsation periods and preliminary Fourier analysis for 16 of the 19 stars were reported by B10. They analysed the LC Kp photometry from Q0 (9.7d interval), Q1 (33.5d) and Q2 (89d) and established the non-Blazhko behaviour of most of the stars. The periods (typical uncertainties of $\pm 3 \times 10^{-5}$ d) and Fourier A_1 amplitudes that they derived are summarized in Columns 3 and 4 of Table 2.

3.2 Period estimation

Pulsation periods for the non-Blazhko stars were derived mainly from analyses of the Kp data alone. Computations were performed with the package PERIOD04 (Lenz & Breger 2005), which carries out multifrequency analyses with Fourier and least-squares algorithms, and with a version of the CLEAN program (see Nemec, Walker & Jeon 2009). Details of the derived periods are given in Table 3, where the best estimates of the periods and times of maximum light are given in Columns 3 and 4, and Column 5 describes the specific data that were analysed. The uncertainties in the periods (given in parentheses) are average values obtained using the three methods available in PERIOD04, i.e. a theoretically expected uncertainty based on analytical considerations, a least-squares method and a Monte Carlo routine similar to the Fisher method of randomization described by Nemec & Nemec (1985). Typically, the periods derived using the Q0–Q5 LC data alone are accurate to 1–2 $\times 10^{-7}$ d. The uncertainty is expected to decrease further as more *Kepler* observations become

Table 3. Pulsation and Fourier parameters for the *Kepler* non-Blazhko ab-type RR Lyr stars.

Star	⟨*Kp*⟩ (mag)	Period (d)	t_0 (BJD)	Observational data (no. of pts)	σ (mmag)	A_1 (mag)	R_{21}	R_{31}	ϕ^s_{21} (rad)	ϕ^s_{31} (rad)
(1)	(2)	(3)	(4)	(5)	(6)	(7)	(8)	(9)	(10)	(11)
(a) Results from analysis of the Q0–Q5 *Kp* photometry										
NR Lyr	12.683	0.682 0264(2)	54964.7381	LC:Q1–Q5 (18 333)	0.69	0.266	0.456	0.352	2.416	5.115
V715 Cyg	16.265	0.470 704 94(4)	54964.6037	LC:Q1–Q5 (18 374)	1.74	0.338	0.479	0.358	2.314	4.901
V782 Cyg	15.392	0.523 6377(1)	54964.5059	LC:Q1–Q5 (18 381)	0.79	0.190	0.488	0.279	2.777	5.808
V784 Cyg	15.370	0.534 0941(1)	54964.8067	LC:Q1–Q5 (18 364)	0.96	0.234	0.487	0.253	2.904	6.084
KIC 6100702	13.458	0.488 1457(2)	54953.8399	LC:Q0–Q4 (14 404)	0.66	0.209	0.493	0.279	2.743	5.747
NQ Lyr	13.075	0.587 7887(1)	54954.0702	LC:Q0–Q5 (18 759)	0.65	0.280	0.471	0.356	2.389	5.096
FN Lyr	12.876	0.527 398 45(1)	54953.2690	SC:Q0+Q5 (149 925)	0.60	0.380	0.445	0.354	2.321	4.817
	12.876	0.527 398 471(4)	54953.2690	LC:Q1–Q5 (18 338)	0.68	0.379	0.442	0.346	2.324	4.819
KIC 7021124	13.550	0.622 4926(7)	54965.6471	LC:Q1 (1595)	1.10	0.283	0.512	0.351	2.372	5.060
KIC 7030715	13.452	0.683 6137(2)	54953.8434	LC:Q0–Q5 (18 802)	0.71	0.231	0.494	0.303	2.683	5.606
V349 Lyr	17.433	0.507 0740(2)	54964.9555	LC:Q1–Q5 (18 314)	3.24	0.346	0.450	0.352	2.328	4.845
V368 Lyr	16.002	0.456 4851(1)	54964.7828	LC:Q1–Q5 (18 273)	1.57	0.405	0.464	0.341	2.272	4.784
V1510 Cyg	14.494	0.581 1436(1)	54964.6695	LC:Q1–Q5 (18 394)	0.82	0.345	0.473	0.355	2.389	5.068
V346 Lyr	16.421	0.576 8281(1)	54964.9211	LC:Q1–Q5 (18 362)	2.83	0.330	0.473	0.352	2.372	5.060
V350 Lyr	15.696	0.594 2369(1)	54964.7795	LC:Q1–Q5 (18 326)	1.67	0.340	0.485	0.342	2.389	5.124
V894 Cyg	13.293	0.571 3866(2)	54953.5627	LC:Q1–Q5 (18 362)	0.91	0.377	0.490	0.338	2.364	5.067
V2470 Cyg	13.300	0.548 5894(1)	54953.7808	LC:Q0–Q5 (18 794)	0.79	0.220	0.488	0.282	2.745	5.737
V1107 Cyg	15.648	0.565 7781(1)	54964.7532	LC:Q1–Q5 (18 373)	0.99	0.280	0.495	0.350	2.421	5.196
V838 Cyg	13.770	0.480 2799(1)	54964.5731	LC:Q1–Q5 (18 241)	1.22	0.393	0.465	0.349	2.300	4.853
AW Dra	13.057	0.687 2158(6)	54954.2160	SC:Q0 (14 240)	0.55	0.305	0.527	0.348	2.731	5.563
	13.053	0.687 217(1)	54954.2160	LC:Q1 (1614)	0.69	0.306	0.524	0.342	2.730	5.561
	13.053	0.687 2158(2)	54954.2160	LC:Q5 (4474)	0.79	0.306	0.524	0.343	2.728	5.557
	13.053	0.687 216 32(3)	54954.2160	SC:Q5 (135 380)	0.71	0.308	0.527	0.347	2.729	5.558
(b) Results from (re-)analysis of high-precision ground-based *V* photometry										
NR Lyr	–	0.682 0264	54964.7381	Benkő & Nuspl (183)	5.7	0.322	0.445	0.343	2.32	4.94
FN Lyr	12.810	0.527 397 16	54953.2630	Layden unpub. (124)	30.1	0.436	0.433	0.344	2.25	4.67
AW Dra	12.823	0.687 1941	49918.2925	Castellani et al. (112)	11.6	0.357	0.510	0.353	2.63	5.43
(c) Results from re-analysis of the ASAS *V* photometry (http://www.astrouw.edu.pl/asas)										
NR Lyr	12.44	0.682 00(5)	54964.7383	190827+3848.8 (82)	61	0.24	0.45	0.35	2.2	4.9
KIC 6100702	13.64	0.488 17(2)	54953.8398	185038+4125.4 (79)	71	0.23	0.59	0.32	2.4	4.8
NQ Lyr	13.36	0.587 79(3)	54954.0702	190749+4217.9 (68)	68	0.30	0.56	0.40	2.4	5.2
FN Lyr	12.78	0.527 40(3)	54953.2690	191022+4227.6 (82)	76	0.41	0.49	0.36	2.3	4.8
KIC 7030715	13.24	0.683 62(3)	54953.8434	192325+4231.7 (84)	103	0.26	0.56	0.35	2.4	5.4
V894 Cyg	12.92	0.571 40(2)	54953.5625	193301+4614.3 (76)	108	0.37	0.41	0.38	2.2	4.8
V2470 Cyg	13.53	0.548 57(1)	54953.7808	191958+4653.3 (78)	62	0.25	0.42	0.33	2.7	5.6
V838 Cyg	14.25	0.480 30(2)	54964.5731	191404+4812.1 (68)	105	0.44	0.39	0.38	2.2	4.7
AW Dra	12.85	0.687 21(1)	54954.2158	190048+5005.5 (86)	49	0.37	0.53	0.36	2.5	5.4

available. The most uncertain period is that for KIC 7021124 which so far has been observed only in Q1. Also given in Section (a) of Table 3 are the mean *Kp* magnitudes obtained from the KIC. In Column 5 the abbreviations 'LC' and 'SC' stand for 'long-cadence' (30-min) and 'short-cadence' (1-min) *Kepler* data. Columns 6–11 contain Fourier-based results and are described below.

In general, the new periods compare favourably with the GEOS and B10 periods (see Table 2), with the newer values being more precise and more accurate. The largest differences are for V715 Cyg and AW Dra, both of which have significantly longer periods than given in the GEOS catalogue. In Section 3.4, the periods derived directly from the *Kp* data are compared with the values from O − C diagrams.

3.3 Light curves, amplitudes and risetimes

Phased light curves for the *Kepler* non-Blazhko ab-type RR Lyr stars are plotted in the left-hand panel of Fig. 2, assuming the pulsation periods and times of maximum light given in Table 3. The light curves have been ordered from smallest to largest amplitude (measured from minimum to maximum light), with each star offset from the next by 0.5 mag. This arrangement shows that there is a clear trend in light-curve shape and RT, with the lowest amplitude stars having the longest RTs and the most symmetric light curves, and the largest amplitude stars having the shortest RTs and most asymmetric light curves.

The largest amplitude star is V368 Lyr, with $A_{\rm tot} = 1.133$ mag. This star also has the most asymmetric light curve and the shortest period, $P = 0.456$ d. At the top of the stack of light curves the star with the smallest amplitude is V782 Cyg with $A_{\rm tot} = 0.523$ mag; however, its period, $P = 0.524$ d, is *not* the longest. That distinction belongs to three stars with approximately equal periods: AW Dra (0.687 d), NR Lyr (0.682 d) and KIC 7030715 (0.684 d). These three stars all have intermediate amplitudes, and are shown below to have considerably lower metallicities than V782 Cyg (see Section 6.1 and Figs 7–9).

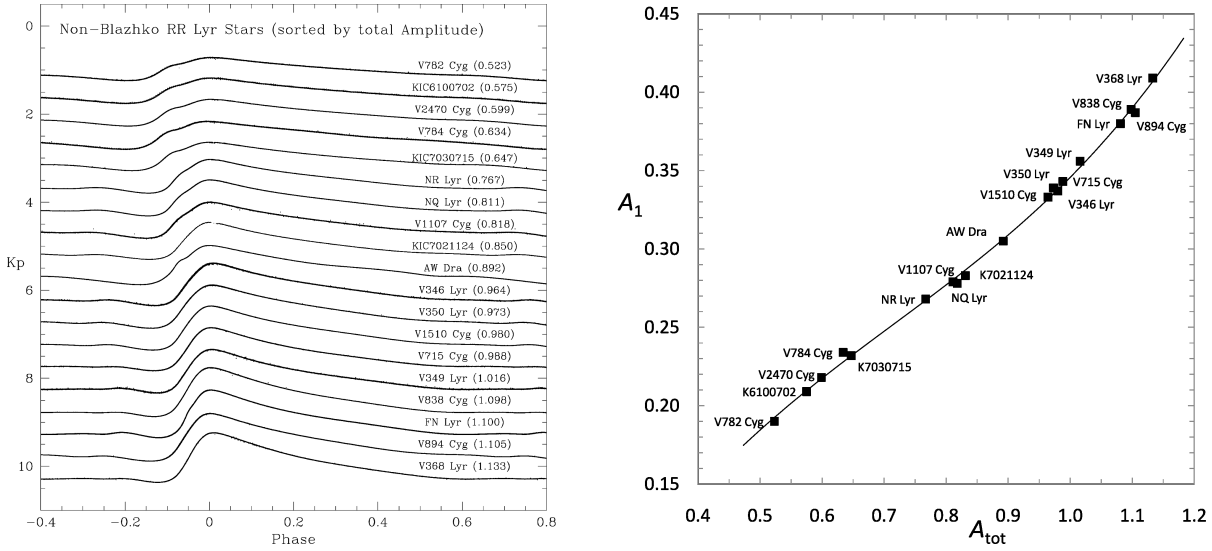

Figure 2. Left: phased light curves for the 19 non-Blazhko ab-type RR Lyr stars observed with the *Kepler* telescope. The quantities in parentheses following the star names are the total *Kp* amplitudes (Table 1, Column 8), ranging from $A_{tot} = 0.52$ to 1.13 mag. Almost all of the light curves contain over 18 000 points with a spread of less than 1 millimagnitude. Right: graph comparing A_{tot} values and the Fourier A_1 coefficients (in Column 8 of Table 3), all derived from the *Kp* photometry. The fit to the points is described by the cubic equation $A_1 = 0.443\,A_{tot}^3 - 0.950\,A_{tot}^2 + 0.973\,A_{tot} - 0.120$, with fit standard error $\sigma = 0.003$ mag.

The right-hand panel of Fig. 2 also shows a comparison of the total amplitudes, A_{tot} (Table 1, Column 9), and the Fourier A_1 coefficients (see the next section), both derived from the *Kp* photometry. Although A_1 is approximately proportional to A_{tot} it is clear that the relationship is non-linear. When a cubic equation was fitted to the graph the resulting standard error of the fit amounted to only 3 mmag. It is doubtful that this (slight) curvature would have been detected without the high precision of the *Kepler* data. In general, the relationship is roughly approximated by non-linear hydrodynamic models (see Section 7, in particular the top-left panel of Fig. 14).

The RTs, magnitude ranges and total amplitudes given in Table 1 (Columns 7–9) were calculated numerically from the fitted *Kp* light curves. The magnitudes at maximum and minimum light are the values at which the slopes of the light curves were found to be zero, from which magnitude ranges and precise total amplitudes were calculated. The phases at the light minima and maxima were used to calculate the RTs.

It is informative to compare the *Kp*-based RTs with those given in the GEOS data base and with RTs based on the ASAS *V* photometry. Since RTs are not given at the ASAS online website the values given in Column 5 of Table 2 were derived in the same way that the *Kp* values were computed. For the nine stars with *Kp* and ASAS RTs the agreement is excellent, the mean difference being 0.002 (ASAS minus *Kp*, standard deviation 0.014). For Miller's three Vatican variables (values are given in parentheses in Column 5 of Table 2) there is reasonable agreement, with the mean difference being −0.024 (Miller minus *Kp*, standard deviation 0.021). The largest differences occur for NR Lyr and V838 Cyg, where the GEOS data base gives RT = 0.27 and 0.40, respectively, compared with the averages of the *Kp* and ASAS estimates of 0.147 and 0.132. An independent estimate of 0.141 for NR Lyr comes from our analysis of the unpublished *V* CCD photometry of Benkő and Nuspl, which agrees well with the *Kp* value.

3.4 O − C diagrams and period change rates

O − C diagrams can be used to improve the precision of estimated pulsation periods, to detect slowly changing periods and to derive accurate period change rates. The longer the time baseline the greater the leverage on the period and the greater the probability of detecting curvature signifying a changing period. For those *Kepler* stars with over 1 year of nearly continuous high-precision photometry (Q0–Q5) we have seen that it is possible to derive periods accurate to $\sim 1\times 10^{-7}$ d using only the *Kepler* photometry. When the *Kepler* data are combined with the long-baseline historical photometry (in some cases as many as 105 years – see e.g. Le Borgne et al. 2007) even more accurate periods (and possible d*P*/d*t* values) can be calculated.

Fig. 3 shows O − C diagrams for the eight *Kepler* non-Blazhko stars that have ephemeris information in the GEOS data base. The ordinate represents the 'observed minus calculated' phase at which maximum light occurs, assuming the GEOS period and time of maximum light given in parentheses at the top of each panel; the abscissa is the Heliocentric Julian Date.[2] At each epoch, the O − C value was calculated by taking the observed time of maximum light *minus* the assumed GEOS time of maximum light (t_0), and dividing the resultant by the assumed (constant) GEOS period (*P*). This gave the number of pulsation cycles since t_0, and the remainder after subtracting an integer number of cycles (E) is the observed fractional phase shift from the expected value. For five of the stars linear fits to the observations are given, a positive (negative) slope indicating that the assumed period is too short (long). Quadratic fits are shown for V782 Cyg, FN Lyr and AW Dra (shown twice, the second graph representing the last ∼13 years), where the upwards curvature indicates an increasing period, the period change rate,

[2] Since the offset between BJDs used by *Kepler* is very small compared to the HJDs usually used by ground-based observers, the two types of dates have been used interchangeably in this paper.

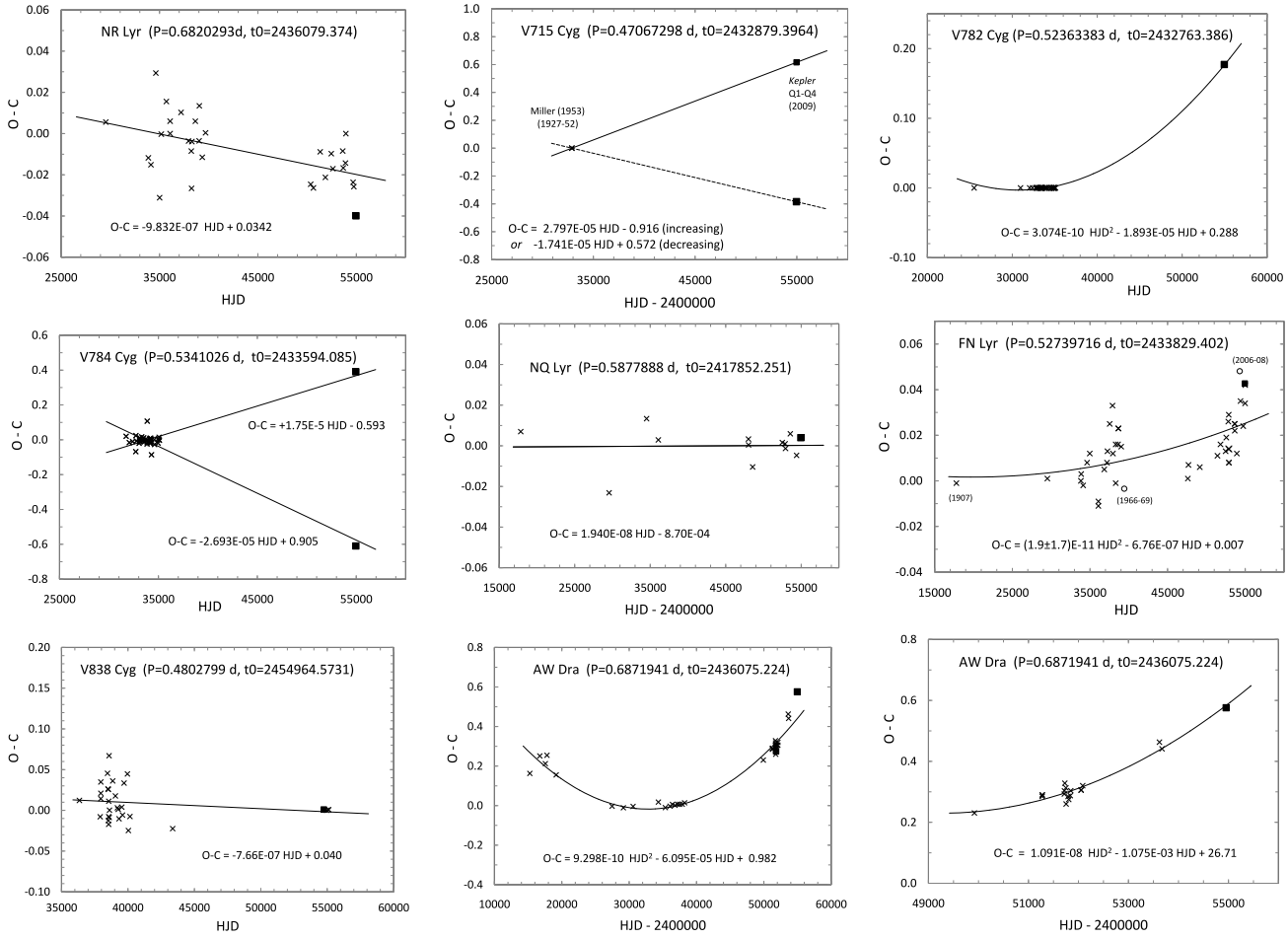

Figure 3. O − C diagrams for the eight *Kepler* non-Blazhko stars with previous photometry in the GEOS atlas (AW Dra is shown twice, with different time-scales). In each panel the O − C value derived from the *Kepler* data is plotted as a solid black square at HJD ∼55000, and the crosses are the O − C values at the various previous epochs. Error bars for the *Kepler* points are comparable to the size of the square and have not been plotted. The fitted lines (or curves) plotted in each panel, the equations of which are given in each graph, are discussed in the text. For V715 Cyg and V784 Cyg two, of many, possible solutions are plotted.

dP/dt, being given by $2Pc^2$ where P is the assumed GEOS period, and c is the curvature coefficient in the quadratic equation. None of the stars represented in Fig. 3 was studied by Le Borgne et al. (2007).

For the three Vatican Variables (V715 Cyg, V782 Cyg, V784 Cyg) there is an ∼60 year gap between the 2009–10 *Kepler* data and the earlier observations. Over such a long time interval one cannot hope to keep track of cycle counts and there is little hope of using the O − C diagrams to either improve the period or calculate dP/dt. To illustrate the cycle-count problem the panels for V715 Cyg and V784 Cyg show two (of many) possible linear solutions, where, in all the cases there is a large O − C shift between the *Kepler* and earlier epochs.[3] However, comparison of the assumed periods with the periods derived from the *Kepler* data do give some indication of either a period change or incorrect period. For V715 Cyg, the *Kepler* period, 0.470 7045(1) d, is significantly longer than the GEOS period, 0.470 67298(43) d, suggesting a period increase. Moreover, for V784 Cyg the *Kepler* period, 0.534 0941(1) d, is significantly shorter than that derived by Miller (1956), 0.534 1026(11) d.

Miller's (1956) data for V782 Cyg provide 46 times of maximum light at epochs between 1928 and 1954, and with these Miller derived $P = 0.523\,633\,83$ d (adopted in the GEOS data base). Our analysis of the ∼18 419 Q1–Q5 *Kp* photometry gave $P = 0.523\,6377(1)$ d, which is 3.9×10^{-6}d longer than the Miller period (see Column 3 of Table 2). Using the time of maximum light given in Column 5 of Table 1 the O − C phase shift of ∼0.20 (nearest) is undoubtedly significant. The quadratic solution (shown in Fig. 3) gives dP/d$t = 0.06$ d Myr^{-1}, which predicts, for 2010, the period 0.523 6379 d, a value that is only $0.2\times\ 10^{-6}$d longer than the measured *Kepler* period. While this agreement strongly supports the increasing period it is also possible that the period changed abruptly in the 60-yr gap.

For V838 Cyg, a total of 31 times of maximum light are available in the GEOS data base: 26 epochs between 1958 and 1968, a single epoch in 1977, and four recent epochs from 2008 to 2009. Although the 10- and 30-yr gaps may be problematic, the *Kepler* ephemeris gives an O–C value near zero for every epoch, suggesting either a constant or very slowly changing period since 1958. A linear fit to the O − C diagram (Fig. 3, bottom-left panel) predicts a

[3] Miller (1953) did not bin his V715 Cyg (VV 14) observations into separate epochs, and the GEOS data base simply adopted for its zero-phase epoch the time of maximum light given in the Miller ephemeris. Future period change rate studies of this star might want to bin Miller's photometry into separate epochs rather than just let one epoch (1948) represent the extended 1927–1952 data.

(constant) true period $P = 0.480\,2797(2)$ d, which matches, to within the uncertainties, the *Kepler*-based period $P = 0.480\,2799(1)$ d and the GEOS period $P = 0.480\,2795$ d. A parabolic fit suggests $\mathrm{d}P/\mathrm{d}t = +0.05 \pm 0.04$ d Myr^{-1}, with the assumed period 0.480 2799 d occurring at BJD 48438. The fit standard error in both cases is only 0.021 (phase units).

For NR Lyr (Fig. 3, top-left panel) the 31 historical points and the new *Kepler* data are consistent with a shorter period than assumed in the GEOS data base. The negative slope suggests a period shorter by 0.46×10^{-6}d than the assumed P(GEOS), i.e. P(true) = 0.682 0288 d; this period is significantly longer than the estimate based on the 18 358 *Kepler* Q1–Q5 data points, 0.682 0264 (2) d.

The 13 historical points and the *Kepler* data for NQ Lyr produce consistent period estimates, with a difference of only 0.1×10^{-6}d between the two periods. Thus the assumed (GEOS) period of 0.587 7888 d is to be compared with 0.587 7887(1) d derived using the 18 759 *Kepler* Q0–Q5 data points.

The O − C diagram for FN Lyr (middle-right panel of Fig. 3) assumes $P = 0.527\,397\,16$ d and $t_0 = 33\,829.402$ (GEOS values), and includes 34 O − C values from as early as 1907 ($t = 177\,93$) to as recent as 2009 ($t = 549\,95$). All but one of the phase shifts is near zero (a visual observation from 1937 was considered an outlier and excluded from our analysis). The diagram includes a point from the 1966 photoelectric V photometry of Bookmeyer et al. (1977) at $t = 39\,416.6457$, and a point from unpublished 2006–08 CCD V photometry by Layden at $t = 54\,288.7454$ (see Section 4.4 for further discussion of these data). These two points, which differ in time by ∼40 yr, have been plotted as open circles and differ in phase by ∼0.055. The O − C value derived for FN Lyr from the *Kepler* data (epoch 2009) is almost identical to the Layden O − C value (see Table 2). Considering that the total baseline is longer than 100 yr the O − C phase shifts are very near zero. Nevertheless, there appears to be a slight upwards trend, and possibly a small amount of curvature. A parabolic solution gives $\mathrm{d}P/\mathrm{d}t = 0.004 \pm 0.004$ d Myr^{-1}, with the GEOS period occurring at $t = 18\,100$, a residual standard error of the fit of 0.011 and a predicted period 0.527 3975 d for the current epoch (2010-11). Since the curvature term does not differ significantly from zero (p-value = 0.27) the question of a changing period remains unanswered. A linear solution is also consistent with the data, in which case a revised constant period of 0.527 397 41(5) d is suggested by the data. Again, the residual standard error of the fit was only 0.011. When the 136 140 SC observations made in Q5 were combined with the 14 280 SC observations made in Q0, a period 0.527 398 45(1) d with residual standard error 0.60 mmag was derived, borderline consistent with both the constant period and small $\mathrm{d}P/\mathrm{d}t$ hypotheses.

Finally, the GEOS data for AW Dra have many epochs with O − C phases that appear to be outliers. These include a single point at $t \sim 20\,000$ with O − C ∼ −0.20, and a clump of ∼ 20 points at $t \sim 52\,000$ with O − C ∼ −0.30. If these values are correct then they present a challenge for modelling period variations. We have chosen to discard them as outliers leaving the O − C diagram shown in the bottom middle panel of Fig. 3. The parabolic fit suggests an increasing period amounting to 0.32 d Myr^{-1}, and predicts a period 0.687 214 d for the *Kepler* Q5 epoch. However, close inspection of the diagram shows that the last three points, one of which is that derived from the *Kepler* data, deviate substantially from the fitted curve. If the analysis is restricted to epochs since HJD 49000 (the first point is from the Castellani et al. 1998, study of AW Dra) *and* if the suspected outliers identified above are excluded, then the O − C diagram is as shown in the bottom-right panel of Fig. 3. In this case, the period increases smoothly at the rate $\mathrm{d}P/\mathrm{d}t = 3.76$ d Myr^{-1}, with the assumed period of 0.687 1941 d having occurred at HJD 49267. For the *Kepler* Q1 and Q5 LC data (6117 points) the predicted period is 0.687 2156(2) d. The period from the combined Q0 and Q5 SC data (149 222 points) is similar, 0.687 2162(1) d, with a fit standard error 7.3 mmag. Both periods agree, are significantly longer than the GEOS period and are consistent with AW Dra having an increasing period. Comparing this period with the predicted periods the new data favour the smaller $\mathrm{d}P/\mathrm{d}t$ value.

To summarize this section, periods based on O − C diagrams were calculated for NR Lyr and NQ Lyr, both of which seem to have constant periods, and $\mathrm{d}P/\mathrm{d}t$ values have been calculated for FN Lyr and AW Dra. AW Dra is the only star for which we can at present be confident that the period is changing (assuming that the outliers really should be omitted from consideration) – depending on the assumed data set the rate is either $\mathrm{d}P/\mathrm{d}t = 3.786$ d Myr^{-1} (for the more recent data), or 0.32 d Myr^{-1} (all data) with the possibility of variations on top of this. For FN Lyr the period *either* is very nearly constant *or* is increasing at a very slow rate. For the other four stars with GEOS times of maximum light the large gaps in the observation record prevent improvement over the GEOS or *Kepler* periods. The ongoing high-precision *Kepler* observations should remedy this lack of knowledge (for the modern era), not only for the eight *Kepler* non-Blazhko stars in the GEOS data base but also for all the *Kepler* non-Blazhko stars.

4 FOURIER ANALYSIS

The use of Fourier methods to characterize the shapes of RR Lyr light curves began with the work of Simon and his collaborators (Simon & Lee 1981, Simon & Teays 1982, Simon & Clement 1993) and has continued through the more recent papers by Kovács, Jurcsik, Morgan and others. The goal of these studies has been to establish empirical correlations employing a minimum number of observed parameters (periods, amplitude ratios, phase parameters) from which physical characteristics can be derived (see Section 6). Calibration of the equations follows from independent observations (high dispersion spectroscopy, parallax measurements, etc.) and from theory (e.g. hydrodynamic pulsation models, stellar evolution models). After Simon (1988) discovered that the Fourier phase parameter ϕ_{21}^c decreases with decreasing metallicity (for field RRab stars with $P < 0.575$ d), Kovács & Zsoldos (1995) proposed that correlations involving period and the Fourier phase parameter ϕ_{31} can be used to derive [Fe/H] values. The first application of this method to field and GC RR Lyr stars was the study by Jurcsik & Kovács (1995, 1996), and subsequent calibrations have been made by Jurcsik (1998, hereafter J98) and Kovács & Walker (1999, 2001). From the beginning Jurcsik & Kovács (1995) warned that the Fourier ϕ_{31} method 'is not applicable for the estimation of [Fe/H] in peculiar stars (e.g. in Blazhko variables, highly evolved stars . . .)', and subsequently JK96 and Kovács & Kanbur (1998) introduced a 'compatibility test' for identifying 'peculiar' stars. Indeed, when such stars were omitted from the ASAS-South data base, agreement between Fourier-based metallicities and low-dispersion spectroscopic metallicities reached the 0.16 dex level (see Kovács 2005).

4.1 Coefficients and fitted light curves

Fourier decomposition of the *Kepler* light curves was performed for each of the 19 non-Blazhko stars by fitting the following Fourier

sine series to the observed photometry:

$$m(t) = A_0 + \sum_{i=1}^{F} A_i \sin[i\omega_0(t - t_0) + \phi_i], \quad (1)$$

where $m(t)$ is the apparent magnitude [either *Kp* for the *Kepler* data or $m_V(t)$ for the ground based V photometry], F is the number of fitted terms, ω_0 is the angular pulsation frequency of the star ($= 2\pi f_0$, where $f_0 = P_0^{-1}$), t is the observed time of the observation (BJD 54953 for the *Kepler* data, HJD for the ground-based V photometry), t_0 is the time of maximum light (used to phase the light curves so that maximum light occurs at zero phase), and the A_i and ϕ_i are the amplitude and phase coefficients for the individual Fourier terms. The Fourier calculations were made with two FORTRAN programs, one kindly provided by Dr. Géza Kovács, and the other by Dr. Pawel Moskalik. The assumed pulsation periods were those derived either from the *Kepler* data or from the period change rate analysis (Section 3.4), and the t_0 values were calculated numerically. The derived periods and t_0 values are summarized in Table 1 (Columns 4 and 5) and the details are given in Table 3.

4.2 *Kepler Kp* photometry

Initially, the *Kepler* magnitudes were fitted with a Fourier series having seven to 15 terms; the larger number being needed when the skewness is greatest, i.e. the RT is shortest. Inspection of the residuals from the fitted light curves revealed that because most of the stars show a sharp rise to maximum light, with additional detailed bumps and features, many more terms were needed. Fig. 4 illustrates 38-term Fourier fits for two non-Blazhko stars, AW Dra on the left and FN Lyr on the right. These two stars have both *Kp* photometry (top diagrams) and high-precision ground-based V-band photometry (bottom diagrams). For AW Dra the *Kepler* data are Q5 SC observations, i.e. brightness measurements every minute over 94.7 d, resulting in 135 380 data points; and for FN Lyr the *Kepler* data are Q1–Q5 LC observations, i.e. a measurement every 30 min over 417 d, resulting in 18 338 points. In both cases the standard deviation of the fit to the *Kepler* data is less than 1 millimagnitude (see Column 6 of Table 3). However, the residuals still show systematic variations with the largest residuals occurring on the rise to maximum light where the slope of the light curve is steepest. To achieve residuals showing normally distributed white noise perhaps 50–100 terms would be needed.

For each of the program stars epoch-independent phase differences $\phi^s_{i1} = \phi_i{}^s - i\phi^s_1$, and amplitude ratios $R_{i1} = A_k/A_1$, were computed from the Fourier coefficients derived from the *Kp* photometry. The superscripts 's' and 'c' signify phases and phase-parameters computed with sine and cosine series, respectively (e.g. Fig. 7). The sine and cosine ϕ_{31} phase parameters differ by π radians, that is, $\phi^c_{31} = \phi_{31}{}^s - 3.141\,59$, and the ϕ_{21} parameters differ by $\pi/2$ rad, i.e. $\phi^c_{21} = \phi_{21}{}^s + 1.5708$.

Table 3 also contains the Fourier parameters needed for computing physical characteristics. In Section (a) results derived from various combinations of SC and LC *Kp* data (see Column 5) are given. The A_1 coefficients (Column 7) are practically identical to the A_1 coefficients calculated by B10 using the Q0–Q2 photometry (given in Column 6 of Table 2). Columns 8 and 9 contain the amplitude ratios, R_{21} and R_{31}; and Columns 10 and 11 contain the Fourier phase parameters, ϕ^s_{21} and ϕ^s_{31}. The accuracy of the *Kp*-based Fourier parameters is at least one part in 1000, and higher in many cases. For example, the parameters derived for FN Lyr from a 38-term fit of the 18 338 Q1–Q5 LC data points have formal values (including uncertainties) as follows: $R_{21} = 0.44\,208(2)$, $R_{31} = 0.346\,10(2)$, $\phi^s_{21} = 2.324\,17(7)$ and $\phi^s_{31} = 4.819\,16(9)$. Correlations and graphical representations of these parameters are discussed below.

4.3 Cycle-to-cycle variations and stationarity

To examine cycle-to-cycle variations in the *Kepler* light curves the Fourier parameters were re-calculated after binning the data so that each bin included data for one pulsation period (i.e. each bin represented a single pulsation cycle). For the LC (30 min) data there were ∼24 observations per bin for an RRab star with a period of 12 h, and fewer (more) observations per cycle for stars with shorter (longer) periods. None of the 19 stars exhibits the recently discovered 'period doubling' effect, thus confirming the result found earlier by Szabó et al. (2010).

For the Fourier calculations 'direct Fourier fitting' (DFF) rather than 'template Fourier fitting' (TFF) methods were used (see Kovács & Kupi 2007), and for each star the resulting time series were plotted for four Fourier parameters: A_1, the first term in the Fourier series (see the right-hand panel of Fig. 2); ϕ_1, the phase of the first term; R_{21}, the amplitude ratio A_2/A_1; and ϕ^s_{31}, the Fourier parameter found by Simon, Kovács and others to be one of the most significant variables for deriving physical characteristics. Typical time series are illustrated in Fig. 5: on the left for the unmodulated RRab star NQ Lyr having intermediate amplitude ($A_1 = 0.279$ mag) and intermediate brightness ($\langle Kp \rangle = 13.075$ mag), and on the right for V783 Cyg, a low-amplitude Blazhko star with the shortest Blazhko period ($P_B = 27.7 \pm 0.04$ d; see B10) among the stars in our sample.

For NQ Lyr linear trend lines were fit to each time series and in almost every case the slope is zero to within the systematic and random uncertainties. The mean values for the four parameters are as follows: $\phi^s_{31} = 5.0958 \pm 0.0023$, with residual standard error, $\sigma = 0.002$; $R_{21} = 0.4710 \pm 0.0006$, with $\sigma = 0.0006$; $\phi^s_1 = 3.961 \pm 0.001$, with $\sigma = 0.001$; and $A_1 = 0.280\,16 \pm 0.000\,14$ mag, with $\sigma = 0.0001$. Since the other non-Blazhko stars show random variations of the Fourier parameters similar to those shown here for NQ Lyr these means and errors provide a measure of the typical uncertainties.

Inspection of the NQ Lyr time series in Fig. 5 shows that the stability over the ∼ 420 d interval (Q0–Q5) is exceptional, not only for each Fourier parameter but also for the ensemble of parameters. To better illustrate the remarkable stationarity of the light curves for all 19 sample stars a set of 'animated gif' light curves has been prepared and these are available in the electronic version of the article, along with the data files (see Supporting Information).

For the Blazhko star V783 Cyg the time plots of the four Fourier parameters are in striking contrast to the stochastic noise exhibited by NQ Lyr and by the candidate non-Blazhko star V349 Lyr. For V783 Cyg pronounced periodic variations are seen over the 27.7 d Blazhko cycles. There does appear to be a slight discontinuity at around 140 d, but this is certainly a data-processing defect. Over the 11 Blazhko cycles seen, there is very little difference from cycle-to-cycle; this is not always the case for Blazhko stars where large cycle-to-cycle differences are often seen.

4.4 High-precision *V* photometry

By comparing the light curves and Fourier parameters for the *Kp* and V photometric systems it is possible to test (in a limited way) the hypothesis that the two broad-band filters give similar results. If this hypothesis is true then the Fourier parameter correlations established for the V-band system by Simon, Kovács, Jurcsik, Sandage and others *might* be applied to the *Kp* magnitudes and be used to

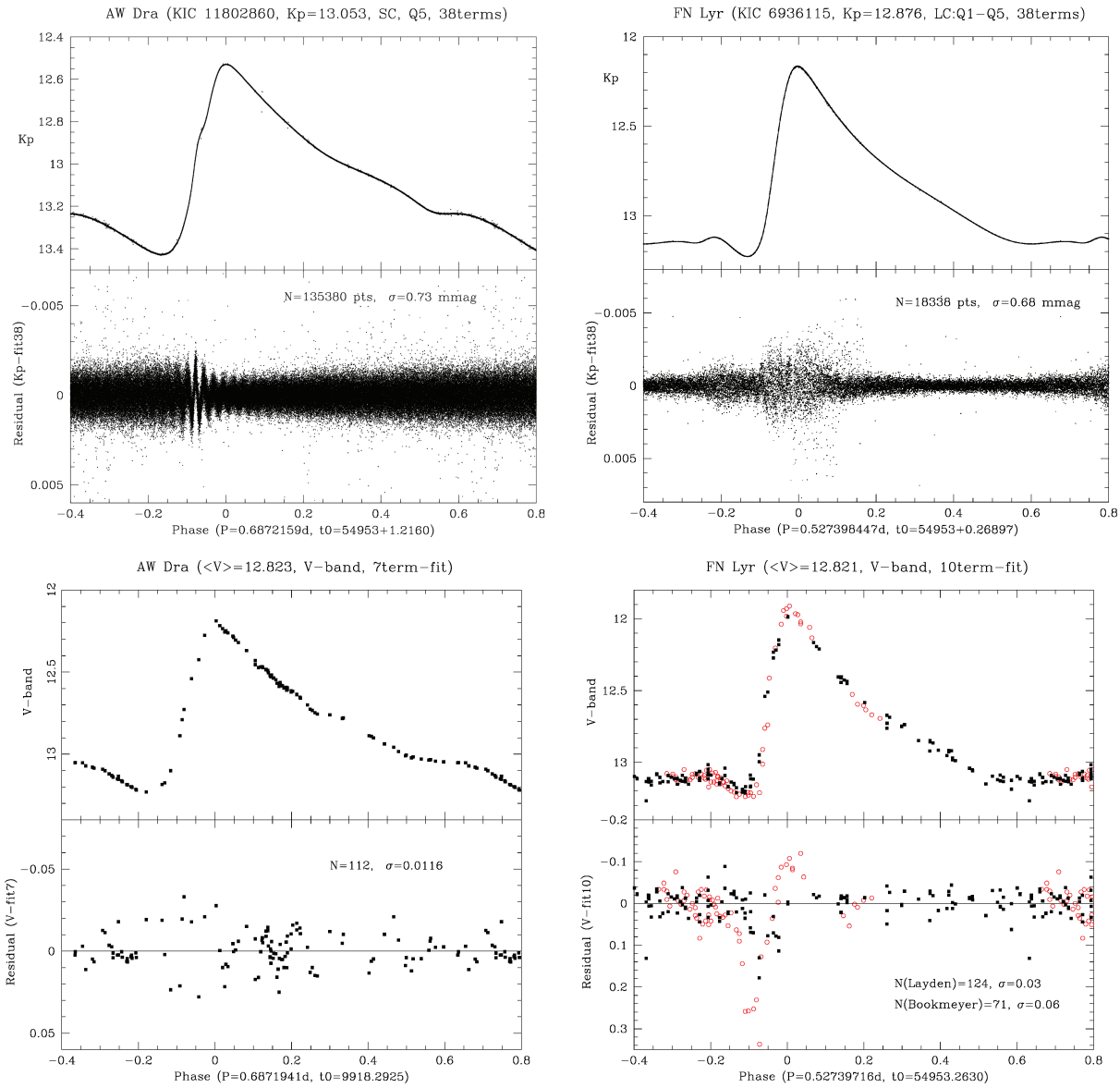

Figure 4. Light curves and residual plots for AW Dra (left) and FN Lyr (right). The top diagrams show *Kp* photometry and the bottom diagrams *V*-band photometry, and within each diagram the light curves are on top and the residual plots on the bottom. The *Kp* photometry is SC(Q5) data for AW Dra and LC(Q1–Q5) data for FN Lyr. The *x*-axis labels give the assumed pulsation periods (P_0) and times of maximum light (t_0). The diagram labels indicate the data plotted and the number of terms in the fitted Fourier series, and the number of data points (N) and standard deviations of the fits (σ) are stated in each diagram.

derive first-order physical characteristics (see Section 6). Unfortunately, there is very little *high-precision* published ground-based *V*-band photometry for our *Kepler* stars. Three exceptions are NR Lyr, AW Dra and FN Lyr. Using the available *V* photometry for these stars Fourier parameters were derived and compared with the *Kp* parameters. The results are given in the middle section of Table 3 (Section b).

4.4.1 AW Dra

The light curve and residuals derived from the *V* photometry of Castellani et al. (1998) are plotted in the lower-left diagram of Fig. 4. The 112 points are from CCD observations made in 1995 with the 72-cm Teramo/Scuola Normale Telescope, modelled with a seven-term Fourier series fit. The shape of the *V* light curve is very similar to the light curve based on the *Kepler* data, and the Fourier parameters (Table 3) support this observation. Notice also that, although the *V*-data have a residual standard error of only 0.0116 mag, the residuals are ∼16 times larger than the *Kp*-residuals (Fig. 4, upper-left panel). On the other hand, the RTs are quite similar: 0.165 for the *Kp* photometry and 0.174 for the *V* photometry. The joined points in the RT graphs below (lower-left panel of Fig. 9 and left-hand panel of Fig. 10) give a visual representation of these differences.

4.4.2 FN Lyr

For FN Lyr, the *V* photometry shown in the lower-right panels of Fig. 4 is from two sources: Bookmeyer et al. (1977) and Layden (2011, unpublished). The Bookmeyer et al. data comprise 71 *UBV* photoelectric observations made in 1966 (21) and 1969 (50), and the Layden *V* photometry constitute 124 *VR* CCD observations made

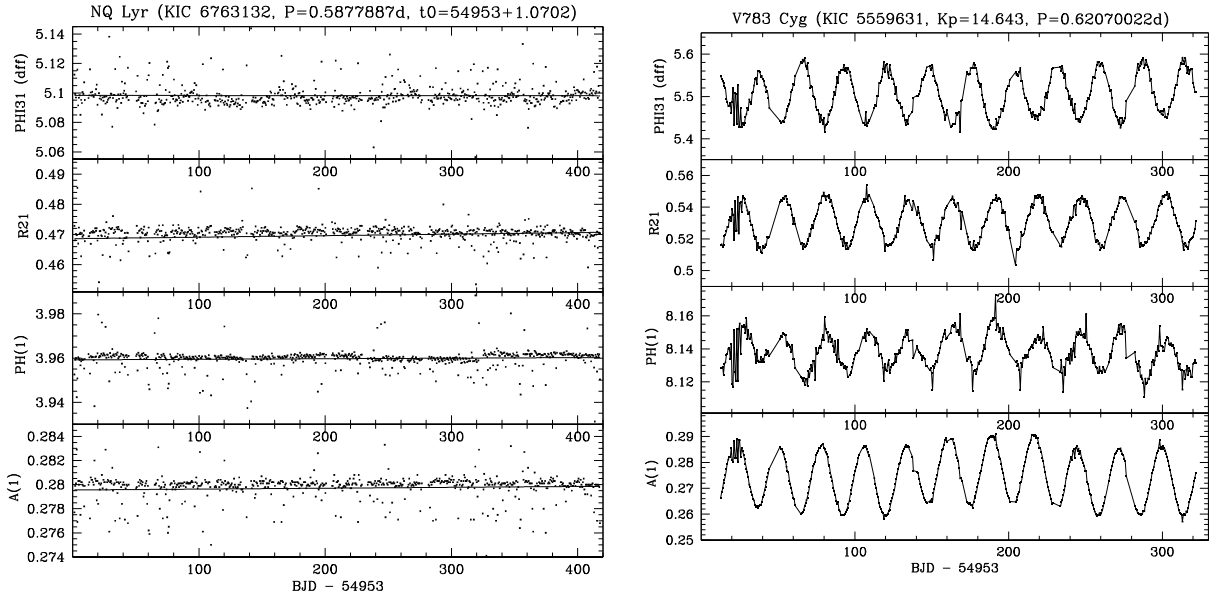

Figure 5. Variations in time of the Fourier parameters ϕ_{31}^{s}, R_{21}, ϕ_{1}^{s} and A_1 (all sine-series) derived for the typical non-Blazhko star NQ Lyr (left-hand panel) and for the known low-amplitude Blazhko star V783 Cyg (right-hand panel). Each point corresponds to the variable of interest as determined from a single pulsation cycle.

in 2006–08. When the two data sets, which are separated by ∼40 yr, were combined and plotted as single light curve (i.e. the same period and time of maximum light) a phase shift amounting to 5.5 per cent of the period (0.029 d) was seen, with the Layden data having the larger phases. The shift corresponds to the offset of the two O − C values seen in Fig. 3 (middle right panel, where the O − C values for the two data sets are plotted as open circles and are labelled '1966–69' and '2006–08'). Our period change rate analysis suggested that the shift is probably due *either* to the assumed period (0.527 397 16 d) being too small *or* to a slowly increasing period ($\mathrm{d}P/\mathrm{d}t = 0.004 \pm 0.004\ \mathrm{d\,Myr^{-1}}$).

Fig. 4 (lower right) shows the composite *V* light curve for FN Lyr, where the Layden data (solid black squares) are plotted alongside 'the Bookmeyer data shifted in phase by +0.055' (red open circles). There is a reasonably good match between the Layden and Bookmeyer light curves, the chief differences being: (1) only two (very close) Layden data points were acquired near maximum light, and they are fainter than the Bookmeyer observations near maximum light; (2) the slope of the rise to maximum light is shallower for the Layden data than for the Bookmeyer data and (3) the Layden data are uniformly distributed in phase while the Bookmeyer data show two large gaps on the descent to minimum light.

Fourier coefficients and parameters were calculated using the composite 'Layden *plus* shifted-Bookmeyer' data, and using the 124 Layden *V* data points only (the former were found to be less reliable than the latter). Owing to the large gaps it was not possible to obtain a reliable Fourier fit using only the Bookmeyer data. Table 3 gives the Fourier decomposition results based on the Layden-only *V* photometry. The *V*-residuals shown in the bottom-right panel of Fig. 4 were calculated with respect to the Layden-only fit. The Layden data have a residual standard error of 0.03 mag, while the fit for the Bookmeyer data is poorer (∼0.06 mag). In both cases (as for the *Kepler* data) the largest residuals occur on the rise to maximum light. The observed smaller total amplitude and longer RT for the Layden *V* photometry compared with the Bookmeyer photometry might be expected if FN Lyr is a low-amplitude Blazhko variable. The available data are insufficient to check this possibility but as additional *Kepler* observations are acquired the answer may be evident.

4.4.3 NR Lyr

In 2008 *B*, *V*, *R*, *I* CCD observations of NR Lyr were made by J. Benkő and J. Nuspl using the Konkoly telescope. At present the 183 data points per filter are on the instrumental system of the telescope; however, the photometric colour constant is very small and the *V* data differ from the Johnson *B*, *V* system by only a zero-point shift. Because the data completely cover the phase range and are of high precision the *V* data were Fourier analysed (using the period and t_0-value favoured by the *Kepler* data) and the results are summarized in Table 3. When the Fourier parameters are compared with those for FN Lyr and AW Dra (see Figs. 6, 9 and 10) all three sets of observed offsets are in excellent agreement (see Section 5.2).

4.5 ASAS *V* photometry

For the nine non-Blazhko RR Lyr stars in the ASAS-North survey (see Section 3.1) the online *V* photometry was re-analysed and the results reported in section (c) of Table 3. The derived $\langle V \rangle$ magnitudes (Column 2) have uncertainties of ±0.01 and range from 12.44 to 14.24. A comparison of the $\langle V \rangle$ and $\langle Kp \rangle$ magnitudes shows the following trend over the observed range: $\langle V \rangle = (1.45 \pm 0.24)\langle Kp \rangle - (5.97 \pm 3.20)$. Until further *V* photometry fainter than 14th mag is obtained it is unclear whether this trend of *V* magnitudes fainter than the *Kp* magnitudes will continue. Pulsation periods (with uncertainties in parentheses) derived from our re-analysis of the *V* data are given in Column 3; in general these agree with the periods given at the ASAS website and with those derived from the *Kepler* data (see Tables 2–3). Columns 4–6 contain, respectively, the assumed time of maximum light, the ASAS name of the star and the spread of the Fourier fit about the mean light curve (found to range from 49 to 108 mmag). Fourier parameters derived using the online *V* data are given on the right-hand side of Table 3. These were computed

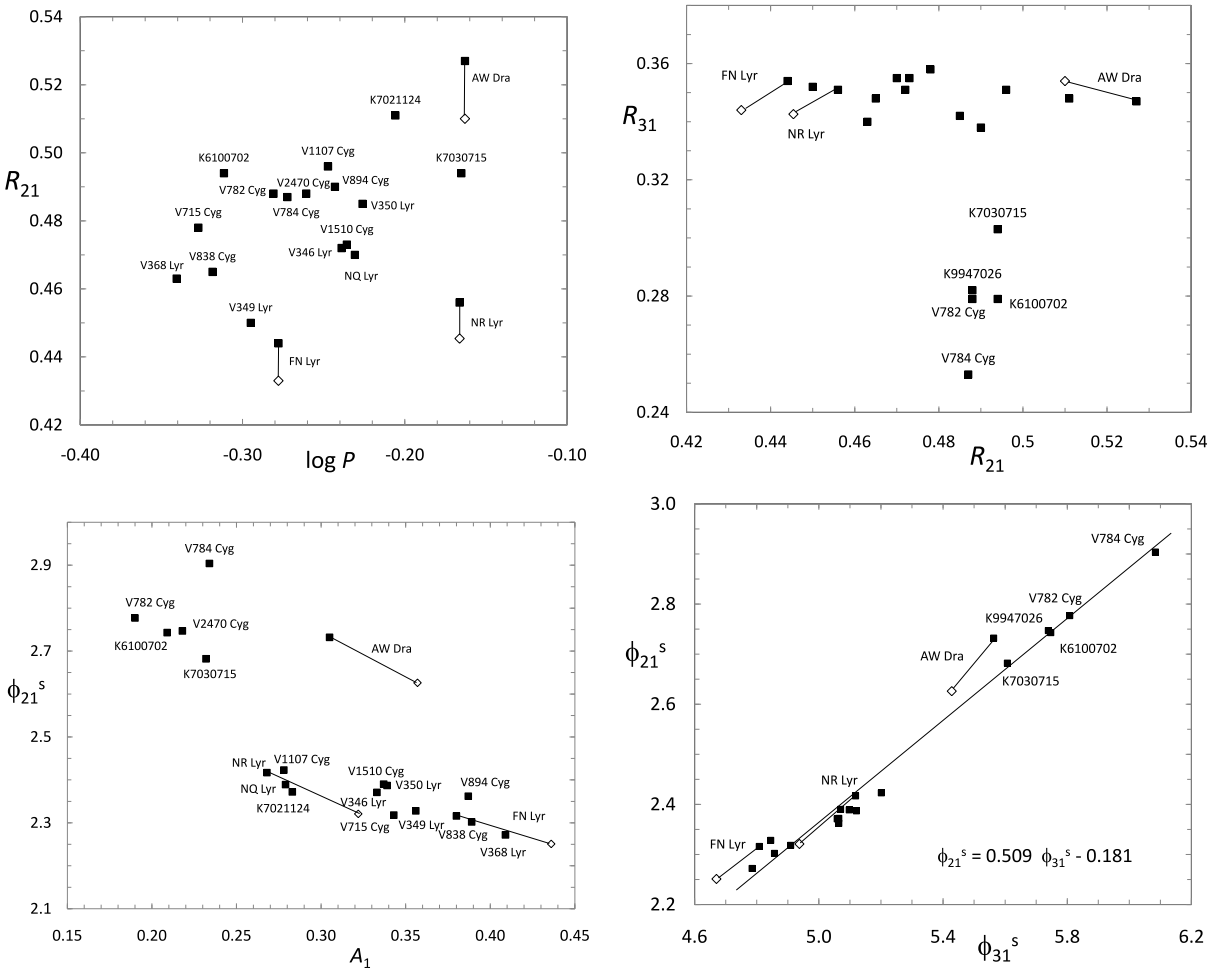

Figure 6. Four panels comparing various Fourier parameters derived from the *Kp* photometry for the 19 *Kepler* non-Blazhko stars. The open diamonds for AW Dra, FN Lyr and NR Lyr were derived from the *V* photometry of Castellani et al. (1998), Layden (2011, unpublished) and Benkő & Nuspl (2011, unpublished), respectively.

using the accurate *Kepler* periods and times of maximum light. The uncertainties typically are ±0.04 for R_{21}, ±0.01 for R_{31}, ±0.08 for ϕ_{21} and ±0.1 for ϕ_{31}, and in several cases are larger.

5 FOURIER PARAMETER CORRELATIONS

5.1 *Kp* correlations

Fig. 6 shows four graphs relating the Fourier parameters A_1, R_{31}, R_{21}, ϕ^s_{21} and ϕ^s_{31}, derived from the sine-series decomposition of the *Kp* photometry of the 19 *Kepler* non-Blazhko stars. Each star is represented by a solid black square, and is labelled for easy identification. Also plotted in Fig. 6 are the *V*-band Fourier parameters for AW Dra, FN Lyr and NR Lyr (Section 4.3) which are shown as open diamonds connected to the corresponding *Kp* points by lines. The offsets between the *Kp* and *V* points appear to be systematic (i.e. generally go in one direction) and are not very large, even in the case of R_{31} which is the least certain of the parameters. Perhaps this relationship between *V* and *Kp* is not surprising because both passbands are quite wide.

The upper-left panel of Fig. 6 shows that there is very little correlation between R_{21} and period (except possibly a slight increase in R_{21} with increasing period). The R_{21} values from the *V* photometry are all slightly smaller than from the *Kp* photometry, and the R_{21} values for FN Lyr and NR Lyr are significantly smaller than that for AW Dra.

The upper-right panel shows 14 stars (including AW Dra, FN Lyr and NR Lyr) with R_{31} between 0.34 and 0.36, and five stars with R_{31} values smaller than 0.31. In particular, AW Dra, FN Lyr and NR Lyr are seen to have similar R_{31} values even though the R_{21} values for FN Lyr and NR Lyr are significantly smaller than that for AW Dra. Although the overall bimodal distribution is striking, we shall see below (upper-right panels of Figs 7 and 8) that RR Lyr stars with relatively low R_{31} values are quite common and can be simulated with hydrodynamic models (Section 7).

In the lower-left panel the stars separate into high- and low-ϕ^s_{21} stars, with a discontinuity at $A_1 \sim 0.25$ mag. AW Dra and V784 Cyg (suspected of having a relatively high metallicity) appear to stand out from the other stars; even when compared with RR Lyr stars in GCs (Section 5.3) these two stars appear extreme.

Finally, the lower-right panel shows that ϕ^s_{21} is roughly proportional to ϕ^s_{31}, where the linear relationship is given by $\phi^s_{21} = 0.509\,\phi_{31}{}^s - 0.181$. For AW Dra, FN Lyr and NR Lyr the phase parameters are smaller for the *V* data than the *Kp* data, and the offsets are parallel to the fitted line.

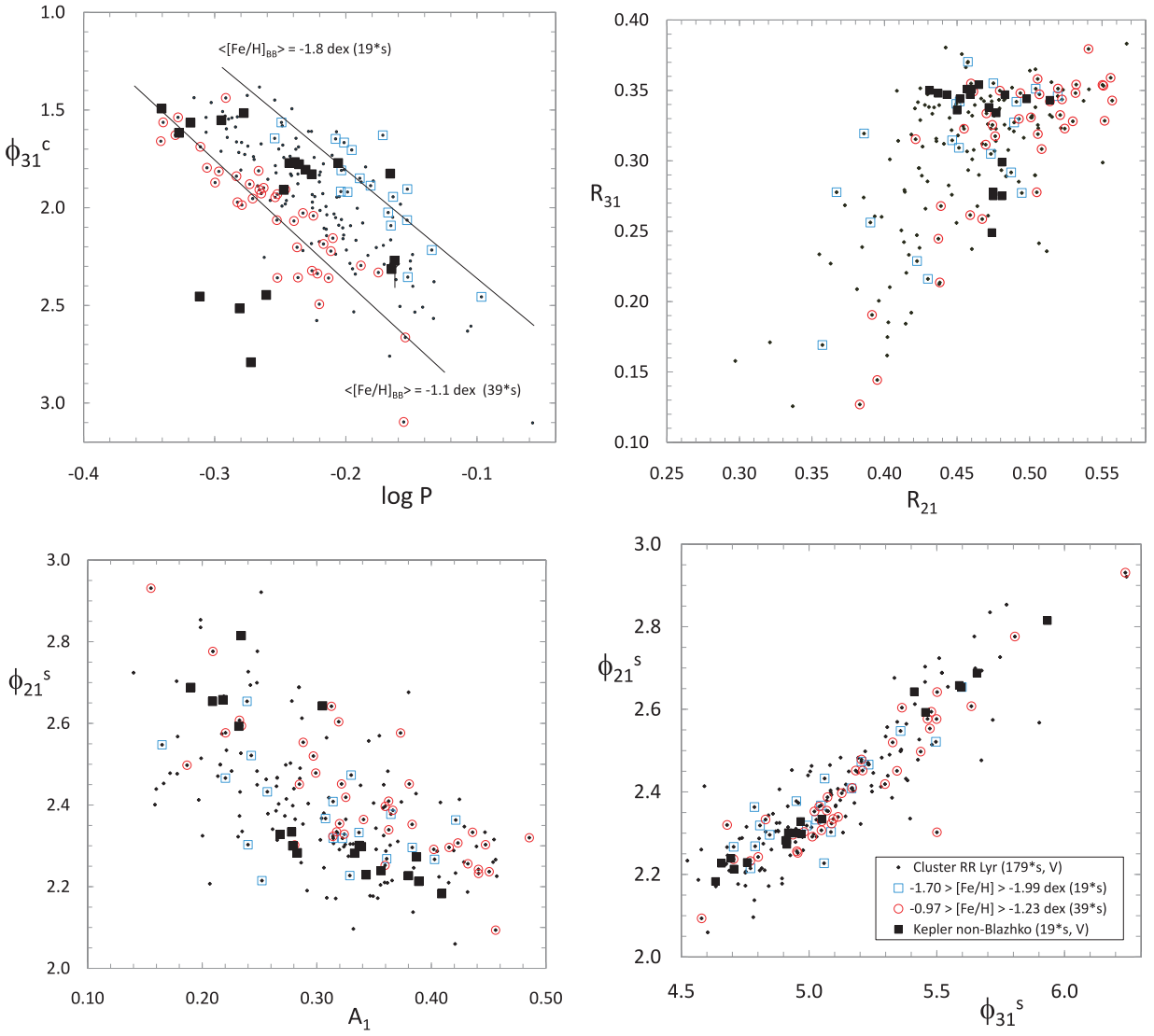

Figure 7. Four panels comparing the Fourier parameters (transformed to the *V* band) for the *Kepler* non-Blazhko stars (large black squares) and for the 177 RR Lyr stars located in several Galactic and LMC GCs (small black dots). The cluster RR Lyr stars (from Kovács & Walker 2001) are in the GCs M2 (12 stars), M4 (four), M5 (12), M55 (four), M68 (five), M92 (five), NGC 1851 (11), NGC 5466 (six), NGC 6362 (12), NGC 6981 (20), IC 4499 (49), Ruprecht 106 (12), NGC 1466 (eight), Reticulum (eight) and NGC 1841 (nine). The points for the 19 most metal poor GC stars are surrounded by blue squares, and the points for the 39 most metal rich GC stars are circled in red.

5.2 *Kp–V* offsets

Since the offsets between the *Kp* and *V* Fourier parameters for AW Dra, FN Lyr and NR Lyr appear to be small and systematic (Figs 6, 9, 10; Table 3), transformation from *Kp* to *V* should be possible using the high-precision *V* parameters (inclusion of the ASAS parameters would not have been helpful owing to their relatively large uncertainties). Transformation to the *V* system allows the derivation of physical characteristics through the application of well-established *V*-band Fourier relations (see Section 6). Because the three stars exhibit a range of periods (0.53 d to 0.69 d) and light-curve shapes ($\phi^s_{31} = 4.8$ to 5.6) and mean colours (see Fig. B1), confounding effects that depend, for example, on location in the 'IS' are likely to have been revealed. On the other hand, if the offsets depend on [Fe/H] such an effect might not have been detected because all three stars appear to have low metal abundances (see Table 4).

Our approach to estimating the *Kp–V* offsets was simply to average the observed differences for AW Dra, FN Lyr and NR Lyr, taking the standard deviation as a measure of the uncertainty. In this way we arrived at the following *Kp–V* transformations:

$$\begin{aligned}
A_{\rm tot}(V) &= A_{\rm tot}(Kp) + (0.14 \pm 0.01),\\
{\rm RT}(V) &= {\rm RT}(Kp) + (0.002 \pm 0.006),\\
A_1(V) &= A_1(Kp) + (0.054 \pm 0.002),\\
A_3(V) &= A_3(Kp) + (0.018 \pm 0.003),\\
R_{21}(V) &= R_{21}(Kp) - (0.013 \pm 0.004),\\
R_{31}(V) &= R_{31}(Kp) - (0.004 \pm 0.009),\\
\phi_{21}(V) &= \phi_{21}(Kp) - (0.089 \pm 0.021),\\
\phi_{31}(V) &= \phi_{31}(Kp) - (0.151 \pm 0.026).
\end{aligned} \quad (2)$$

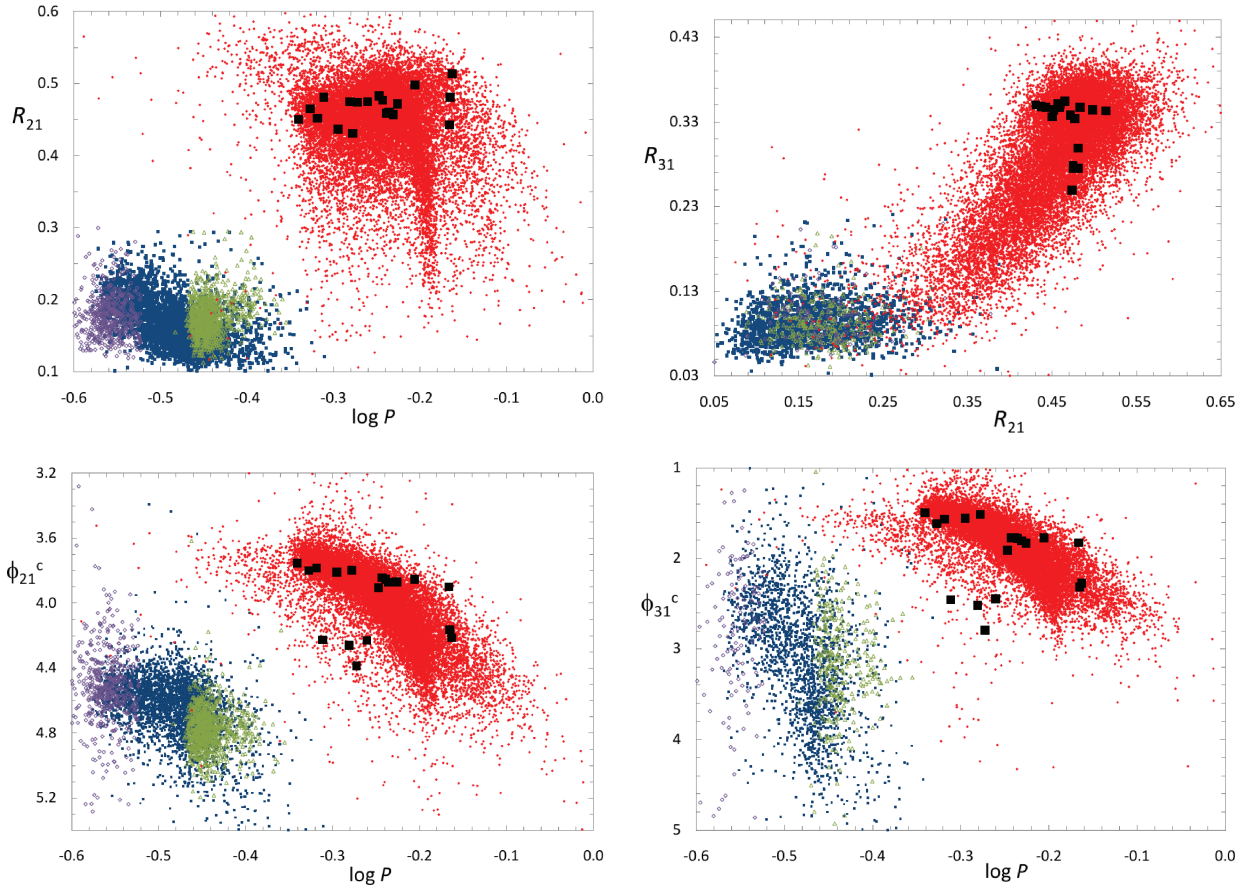

Figure 8. Four panels comparing Fourier parameters (V band) for the *Kepler* non-Blazhko ab-type RR Lyr stars (large black squares) and for 24 905 RR Lyr stars in the central regions of the LMC. The LMC data are from the Soszynski et al. (2009) OGLE-III study, with colour and symbol coding as follows: red filled dots (17 693 RRab stars); blue filled squares (4957 RRc stars); green open triangles (986 RRd stars) and purple open diamonds (1269 RRe stars). Because of the limited x- and y-ranges not all of the LMC RR Lyr stars are represented in the graphs.

Table 4. Metal abundances based on the *Kp* photometry and the equations of J98 and S04.

Star	[Fe/H]			
	ϕ_{31}^{s} J98eq1 CG, ZW, C9	ϕ_{31}^{c} S4eq3 ZW	$A_{\rm tot}$ S4eq6 ZW	RT S4eq7 ZW
(1)	(2)	(3)	(4)	(5)
NR Lyr	−2.04, −2.34, −2.32	−2.28	−2.13	−2.16
V715 Cyg	−1.18, −1.44, −1.34	−1.45	−1.17	−0.74
V782 Cyg	−0.25, −0.47, −0.29	−0.51	−0.86	−0.76
V784 Cyg	+0.06, −0.14, +0.07	−0.18	−1.09	−0.87
KIC 6100702	−0.14, −0.35, −0.17	−0.38	−0.69	−0.48
NQ Lyr	−1.55, −1.83, −1.77	−1.86	−1.68	−1.57
FN Lyr	−1.62, −1.90, −1.84	−1.94	−1.70	−1.31
KIC 7021124	−1.79, −2.08, −2.04	−2.08	−1.91	−1.83
KIC 7030715	−1.39, −1.66, −1.58	−1.60	−1.97	−1.96
V349 Lyr	−1.46, −1.73, −1.66	−1.77	−1.47	−1.08
V368 Lyr	−1.27, −1.53, −1.44	−1.53	−1.27	−0.64
V1510 Cyg	−1.56, −1.83, −1.77	−1.86	−1.89	−1.57
V346 Lyr	−1.55, −1.83, −1.76	−1.86	−1.84	−1.52
V350 Lyr	−1.56, −1.84, −1.78	−1.86	−1.96	−1.62
V894 Cyg	−1.51, −1.79, −1.72	−1.82	−2.01	−1.46
V2470 Cyg	−0.48, −0.71, −0.55	−0.74	−1.13	−0.99
V1107 Cyg	−1.30, −1.56, −1.48	−1.60	−1.56	−1.38
V838 Cyg	−1.30, −1.56, −1.48	−1.58	−1.40	−0.84
AW Dra	−1.47, −1.74, −1.67	−1.68	−2.34	−2.06

The most uncertain of these equations are those for RT and R_{31}. While the per cent uncertainties are large the offsets are small; and besides, these two quantities are rarely used in correlations to derive physical properties.

A comparison of the ASAS $A_{\rm tot}(V)$ values (given in Table 2, Column 7) with the *Kp* values (given in Column 8 of Table 1) is not helpful since several of the stars show larger than expected differences (e.g. V838 Cyg). The accuracy of the above transformation equations is expected to improve with future *BVI* photometry. In Section 6, these offset equations are used to convert the well-established V-band correlations relating Fourier parameters and physical characteristics to *Kp* correlations.

5.3 *Kepler* versus globular cluster RR Lyr stars

In Fig. 7 the Fourier parameters for the 19 non-Blazhko stars in the *Kepler* field (derived using the *Kp* photometry but transformed to V values using the offsets given in equation 2) are compared with parameters derived from V photometry for 177 RR Lyr stars in several well-studied GCs (from Kovács & Walker 2001). The same symbols and colour coding are used in all four panels.

The upper-left panel is analogous to the $P - A_{\rm tot}$ diagram and can be used to derive metallicities (see Section 6.1). The two diagonal lines represent mean relations when the GC data (small black dots) are sorted into two $[{\rm Fe/H}]_{\rm BB}$ bins (here 'BB' refers to the

Butler–Blanco system, which approximates the Carretta–Gratton system – see below): a metal-poor bin consisting of 19 stars (surrounded by blue squares) with metallicities between −1.70 and −1.99 dex and average −1.8 dex (BB-scale); and an intermediate-metallicity bin consisting of 39 stars (circled in red) with $[Fe/H]_{BB}$ between −0.97 and −1.23 dex and average −1.1 dex. The equations of the lines are: $\phi_{31}^c = 5.556 \log P + 0.2920$ (upper metal-poor bin) and $\phi_{31}^c = 6.200 \log P + 3.615$ (lower intermediate-metallicity bin). Four of the *Kepler* non-Blazhko stars are clearly richer than $[Fe/H]_{BB} = -1.1$ dex, while the remainder are apparently more metal poor.

The axes of the other three panels in Fig. 7 are similar to those in Fig. 6. The upper-right panel shows that the *Kepler* stars appear to be drawn from a distribution similar to that of the GCs. In particular, the *Kepler* stars with low R_{31} values are not unusual, except possibly that they all have relatively high R_{21} values. Since the GC stars of higher metallicity (red open circles) all tend to reside on the right side of the diagram this separation is probably a metallicity effect, supporting our conclusion that V784 Cyg, V782 Cyg, KIC 6100702 and V2470 Cyg are metal-rich. Likewise, the lower-left panel shows that the majority of the *Kepler* stars do not differ from the stars in GCs. Note too that there is very little metallicity discrimination in this plane. The two stars located at the extreme upper edge of the envelope of the GC distribution are AW Dra and V784 Cyg. Finally, the lower-right panel shows close agreement between the phase parameters of the *Kepler* and GC RR Lyr stars, which supports the conclusion drawn earlier (lower-right panel in Fig. 6) that there is a strong approximately linear correlation between ϕ_{21}^s and ϕ_{31}^s. The diagram also shows very little dependence on metallicity.

5.4 *Kepler* versus LMC field RR Lyr stars

In Fig. 8 we compare the R_{21}, R_{31}, ϕ_{21}^c and ϕ_{31}^c Fourier parameters for the 19 *Kepler* non-Blazhko RR Lyr stars with those for the field RR Lyr stars in the central regions of the LMC. The LMC data are from the massive OGLE-III Catalogue of Variable Stars by Soszynski et al. (2009), which comprises almost 25 000 RR Lyr stars. All the parameters are *V*-band values, the LMC values having been transformed from *I* to *V* using the transformation equations given by Morgan, Simet & Bargenquast (1998), and the values for the *Kepler* RR Lyr stars from *Kp* to *V* using the equation (2) offsets.

The upper-left panel shows that the *Kepler* stars have R_{21} values in the narrow range 0.43 to 0.51, which is much smaller than the range seen for the LMC stars, 0.25 to 0.55. In particular, none of the *Kepler* RRab stars is among the LMC RRab stars in the 'R_{21} dropdown' at $\log P \sim -0.19$, i.e. $P \sim 0.65$ d. Note that the upper-left panel of Fig. 6 can be used to identify individual *Kepler* stars.

The R_{21} and R_{31} amplitude ratios are compared in the upper-right panel of Fig. 8. This graph, which is similar to the upper-right panels of Figs 6 and 7 (and again, Fig. 6 can be used to identify individual *Kepler* stars), further puts into perspective the small ranges of R_{21} and R_{31} seen for the *Kepler* RRab stars, both relative to that for the LMC RRab stars, and relative to the ranges seen for the other types of RR Lyr stars (RRc, RRd and RRe).

The bottom panels of Fig. 8 are both 'metallicity diagnostic' diagrams, such as those discussed in Section 6.1. We have already seen (upper-left panel of Fig. 7) that the *Kepler* stars sort into four metal-rich and 15 metal-poor stars, that the metal-poor stars are similar to the RRab stars found in both Oosterhoff type I and type II Galactic GCs, and that the metal-rich stars have no counterparts among the Kovács & Walker (2001) sample of GC RR Lyr stars. Here we see that both the metal-rich *Kepler* stars (the clump of four stars at $\log P \sim -0.3$ and $\phi_{21}^c \sim 4.3$) and the metal-poor *Kepler* stars have counterparts in the LMC, and that the metal-rich stars appear to have relatively long periods for metal-rich RRab stars (i.e. the subgroup of LMC RRab stars with shorter periods at a given ϕ_{31}^c).

6 PHYSICAL CHARACTERISTICS

RR Lyrae stars provide fundamental insight into the late evolution of low-mass stars, and in particular the IS region of the horizontal branch (HB). Being present in many GCs (and galaxies) exhibiting different HB types[4] their properties are related to the evolutionary and chemical histories of these systems. Thus, it is desirable to derive (from photometry, spectroscopy and detailed pulsation and stellar evolution models) their physical characteristics, such as the mass $\mathcal{M}$, luminosity *L*, effective temperature $T_{\rm eff}$, iron abundance [Fe/H], chemical composition (X,Y,Z), age, *etc.* An equally important goal is to understand the interdependencies of these quantities. Significant early contributions are summarized in the papers by Christy (1966), Iben (1971), Smith (1995), Sandage & Tammann (2006, hereafter ST6) and Catelan (2009). This knowledge becomes critical when RR Lyr stars (and Cepheids) are used to derive *accurate* distances within and beyond our Galaxy (see Tammann, Sandage & Reindl 2008, hereafter TSR8; Sandage & Tammann 2008, hereafter ST8).

Of course, high-dispersion spectroscopy permits direct measurements to be made of some of these quantities; however, such observations are time-consuming and often impractical. Thus efforts have been on-going to derive physical characteristics from photometry only, in particular from pulsation periods, mean magnitudes and colours, quantities that characterize the shapes of the light curves (e.g. amplitudes, RTs, Fourier phase parameters) and, most recently, from fitting detailed light-curve shapes to non-linear convective pulsation models (see Bono, Castellani & Marconi 2000; Marconi & Clementini 2005; Marconi & Degl'Innocenti 2007).

A potential difficulty for the present Fourier investigation is that almost all the available calibration relations use empirical correlations derived from *V*-band photometry, while for the stars studied here we have *Kp* photometry, and only a limited amount of high-precision *V* photometry and colour information. Furthermore, the mean *Kp* magnitudes from the KIC are somewhat uncertain for giant stars. Despite these limitations we have shown in the previous section, at least for AW Dra, FN Lyr and NR Lyr, three RR Lyr stars with quite different periods and light-curve shapes, that differences between the *V* and *Kp* Fourier parameters appear to be small and systematic. For this reason, we have chosen to present approximate physical characteristics based on the extant *V*-band correlations applied to *Kp* correlations transformed using the observed *Kp*–*V* parameter offsets. Our results are summarized in Tables 4–6 and their derivation is discussed next.

6.1 Iron abundances

6.1.1 Background: [Fe/H] from P-shifts in P–A diagram

Starting with the papers by Oosterhoff (1939, 1944), Arp (1955) and Preston (1959), the period-amplitude (*P*–*A*) diagram, also known as the 'Bailey diagram', has been found to be a useful tool for deriving

[4] The HB type of a GC is defined as (B−R)/(B+V+R), where B, R and V are the number of blue HB stars in the cluster, the number of red HB stars and the number of RR Lyr stars, respectively (Lee 1989). A table of values is given in Lee, Demarque & Zinn (1994, hereafter LDZ94).

Table 5. Galactic coordinates, reddenings, extinctions, dereddened colours and distances.

Star	⟨*Kp*⟩ (mag)	⟨*V*⟩ (mag)	*l*(II) (°)	*b*(II) (°)	$E(B-V)$ (mag)	A_V (mag)	$(B-V)_0$ J98, KW01	*d* (kpc)
(1)	(2)	(3)	(4)	(5)	(6)	(7)	(8)	(9)
NR Lyr	12.683	12.44	69.866 86	13.552 58	0.175(0.009)	0.532	0.369, 0.372	3.0
V715 Cyg	16.265		72.926 58	07.728 90	0.170(0.009)	0.517	0.321, 0.327	14.2
V782 Cyg	15.392		75.144 35	06.947 25	0.509(0.024)	1.606	0.358, 0.363	15.1
V784 Cyg	15.370		76.411 26	06.566 89	0.343(0.010)	1.088	0.351, 0.353	11.8
KIC 6100702	13.458	13.64	71.0171	17.7007	0.103(0.006)	0.324	0.348, 0.353	3.9
NQ Lyr	13.075	13.36	73.112 19	15.064 21	0.068(0.003)	0.207	0.352, 0.358	3.7
FN Lyr	12.876	12.79	73.458 62	14.692 86	0.104(0.007)	0.320	0.323, 0.328	2.9
KIC 7021124	13.550		73.5605	14.7208	0.113(0.006)	0.366	0.357, 0.361	4.1
KIC 7030715	13.452	13.24	74.5488	12.5345	0.108(0.006)	0.334	0.376, 0.377	3.8
V349 Lyr	17.433		72.234 72	18.378 38	0.102(0.013)	0.301	0.324, 0.330	22.7
V368 Lyr	16.002		74.405 57	14.986 18	0.061(0.003)	0.189	0.306, 0.308	11.0
V1510 Cyg	14.494		78.7859	07.2303	0.484(0.030)	1.480	0.340, 0.345	10.4
V346 Lyr	16.421		73.655 39	19.490 70	0.052(0.001)	0.160	0.340, 0.345	13.8
V350 Lyr	15.696		75.654 35	19.589 72	0.051(0.001)	0.158	0.341, 0.345	9.9
V894 Cyg	13.393	12.92	78.737 02	12.607 55	0.112(0.005)	0.346	0.329, 0.331	3.2
V2470 Cyg	13.300	13.54	78.3633	14.9140	0.068(0.001)	0.211	0.357, 0.360	3.7
V1107 Cyg	15.648		78.548 73	15.032 95	0.070(0.002)	0.219	0.348, 0.355	9.7
V838 Cyg	13.770	14.24	79.203 99	16.346 90	0.067(0.002)	0.210	0.314, 0.318	5.3
AW Dra	13.053	12.85	80.230 54	19.053 92	0.047(0.001)	0.146	0.363, 0.365	3.0

Table 6. Fundamental physical properties of the *Kepler* non-Blazhko RR Lyr stars.

Star	$T_{\rm eff}$ KW01, S06 eq11, eq18	M_V J98, F98, BCD7, CC8 eq2, eq2, eq10, eq4a	log *g* J98, KW99 eq15, eq12	*L*(puls) J98, J98 eq16, eq17	*L*(evol) S06, S06, S06 eq8, eq10, eq12	$\mathcal{M}$(puls) J98, J98 eq14, eq22	$\mathcal{M}$(evol) S06, BCD7 eq15, eq7
(1)	(2)	(3)	(4)	(5)	(6)	(7)	(8)
NR Lyr	6242, 6124	0.63, 0.64, 0.67, 0.47	2.677, 2.689	46.9, 47.3	58.7, 54.1, 61.1	0.66, 0.62	0.73, 0.72
V715 Cyg	6607, 6603	0.86, 0.81, 0.81, 0.67	2.874, 2.882	38.0, 36.7	47.6, 45.1, 48.6	0.60, 0.55	0.64, 0.64
V782 Cyg	6493, 6512	0.96, 0.95, 1.03, 0.84	2.817, 2.826	32.0, 34.6	30.5, 34.4, 40.3	0.53, 0.50	0.57, 0.58
V784 Cyg	6546, 6577	0.95, 0.98, 1.08, 0.88	2.807, 2.815	31.0, 33.3	27.2, 32.2, 38.9	0.49, 0.49	0.56, 0.56
KIC 6100702	6564, 6605	0.99, 0.98, 1.08, 0.87	2.855, 2.863	31.0, 33.1	27.4, 32.3, 38.9	0.52, 0.49	0.56, 0.56
NQ Lyr	6382, 6358	0.75, 0.73, 0.72, 0.57	2.756, 2.767	42.1, 42.2	55.2, 50.3, 54.3	0.63, 0.58	0.68, 0.68
FN Lyr (*Kp*)	6531, 6482	0.76, 0.72, 0.71, 0.56	2.814, 2.822	42.7, 40.2	55.8, 50.8, 55.1	0.60, 0.59	0.69, 0.68
FN Lyr (*V*)	6559, 6551	0.76, 0.72, 0.72, 0.56	2.814, 2.823	42.5, 39.4	55.6, 50.6, 54.8	0.60, 0.59	0.69, 0.68
KIC 7021124	6332, 6240	0.70, 0.69, 0.69, 0.52	2.725, 2.737	44.5, 44.4	57.6, 52.4, 57.6	0.64, 0.60	0.71, 0.70
KIC 7030715	6267, 6181	0.69, 0.74, 0.73, 0.58	2.676, 2.688	41.7, 43.7	54.5, 49.8, 53.7	0.58, 0.58	0.68, 0.67
V349 Lyr	6550, 6517	0.80, 0.76, 0.74, 0.60	2.835, 2.843	40.8, 39.0	53.2, 48.8, 52.5	0.61, 0.57	0.67, 0.66
V368 Lyr	6683, 6689	0.84, 0.80, 0.79, 0.65	2.891, 2.898	38.9, 36.2	49.4, 46.3, 49.8	0.57, 0.56	0.65, 0.65
V1510 Cyg	6435, 6370	0.73, 0.72, 0.71, 0.56	2.762, 2.772	42.8, 41.8	56.0, 51.0, 55.3	0.60, 0.59	0.69, 0.68
V346 Lyr	6439, 6376	0.74, 0.72, 0.71, 0.56	2.766, 2.776	42.6, 41.6	55.8, 50.8, 55.0	0.60, 0.59	0.69, 0.68
V350 Lyr	6426, 6359	0.72, 0.71, 0.71, 0.55	2.750, 2.760	43.1, 42.1	56.3, 51.2, 55.6	0.58, 0.59	0.69, 0.69
V894 Cyg	6496, 6443	0.72, 0.71, 0.71, 0.55	2.771, 2.781	42.9, 41.0	56.2, 51.1, 55.5	0.56, 0.59	0.69, 0.68
V2470 Cyg	6469, 6470	0.90, 0.91, 0.94, 0.79	2.793, 2.802	33.9, 36.1	36.4, 38.1, 42.9	0.53, 0.51	0.59, 0.60
V1107 Cyg	6425, 6375	0.79, 0.77, 0.76, 0.62	2.776, 2.786	40.1, 40.3	51.8, 47.9, 51.4	0.61, 0.57	0.66, 0.66
V838 Cyg	6627, 6617	0.82, 0.78, 0.77, 0.64	2.863, 2.871	39.5, 37.3	50.8, 47.2, 50.7	0.58, 0.56	0.66, 0.65
AW Dra (*Kp*)	6306, 6217	0.65, 0.71, 0.70, 0.54	2.673, 2.685	43.4, 44.1	56.7, 51.5, 56.1	0.55, 0.59	0.70, 0.69
AW Dra (*V*)	6303, 6276	0.65, 0.70, 0.70, 0.54	2.673, 2.684	43.3, 43.3	56.6, 51.4, 56.0	0.51, 0.59	0.70, 0.69

iron-to-hydrogen ratios for field and cluster/galaxy RR Lyr stars. The amplitude usually employed is the *B* or *V* total amplitude, $A_{\rm tot}$, and often the abscissa is log*P*. The basic $P-A_{\rm tot}$–[Fe/H] correlation is such that for a given value of $A_{\rm tot}$ lower-metallicity stars tend to have longer periods than higher-metallicity stars. Sandage (2004, hereafter S04) has called this the 'OAP period–metallicity correlation'. Other recent discussions of the $P-A$ diagram and period shifts are given by Di Criscienzo et al. (2004), Bono et al. (2007, hereafter BCD7) and Sandage (2006, 2010, hereafter S06 and S10).

The basic explanation for *P*-shifts in the Bailey diagram follows from the 'stacked HB luminosity levels' model first proposed by Sandage (1958), the latest refinement of which is given in S10 (see his figs 1 and 3). Owing to the Ritter (1879) pulsation relation, $P\sqrt{\rho}=Q$ (where *Q* is a constant over a wide range of *L*, $T_{\rm eff}$ and [Fe/H]), lines of constant density (ρ), and therefore period, cut diagonally across HBs of different luminosity (see fig. 13 of Sandage, Katem & Sandage 1981, hereafter SKS). When coupled with a monotonic $A_{\rm tot}$–$T_{\rm eff}$ correlation (in the sense that $A_{\rm tot}$ increases with distance from the red edge of the IS – see e.g. fig. 12 of SKS, and

fig. 12 of Di Criscienzo et al. 2004) one expects to see at a given $A_{\rm tot}$ more luminous HB stars having longer periods. In fact, *P*-shifts and correlations such as the $\log P - A_{\rm tot}$-[Fe/H] correlation are expected in all diagrams where the abscissa is pulsation period and the ordinate is a light-curve descriptor that correlates with $A_{\rm tot}$. Two such descriptors are the RT and the Fourier ϕ_{31} phase parameter (defined in Section 4.2; see Fig. 10). For example, in the RT *versus* log*P* diagram the *P*-shift at a given RT between M3 and M15 amounts to $\Delta\log P = 0.055$ (see fig. 10 of SKS). Period shifting can also be seen between M3 and M2 in the ϕ_{31} *versus* period diagram (see fig. 2 of Jurcsik et al. 2003), and between metal-rich and metal-poor field RR Lyr stars (see fig. 3 of S04). Thus, such correlations have the potential for measuring [Fe/H] (S04; Kovács 2005; Cacciari, Corwin & Carney 2005, hereafter CCC5; S06; S10; Sodor, Jurcsik & Szeidl 2009).

Identifying the less luminous HB in the Sandage model with that of the unevolved zero-age horizontal branch (ZAHB) stars in the IS of a relatively metal-rich system, and the more luminous HB with the same near-ZAHB stars in the IS of a more metal poor system, leads directly to the OAP period–metallicity correlation. Indeed, ZAHB stellar evolution models clearly show that the mean luminosity levels in the IS for metal-poor ZAHB stars are higher than those for more metal rich ZAHB stars (e.g. Faulkner 1966; Faulkner & Iben 1966; Iben & Faulkner 1968; Hartwick, Härm & Schwarzschild 1968; Iben & Rood 1970; Iben 1971; Sweigart & Gross 1976; Lee, Demarque & Zinn 1990, hereafter LDZ90; LDZ94; Dorman 1992; VandenBerg et al. 2000; Demarque et al. 2000, hereafter D00; Cassisi et al. 2004; Pietrinferni et al. 2004, 2009; Dotter et al. 2007, *etc.*). Indeed, in the IS at $\log T_{\rm eff} = 3.85$ the M15 HB is ∼0.22 mag brighter than that for M3 (SKS). For [Fe/H] values ranging from −2.3 to −0.5 the mean absolute magnitudes for the RR Lyr stars range from $\langle M_{\rm V}({\rm RR})\rangle \sim 0.40$ to 0.85 mag, with, for all but the most extreme clusters, little dependence on HB type (see figs 1 and 2 of D00; and fig. 3 of Cassisi et al. 2004). The models also show that in the IS at the luminosity level of RR Lyr stars the variation in L(ZAHB) is due primarily to a difference in mean mass, with $\langle\mathcal{M}\rangle$ being higher in more metal poor systems.[5]

6.1.2 *Period shifts caused by post-ZAHB evolution*

Despite the general success of the Bailey diagram as a tool for deriving [Fe/H] values it has become apparent since the early 1980s that simple correlations of period-shift with metallicity do not exist in all cases and factors other than metal abundance play a role in the interpretation of these diagrams and correlations. Chief among these effects is evolution away from the ZAHB.

All HB stellar evolution models show tracks leading away from the ZAHB toward the asymptotic giant branch, with HB lifetimes ∼50–100 Myr (core helium burning phase). While the evolution can be either redwards or bluewards it almost always is in the direction of higher luminosity, with the pace quickening as the evolution progresses. As L increases the period becomes longer and larger *P*-shifts are seen in the $P - A$ diagram. However, most HB stars are expected to be located near to the ZAHB, with fewer stars in advanced evolutionary phases (CCC5 put the fraction of evolved RR Lyr stars in M3 at ∼14 per cent). Indeed skewed HB *and* RR Lyrae luminosity distributions are observed in many GCs (e.g. fig. 14 of Sandage 1990, hereafter S90). Such skewed distributions are also seen in simulations of HB and RR Lyr stars (see fig. 10 of Marconi et al. 2003, and fig. 3 of Catelan 2004), and in period shift diagrams (see fig. 6 of Kunder & Chaboyer 2009).

As a first step towards identifying and correcting for such evolutionary effects Sandage (1981a,b, hereafter S81a,b) introduced the concept of 'reduced' period, $\log P' = \log P + 0.336\Delta m_{\rm bol}$, where $\Delta m_{\rm bol} = m_{\rm bol}$ minus (−) the mean apparent magnitude of the bulk of the RR Lyr stars in a given cluster, and the multiplicative factor follows from the van Albada & Baker (1971, 1973) version of the $P\sqrt{\rho} = Q$ relation, and demonstrated the existence of a period–luminosity–amplitude relation for equal-metallicity RR Lyrae stars. The net effect of making this correction is to reduce the period shifts of the evolved RR Lyr stars, resulting in tighter correlations in the $A_{\rm tot}$ versus logP' diagram. In this way S81a,b identified several stars in Messier 3 that are extra-luminous with longer periods at a given A_B than the bulk of the RRab stars.[6] Many other GCs are now known to contain extra-luminous large-period-shift stars, including 47 Tuc (V9 – see Storm et al. 1994), NGC 6388 and NGC 6441 (Pritzl et al. 2000, 2001, 2002; Catelan et al. 2006), Messier 5 (Kaluzny et al. 2000, CCC5), NGC 5896 (Alves, Bond & Onken 2001), IC 4499 (V9 and V54 – see CCC5; Kunder et al. 2011; Walker et al. 2011), and Messier 13 (Sandquist et al. 2010).

The reduced-period concept is useful when deriving mean metallicities for ensemble populations of RR Lyr stars in GCs and galaxies (e.g. Dall'Ora et al. 2003), and for field stars that are near the ZAHB (which are assumed to be in the majority), but the method fails for evolved RR Lyrae stars: what looks in the Bailey diagram like a metal-poor ZAHB star might well be an evolved metal-rich star, i.e. an evolved OoI star masquerading as an unevolved OoII star.

Thus, the amount of *P*-shifting is determined by the amount of *L*-evolution, which in turn depends on the HB morphology of the parent population (LDZ90; Lee 1990)[7]. When RR Lyr stars

[5] Based on the $A_{\rm tot} - T_{\rm eff}$ correlation one expects also to see period shifting in the log$T_{\rm eff}$ versus log$P$ diagram, and indeed fig. 11 of SKS shows at 'any given temperature' an observed shift between M3 and M15 of $\Delta\log P = 0.070$. However, when comparing model predictions with observations one must 'let the temperature be cooler for more metal poor RR Lyr stars at their higher luminosities' (Simon & Clement 1993; Sandage 1993 (S93); S06).

[6] Sandage's candidate evolved stars in M3 include V24, V60, V65, V96 and V124, all of which can be seen (labelled) in the S81a fig. 2 $m_{\rm bol}$ versus log$T_{\rm eff}$ diagram and in the S81a fig. 3 period–amplitude diagrams. Subsequent studies of M3 by Kaluzny et al. (1998) and Clement & Shelton (1999) confirmed V65 as an evolved star and also have identified V14 and V104 as post-ZAHB stars. Post-ZAHB evolution in M3 was also investigated by Marconi et al. (2003) and by Jurcsik et al. (2003). The latter used 'luminosity bins' and Fourier parameters and found that RR Lyr 'stars close to the ZAHB show OoI type properties, while the brightest stars have Oo II statistics regarding their mean periods and RRab/RRc number ratios', confirming the earlier result of Clement & Shelton (1999). Thus, again, the Oosterhoff dichotomy seems to be connected with evolutionary effects. More recently, CCC5 confirmed V24 and V14 as evolved stars and identified three more post-ZAHB stars based on their long periods and relatively high luminosities (V3, V35, V67). Most recently, Valcarce & Catelan (2008) identified in M3 ∼15 non-Blazhko and another ∼10 Blazhko RR Lyr stars in an advanced post-ZAHB evolutionary state (see their fig. 2).

[7] The main parameter controlling the distribution of stars along the HBs of GCs is metal abundance (Sandage & Wallerstein 1960), with metal-rich clusters (e.g. NGC 6356, 47 Tuc) having predominantly red HBs and metal-poor systems (e.g. M15, M9) having predominantly blue HBs. Since the discovery by Sandage & Wildey (1967) and van den Bergh (1967) that there is not a unique correlation between [Fe/H] and HB morphology, and the recognition that the GCs with the bluest HBs are not the most metal poor clusters (Renzini 1983), the search has been on for the so-called

originate from a position on the ZAHB that is *within* the IS, which occurs in OoI clusters with HB type near zero, such as M3 and M4 with HB types (from LDZ94) of 0.08 ± 0.04 and -0.07 ± 0.10, respectively, the evolution manifests itself in the IS region of the HR diagram as a vertical widening of the HB with RR Lyr stars of similar mass spread over a range of L and $T_{\rm eff}$ (see S90; and fig. 1 of Jurscik et al. 2003, hereafter J03; and fig. 2 of Valcarce & Catelan 2008). On the other hand, when the original location on the ZAHB was *bluewards and outside of* the IS, which occurs in OoII clusters with HB types that are large and positive, such as M15 (see Sobeck et al. 2011), M92 (see Roederer & Sneden 2011) and M2 (Lee & Carney 1999) with HB types of 0.72 ± 0.10, 0.88 ± 0.08 and 0.96 ± 0.10 (all from LDZ94), respectively, most if not all the RR Lyr stars are evolved and few if any lower-luminosity ZAHB stars are present (see LDZ90, D00). In the case of M2 Lee & Carney (1999) concluded that its RR Lyrae stars are $\sim$0.2 mag more luminous than those in M3, owing to all the M2 stars having evolved away from the blue side of the HB, whilst the bulk of the M3 stars lie near the ZAHB. Additional observational support for this idea comes from the clear correlation of metallicity and HB intrinsic vertical width, with more metal rich systems having greater vertical widths (see fig. 16 of S90). Schematic tracks (along with grid lines of constant period and amplitude) comparing the post-ZAHB evolution of stars in M2 (and M15) with the tracks for M3 (and NGC 6441) are given in fig. 3 of S10. Completing the picture, in clusters with red HBs (i.e. HB types that are large and negative, such as 47 Tuc and M107, with HB types of -1.0 ± 0.03 and -0.76 ± 0.08, respectively) the evolution occurs mainly redwards of the IS and few, if any, RR Lyr stars are expected (exceptions to this rule include systems with red HBs and extended blue HBs, such as NGC 6388 and NGC 6441 – see references above). Thus, the luminosity of an individual RR Lyr star in a given cluster depends not only on its metallicity (usually assumed to be that of the parent cluster) but also on its evolutionary state, which in turn is determined by the HB-type of the parent cluster and the amount of evolution away from the ZAHB.

In closing, a potential solution to the evolution degeneracy problem in the Bailey diagram is to identify the evolved RR Lyrae stars using some sort of light-curve index, such as the JK96 'compatibility criterion' (see Kovács & Kanbur 1998; Clement & Shelton 1999; Nemec 2004; CCC5). Of particular interest in this regard is fig. 14 of CCC5, which shows large P-shifts for several stars in the $A_{\rm B}$ *versus* log$P$ diagram, but no such offset in the ϕ_{31} *versus* log$P$ diagram; whether post-ZAHB stars stand out more in the $P-A$ diagram than in the period-ϕ_{31} diagram remains an open question. In any case it is important to exercise caution when using the individual Fourier-based metallicities derived here.

6.1.3 Metallicity scales

For the *Kepler* non-Blazhko RRab stars we have used the correlations involving all three light-curve descriptors to estimate [Fe/H] values (see Section 6.1.4). The resulting metallicities are reported in Table 4. The metal abundances based on the S04 equations are on the Zinn & West (1984, hereafter ZW) scale, and those based on J98's equation (1) are on the Carretta & Gratton (1997, hereafter CG) scale. For comparison purposes the latter (i.e. the ϕ_{31}^s-metallicities) have been transformed to the ZW scale *and* to the Carretta et al. (2009, hereafter C9) scale. Although several other metallicity systems have been proposed (e.g. Layden 1994; Jurcsik 1995; Butler & Blanco – see S04 and Kraft & Ivans 2003), the C9 scale is most extensive. It is based on a homogeneous data set derived from $\sim$2000 modern spectra, and is gaining considerable favour – see e.g. its adoption by Harris (1996) for his online GC catalogue at http://www.physics.mcmaster.ca/~harris/mwgc.data. In addition, equations are provided for transformation between the various scales. When transforming between the ZW and CG systems the following equation (from S04, footnote 1) has been used: $[{\rm Fe/H}]_{\rm ZW} = 1.05\,[{\rm Fe/H}]_{\rm CG} - 0.20$. When transforming from the ZW and CG scales to the C9 scale we have used (from C9): $[{\rm Fe/H}]_{\rm C9} = 1.137\,[{\rm Fe/H}]_{\rm CG} - 0.003$ and $[{\rm Fe/H}]_{\rm C9} = -4.13 + 0.130\,[{\rm Fe/H}]_{\rm ZW} - 0.356\,[{\rm Fe/H}]^2_{\rm ZW}$.

6.1.4 Metallicities for the Kepler stars

Fig. 9 contains, for the *Kepler* non-Blazhko RRab stars, four such 'metallicity diagnostic diagrams'. The principal observation here is the similarity, to the first order, of the distribution of the points in the four graphs. The top-left panel is the classical P–$A_{\rm tot}$ diagram, with total *Kp* amplitude plotted along the ordinate. Traditionally, lines of constant [Fe/H] serve as metallicity calibration lines; these run diagonally from the upper-left to the lower-right corner (as seen in three of the panels).

The top-right panel has A_1 along the ordinate. As expected, because A_1 and $A_{\rm tot}$ are highly correlated (see Fig. 2), the distribution of the points closely resembles that in the $A_{\rm tot}$ *versus* log$P$ diagram. In principle, the small range of A_1 (only $\sim$0.2 mag) compared with that of $A_{\rm tot}$ (nearly 0.7 mag here, but often larger) makes the P–A_1 diagram less useful for estimating [Fe/H]; but with such high-precision data as provided by *Kepler* the derived [Fe/H] results should, in principle, be similar.

The bottom panels of Fig. 9 show RT (left) and ϕ_{31}^c (right) plotted against log$P$, where both RT (reverse scale) and ϕ_{31}^c (reverse scale) increase with increasing log$P$. The bottom-right panel is the '*Kepler* non-Blazhko RRab only' version of the top-left panel of Fig. 7, and also is similar to Fig. 11. The dashed line in the bottom-right panel (from fig. 14 of CCC5), the equation of which is $\phi_{31}^c = 3.124 + 5.128\log P$, represents the observed V-band relation for the RRab stars in M3 – it is encouraging that the slope of the line appears to agree with the slope of the *Kepler* metal-poor stars. According to this calibration NR Lyr is the most metal-poor star in the sample, followed by KIC 7021124 and FN Lyr, and most of the RRab stars have metallicities similar to those in M3, which has $[{\rm Fe/H}] = -1.50 \pm 0.05$ dex (C9 scale; W. Harris' online catalogue). Metallicities for the other stars, including the four stars suspected of having high [Fe/H] values, are discussed below.

Fig. 10 contains the RT *versus* $A_{\rm tot}$ diagram (left-hand panel) and the ϕ_{31}^s (which is π larger than ϕ_{31}^c) *versus* $A_{\rm tot}$ diagram (right-hand panel) for the *Kepler* stars. In general, as the total amplitude increases, both RT and ϕ_{31}^s decrease, with linear fits described by the equations: $RT = -0.118A_{\rm tot} + 0.256$ and $\phi_{31}^s = -1.75A_{\rm tot} + 6.75$; however, owing to the large scatter about these lines, and the suspected large range in metallicities of the *Kepler* stars, we believe these equations to be unreliable (and for this reason they were not plotted). Theoretical models (see the middle-left panels of Figs 14 and 15) suggest that it is more probable that there are families of

'second parameter'. The two leading candidates are differences in age (see Rood & Iben 1968; LDZ94; Lee et al. 1999, 2007; Rey et al. 2001; Dotter et al. 2010) and variations in the initial helium abundance (see Sandage & Wildey 1967, van den Bergh 1967, Hartwick 1968, Busso et al. 2007). Other candidates include variations in the amount of mass loss along the red giant branch (RGB), rotation rates and the amount of helium mixing deep inside progenitor RGB stars (see Sweigart & Catelan 1998).

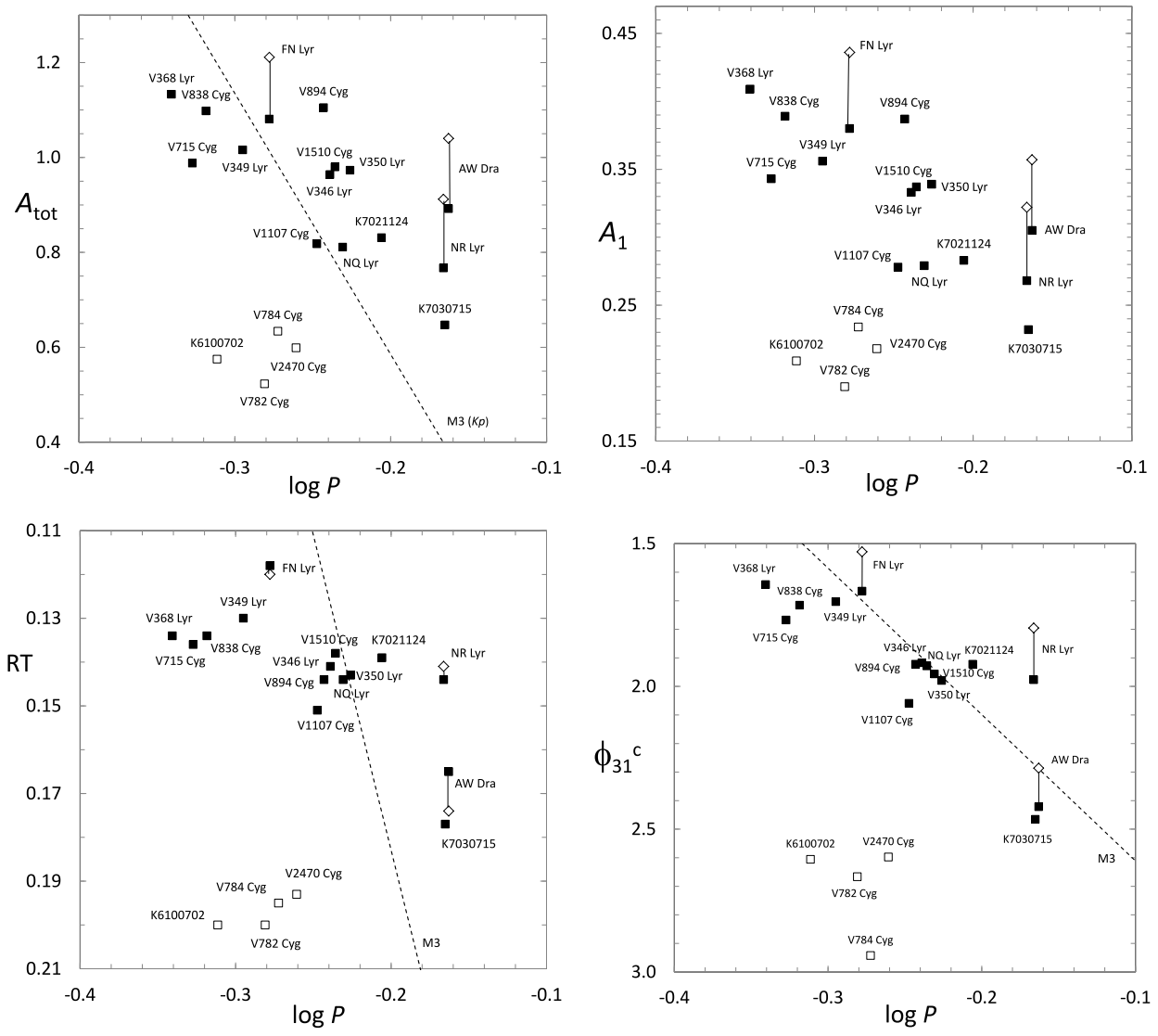

Figure 9. Period–amplitude and three other metallicity diagnostic diagrams for the *Kepler* non-Blazhko RRab stars. For all four graphs the abscissa is log$P$, all the stars have been labelled and the four candidate metal-rich stars are plotted as open squares. AW Dra, FN Lyr and NR Lyr are plotted twice in each panel, with the points derived from the *Kp* photometry (solid black squares) connected to the points derived from the high-precision V-band photometry (open diamonds) – the consistency of the *Kp*–V offsets seen here (and in Figs 6 and 10) is quite striking. The diagonal dashed lines, representing the relations for the M3 RR Lyr stars (assumed to have $[Fe/H]_{ZW} = -1.6$ dex), are from equation (5) (S04eq6, top left), equation (6) (S04eq7, bottom left) and fig. 14 of CCC5 (bottom right).

lines (or curves), one for each metallicity. Unfortunately, the present observational data are insufficient to establish these. It is noteworthy that AW Dra, and to a lesser extent V784 Cyg and V894 Cyg, has larger ϕ_{31}^s values and larger RTs than other stars of comparable A_{tot}. While it appears that all the low-amplitude stars have large RTs and large ϕ_{31}^s values, this conclusion is based on only four low-amplitude candidate metal-rich stars and two low-amplitude long-period candidate metal-poor stars (KIC 7030715, AW Dra), one of which (AW Dra) is a possible outlier in both graphs and which may be a long-period evolved star of intermediate metallicity [if our preliminary Canada–France–Hawaii Telescope (CFHT) spectra result is correct – see Section 6.1.5] rather than a near-ZAHB star of low metallicity. In any case, both KIC 7030715 and AW Dra have considerably longer periods than the four high-metallicity stars.

In Fig. 11, the *Kepler* data are compared with the Galactic field star data analysed by S04 (see his fig. 3). The field RR Lyr stars are the same as those studied by Simon & Lee (1981), Simon & Teays (1982) and Simon (1988), the details of which are given in table 1 of S04. Fig. 11 is comparable to the bottom-right panel of our Fig. 9, which shows only the *Kepler* non-Blazhko stars. Because the Simon et al. stars have known $[Fe/H]_{ZW}$ values from Layden (1994) it is possible to sort them by metallicity. Following Sandage we plotted two subsets of the data, which have average metallicities $\langle[Fe/H]\rangle = -0.35$ and -1.63 dex (ZW scale); the diagonal lines were obtained by substituting these values into equation (3) of S04. This diagram is also the Galactic field star version of the upper-left panel of Fig. 7, which included RR Lyr stars in Galactic and Magellanic Cloud GCs. The chief difference is that the calibration has now been extended to more metal rich stars.

Fig. 11 shows that the stars KIC 6100702, V2470 Cyg, V782 Cyg and V785 Cyg, all of which have long RTs, are solidly in the metal-rich region of the diagram, with the highest ϕ_{31}^c values and all with

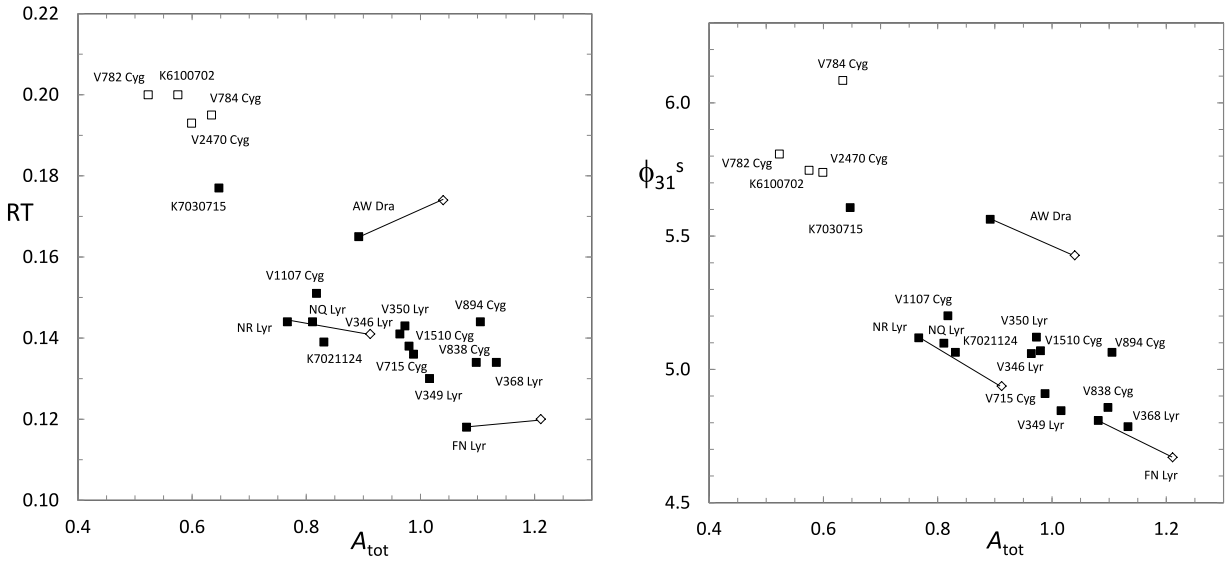

Figure 10. RT versus total amplitude diagram (left-hand panel) and Fourier phase parameter ϕ_{31}^s versus total amplitude diagram (right-hand panel) for the *Kepler* non-Blazhko RRab stars. The symbols are the same as in the bottom-right panel of Fig. 9 (i.e. the four metal-rich stars have been plotted with open squares), and again AW Dra, FN Lyr and NR Lyr are plotted twice in each panel, indicating the magnitudes and directions of the (systematic) *V*–*Kp* offsets.

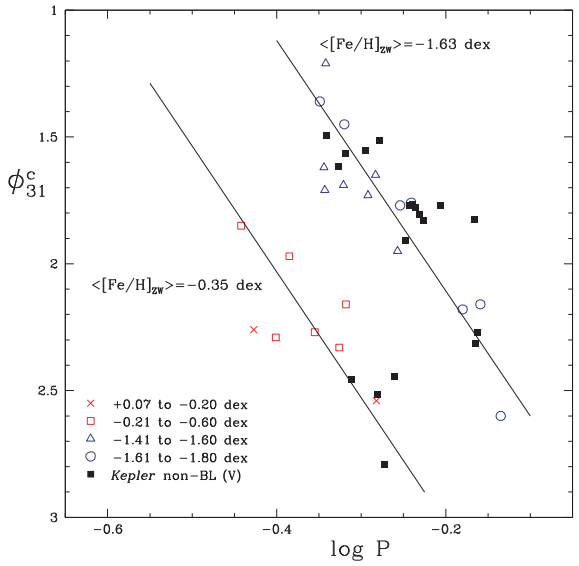

Figure 11. Period–ϕ_{31}^c diagram, comparing the *Kepler* non-Blazhko RR Lyr stars and the Lub-Simon Galactic field stars (from S04). The latter have metallicity estimates (on the ZW scale) from Layden (1994). The symbols are as indicated on the graph: *Kepler* stars (large black squares); two very metal-rich RR Lyr stars (red crosses); six metal-rich RR Lyr stars (red open squares); seven intermediate-metallicity RR Lyr stars (blue open triangles) and nine intermediate-to-low [Fe/H] RR Lyr stars (blue open circles). The *Kepler* stars have been shifted upwards by 0.151 (in accordance with equation 2) and thus are *V* values (as are the values for the Lub-Simon stars).

periods shorter than 0.55 d. The other *Kepler* stars are a better match to the field stars that have $[Fe/H]_{ZW} = -1.63$ dex. AW Dra and KIC 7030715, with long periods, intermediate RTs and high ϕ_{31} values, are seen to have metallicities ~ -1.64 dex (ZW scale). Three of the four metal-rich stars (V782 Cyg, KIC 6100702 and V2470 Cyg) have $[Fe/H]_{ZW} = -0.4$ dex, and V784 Cyg is the most metal rich star in our sample with $[Fe/H]_{ZW} = -0.2$ dex. The most metal poor stars are seen to be more metal poor than $[Fe/H]_{ZW} = -1.6$ dex.

Equation (1) of J98, which is identical to equation (3) of Jurcsik & Kovács 1996, describes lines of constant $[Fe/H]_{CG}$ in the period–$\phi_{31}^s(V)$ diagram. Using the offset formula for ϕ_{31}^s given in equation (2) the *Kp* version of the J98 equation becomes

$$[Fe/H]_{CG} = -5.241 - 5.394\,P + 1.345\,\phi_{31}^s(Kp). \quad (3)$$

Metallicities calculated with this formula are listed in Column 2 of Table 4 under 'J98eq1'. For comparison purposes the corresponding values on the ZW and C9 scales also are listed.

Our second estimate of [Fe/H] is derived from the $[Fe/H]_{ZW} - \log P - \phi_{31}^c$ relation of S04 (his equation 3 – note that the cosine version of the Fourier phase parameter is employed here) – see lower-right panel of Fig. 9. Applying the ϕ_{31}^c offset given in equation (2), Sandage's relation becomes

$$[Fe/H]_{ZW} = -6.217 - 7.012\log P + 1.411\,\phi_{31}^c(Kp), \quad (4)$$

where the intercept term has a total uncertainty of ±0.023, and the ϕ_{31}^c and log*P* coefficients have respective uncertainties of ±0.014 and ±0.071 (from S04). Metallicities derived from equation (4) are listed in Table 4 under 'S4eq3'.

Implementation of the *P*–*A* diagram (see upper-left panel of Fig. 9) for deriving metallicities was via equation (6) of S04, combined with the *Kp*–*V* offset for A_{tot} (equation 2):

$$[Fe/H]_{ZW} = -1.453\,A_{tot}(Kp) - 7.990\log P - 2.348, \quad (5)$$

where the errors in the coefficients (from S04) are ±0.027, ±0.091 and ±0.043, respectively. The derived $[Fe/H]_{ZW}$ values are listed in Table 4 under 'S4eq6'. According to this formula the most metal-poor star is AW Dra, 0.2 dex more metal poor than NR Lyr, and 0.6 dex more metal poor than the estimates derived form the ϕ_{31} equations! Given its location in the ϕ_{31}^c versus log*P* diagram, and our recently derived spectroscopic metallicity of -1.33 ± 0.08 dex, it is our opinion that this is an evolved RR Lyrae star; curiously, it follows the pattern of evolved RR Lyr stars seen in M3 by CCC5 (their fig. 16). The metal-rich stars also are predicted to be more metal poor than the values given by the ϕ_{31} estimates.

Our fourth set of [Fe/H] estimates was based on the RT *versus* log*P* diagram (lower-left panel of Fig. 9). The metallicities were

calculated using Sandage's relation between RT, P and [Fe/H] (his equation 7), combined with our V–Kp offset (equation 2):

$$[\mathrm{Fe/H}]_{\mathrm{ZW}} = 6.33\,\mathrm{RT}(Kp) - 9.11\log P - 4.59, \quad (6)$$

where the S04 intercept has been increased by 0.01 (representing the RT conversion from V to Kp). Application of this equation gave the metallicities listed in Table 4 under 'S4eq7'.

6.1.5 *Discussion of the derived metallicities*

In the absence of spectroscopic metal abundances[8] which of the [Fe/H] values in Table 4 are the most reliable? One area of potential bias comes from the fact that all the metallicity correlations used in Section 6.1.4 assume that the stars are unevolved. This probably is true for most of the *Kepler* non-Blazhko stars; however, there may a few evolved stars in the sample, the most likely candidate being AW Dra. In such a case the period will have been increased by luminosity evolution and the derived [Fe/H] will be systematically smaller than the true value. Another potential bias occurs for the most metal poor stars where the Fourier-based metallicity calibrations may give values systematically too high (see JK96 and Nemec 2004). The implication here is that the most metal poor stars in our sample are even more metal deficient than the values given in Table 4.

In general, the metallicities that are based on the Fourier ϕ_{31} phase parameter (i.e. those derived using equation 1 of J98, and equation 3 of S04) are very similar. This can be seen by comparing the ϕ_{31}^{s} and ϕ_{31}^{c} metallicities (ZW scale) given in Columns 2 and 3 of Table 4. When the ϕ_{31} metallicities are compared with those calculated using A_{tot} (Column 4) and RT (Column 5) a number of systematic differences are present. For all the low-amplitude stars (the four suspected metal-rich stars, and AW Dra and KIC 7030715) the RT and A_{tot} estimates tend to be systematically more metal poor than the ϕ_{31} estimates. On the other hand, for most of the suspected metal-poor stars the A_{tot} and RT equations give more metal rich estimates of [Fe/H] than those derived with the ϕ_{31} equations. For several of the stars (e.g. V1510 Cyg, V346 Lyr, V350 Lyr, V894 Cyg and V1107 Cyg) the RT gives [Fe/H] values richer than the ϕ_{31} values, while the A_{tot} formula gives [Fe/H] values more metal poor. The largest difference occurs for V784 Cyg, where ϕ_{31} suggests $[\mathrm{Fe/H}]_{\mathrm{ZW}} = -0.16$ while A_{tot} and RT imply $[\mathrm{Fe/H}]_{\mathrm{ZW}} = -1$ dex. Our suspicion is that the slope in the RT term of equation (6) is too steep (see M3 line in lower-left panel of Fig. 9).

AW Dra is the only star for which the estimated [Fe/H] can be compared with a previously published metallicity estimate, and, unfortunately, that estimate is quite uncertain. Based on its location in the P–A_V diagram, Castellani et al. (1998) found the metallicity of AW Dra to be in the range -1.9 to -1.4 dex. Our estimate, $[\mathrm{Fe/H}]_{\mathrm{C9}} = -1.67$ dex, is consistent with theirs, but should be more reliable because it is based on much more extensive and higher precision photometry (see Table 3, and footnote 8).

6.2 Reddenings and mean colours

6.2.1 *Dereddened colours*

J98 showed that the dereddened mean $B-V$ colours correlate well with pulsation period P and the Fourier A_1 coefficient, and derived the following relationship (her equation 3):

$$(B-V)_0 = 0.308 + 0.163P - 0.187A_1. \quad (7)$$

Replacing $A_1(V)$ with $A_1(\mathrm{Kp})$ from equation (2) simply reduces the intercept from 0.308 to 0.298. Dereddened $B-V$ colours calculated with our modified equation for the Kp photometry, and with the J98 equation for the V photometry of FN Lyr and AW Dra, are given in Column 8 of Table 5 (under 'J98'). The colour range is from 0.306 (for V368 Lyr) to 0.376 (for KIC 7030715), with a mean colour of 0.343.

Another relationship for $(B-V)_0$ was derived by KW01. Their equation (6) includes an additive A_3 term, and the A_1 and A_3 are derived from V photometry. Using our offsets to convert to the Kp scale gives

$$(B-V)_0 = 0.448 + 0.189\log P - 0.313\,A_1 + 0.293\,A_3, \quad (8)$$

where A_1 and A_3 now are derived from Kp photometry and the KW01 intercept has been modified accordingly. Dereddened colours derived using this equation (and the KW01 equation for the V data of AW Dra and FN Lyr) are also given in Column 8 of Table 5 (under 'KW01'). These estimates are practically identical to the J98 colours and have an overall mean of 0.347. In subsequent analyses we adopt for each star the average of the two colour estimates.

Fig. 12 shows four graphs for the non-Blazhko RR Lyr stars, all with dereddened mean colour, $(B-V)_0$, plotted along the x-axis. In every graph the four high-metallicity stars (V782 Cyg, V784 Cyg, KIC 6100702 and V2470 Cyg), plotted as open squares, stand apart from the other RR Lyr stars. One sees that they also tend to be on the red side of the IS. The three stars with the reddest colours (and coolest temperatures), NR Lyr, AW Dra and KIC 7030715, are all of very low metallicity and have the longest periods ($P \sim 0.68$ d) in our sample, and the three shortest period stars (V368 Lyr, V838 Cyg, V715 Cyg) have the bluest colours and are metal poor but of intermediate metallicity ($[\mathrm{Fe/H}]_{\mathrm{ZW}} \sim -1.5$ dex). Linear regressions were made to the points representing the 15 metal-poor stars, and the equations of the lines are given on the graphs. The colour–metallicity diagram (top left) shows that the reddest metal-poor stars tend to have the lowest metallicities; the colour–period diagram (top right) shows that the metal-poor stars exhibit a correlation such that the reddest stars have the longest periods, and that at a given colour the metal-rich stars have shorter periods than the metal-poor stars; the colour–total amplitude diagram (bottom left) shows that the red metal-poor stars have lower amplitudes than the blue metal-poor stars, and that at a given colour the metal-rich stars have lower amplitudes than the metal-poor stars and the colour–absolute magnitude diagram (bottom right – see discussion in Section 6.4) shows

[8] High-resolution echelle spectra of the brightest 18 *Kepler* RR Lyr stars (non-Blazhko and Blazhko, RRab and RRc) have recently been acquired with the ESPaDOnS spectrograph on the CFHT 3.6-m telescope (Nemec et al., in preparation). These spectra currently are being measured and *preliminary* informative results are available for two of the non-Blazhko RRab stars: (1) for KIC 6100702 a spectroscopic metal abundance of -0.18 ± 0.06 dex has been derived – this compares very favourably with the two ϕ_{31}-based metallicities, $[\mathrm{Fe/H}]_{\mathrm{C9}} = -0.17$ dex and $[\mathrm{Fe/H}]_{\mathrm{ZW}} = -0.38$ dex (see Columns 2 and 3 of Table 4), both of which are more metal rich than the A_{tot} and RT values. Thus for one of the four suspected metal-rich non-Blazhko RRab stars there is spectroscopic confirmation of high metallicity; and (2) for AW Dra a spectroscopic $[\mathrm{Fe/H}] = -1.33 \pm 0.08$ dex has been derived. If correct this is more metal rich than any of the derived photometric estimates. Our suspicion is that AW Dra, which exhibits a large period-shift in the A_{tot} *versus* log$P$ diagram and in the A_1 *versus* log$P$ diagram (see upper two panels of Fig. 9), and is an outlier in the ϕ_{21}^{s} *versus* A_1 diagram and in the ϕ_{21}^{s} *versus* ϕ_{31}^{s} diagram (see bottom two panels of Fig. 6), and an outlier in both Fig. 10 panels, may be in an advanced post-ZAHB evolutionary state (see Section 7). The spectroscopic metallicities for these two stars currently are being firmed up and data reductions are continuing on the other 16 stars for which spectra are in hand.

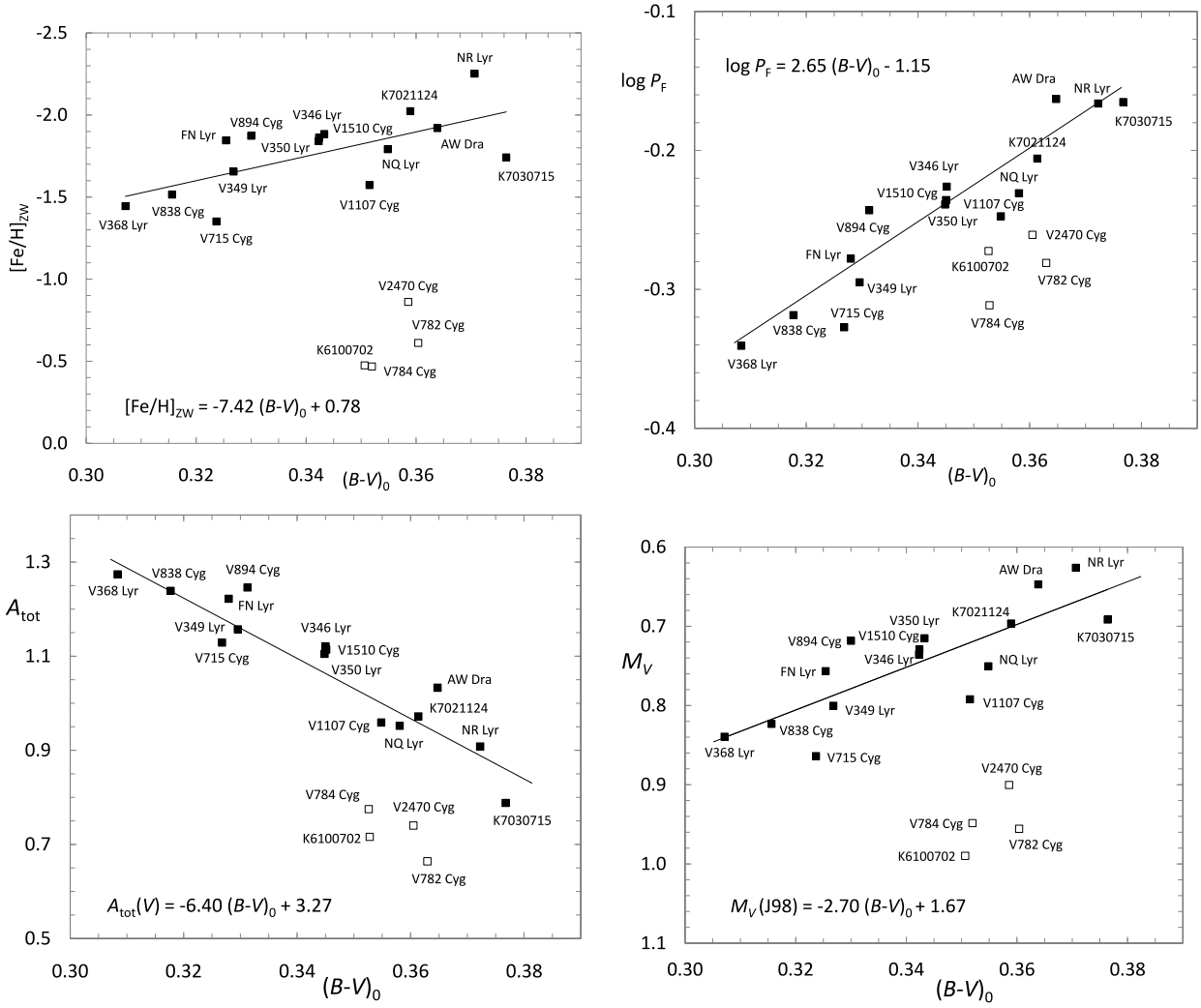

Figure 12. Four diagrams for the non-Blazhko RR Lyr stars, all with dereddened mean colour $(B-V)_0$ (average of the two values given in Column 8 of Table 5) along the abscissa: metallicity *versus* colour (top left), period *versus* colour (top right), total amplitude *versus* colour (bottom left) and absolute magnitude *versus* colour (bottom right). In each panel the line (and its equation) is from a least-squares fit to the points for the 15 metal-poor stars (i.e. those with [Fe/H] < -1.0 dex). The linear correlations show that the reddest metal-poor stars (those nearest the red edge of the IS) are more metal poor, have longer periods and smaller total amplitudes, and are more luminous than the bluest metal-poor stars. The diagrams also show that at a given colour the four metal-rich stars (plotted with open squares) have shorter periods, have smaller amplitudes and are less luminous than the metal-poor stars.

that at a given colour the metal-rich stars have lower luminosity than the metal-poor stars, and that the reddest metal-poor stars are more luminous than the bluest metal-poor stars.

6.2.2 Reddenings and extinctions

Table 5 also contains $E(B-V)$ reddenings (Column 6) derived from the large-scale reddening maps of Schlegel, Finkbeiner & Davis (1998). These were estimated using the NStEd online facility and the Galactic (*l*,*b*) coordinates given in Table 5 (Columns 4 and 5). According to the maps the most reddened stars in our sample are V782 Cyg, V784 Cyg and V1510 Cyg. Total extinctions in the V passband, A_V, were calculated assuming an extinction-to-reddening ratio $A_V/E(B-V) = 3.1$ and are given in Column 7 of Table 5.

For AW Dra, which has calibrated B, V photometry, the above reddenings can be compared with reddenings derived from the Fourier-based dereddened colours and the observed reddened mean $B-V$ colours. Castellani et al. (1998) observed $(B-V)_0 = 0.368$, and from the $P-A$ diagram estimated [Fe/H] $= -1.4$ dex. Using the Burstein & Heiles (1982) reddening maps they adopted the value $E(B-V) = 0.04 - 0.06$ mag, which gives $(B-V)_0 = 0.31$–0.33. This estimate of the reddening is consistent with 0.047 ± 0.001 given in Table 5, but the dereddened colour is bluer than the average of the two Fourier-based values, $(B-V)_0 = 0.364$ (J98, KW01). This difference explains why the Castellani et al. estimates of $T_{\rm eff}$ (see their table 7, and below) are higher than our estimates (Column 2 of Table 4).

6.3 Effective temperatures

Mean $T_{\rm eff}$ values for the RR Lyr stars were estimated using two prescriptions, one from KW01 and the other from S06 [where the relationship between $(B-V)_0$ colour, $T_{\rm eff}$ and [Fe/H], including the effects of such other factors as surface gravity and turbulent velocity, has been reviewed]. For the colour interval $0.20 < (B-V)_0 < 0.30$ S06 adopts the formula given by Carney, Storm & Jones

(1992):

$$(B-V)_0 = -2.632\log T_{\rm eff} + 0.038\,[{\rm Fe/H}]_{\rm ZW} + 10.423. \quad (9)$$

Inverting this equation (equation 18 of S06) gives

$$\log T_{\rm eff} = -0.380\,(B-V)_0 + 0.0144\,[{\rm Fe/H}]_{\rm ZW} + 3.960. \quad (10)$$

This equation, along with our colour and metallicity estimates, was used to calculate $T_{\rm eff}$ for the 19 non-Blazhko stars. These are given in Column 2 of Table 6 (under 'S06'). Since the *Kepler* RR Lyr stars have redder colours than the recommended range of applicability of the S06 equation $T_{\rm eff}$ values also were calculated using equation (11) of KW01. For $[\alpha/{\rm Fe}] = 0$ the metallicity term $[{\rm M/H}]_{\rm CG}$ is equal to $[{\rm Fe/H}]_{\rm CG}$ and we can write

$$\log T_{\rm eff} = 3.8840 - 0.3219\,(B-V)_0 + 0.0167\log g + 0.0070\,[{\rm Fe/H}]_{\rm CG}, \quad (11)$$

which is valid over the colour range of the ab-type RR Lyr stars studied here. Estimates of $T_{\rm eff}$ based on this formula also are given in Table 6 (Column 2, under KW01). In general, the temperatures agree, with an average difference of only 20 K, and one could simply take the average for the best estimate; however, the KW01 temperatures are higher (lower) than the S06 temperatures for the metal-poor (metal-rich) stars. We shall see below that there is reason to believe that the KW01 formula is to be preferred (see Section 6.9, and in particular the bottom left panel of Fig. 13).

Castellani et al.(1998, table 7) found $T_{\rm eff} \sim 6700$ K for AW Dra, assuming fundamental mode pulsation, mass $\sim$0.65–0.75 $\mathcal{M}_\odot$ and luminosity $\sim$65–80 $L_\odot$. This temperature is $\sim$400 K hotter than the corresponding Fourier-based estimate of $T_{\rm eff} \sim 6300$ K. The difference is not surprising given that their assumed mass and luminosity are higher than the Fourier-based values.

6.4 Absolute magnitudes

Following on from the Jurcsik & Kovács (1996) and Kovács & Jurcsik (1996, 1997) papers, J98 gives an equation for absolute magnitude (based on V photometry) that depends on A_1 and ϕ^s_{31} (her equation 2). Application of our V–Kp offsets (equation 2) gives

$$M_V = 1.179 - 1.396\,P - 0.477\,A_1 + 0.103\,\phi^s_{31}, \quad (12)$$

where A_1 and ϕ^s_{31} are Fourier parameters derived from the Kp photometry. The resulting M_V values are given in Column 3 of Table 6 (under 'J98, eq2').

The Fernley et al. (1998) equation relating M_V and metallicity,

$$M_V = (0.20 \pm 0.04)\,[{\rm Fe/H}]_{\rm CG} + (1.03 \pm 0.14), \quad (13)$$

assumes that RR Lyr has $M_V = 0.78(\pm 0.29)$ at $[{\rm Fe/H}]_{\rm CG} = -1.39$ dex and is consistent with the statistical parallax solution for 84 halo RR Lyr stars and with various Baade-Wesselink analyses. M_V values derived using this equation are listed in Column 3 of Table 6 (under 'F98, eq.2'). In general, the F98 and J98 values are similar, with a mean difference (J98 minus F98) of only 0.01 ($\pm$ 0.01) mag. On the downside there has been mounting evidence that the calibration of M_V with [Fe/H] is non-linear (see S06 and TSR8).

Equation (10) of Bono, Caputo & Di Criscienzo (2007) provides a third estimate of M_V. They show that over the entire metallicity range from $[{\rm Fe/H}]_{\rm ZW} = -2.5$ to 0.0 dex the Galactic field variables with Layden metallicities are described by

$$M_V = 1.19\,(\pm 0.10) + 0.50\,[{\rm Fe/H}]_{\rm ZW} + 0.09\,[{\rm Fe/H}]^2_{\rm ZW}. \quad (14)$$

Absolute magnitudes calculated with this quadratic formula are also given in Column 3 of Table 6 (under 'BCD7'). For the metal-poor stars the BCD7 M_V values are very similar to the F98 values; however, because of the non-linear metallicity dependence they are fainter than the F98 values for the four metal-rich stars.

Most recently, Catelan & Cortes (2008) argue that revised values for the trigonometric parallax and reddening of RR Lyr imply that the luminosity scale for RR Lyr stars should be brighter and give the following equation:

$$M_V = (0.23 \pm 0.04)\,[{\rm Fe/H}]_{\rm ZW} + (0.984 \pm 0.127). \quad (15)$$

Absolute magnitudes calculated with this equation (given in Column 3 of Table 6 under 'CC8') are, on average, $\sim$0.15 mag brighter than the values from F98 and BCD7, which in turn are $\sim$0.05 brighter than the J98 values. Note that these differences are smaller than the uncertainties in the individual M_V estimates (which are $\sim$0.20 mag). The colour–M_V diagram plotted in Fig. 12 (bottom-right panel) was constructed using the M_V values calculated with equation (2) of J98.

6.5 Distances

Approximate distances for the non-Blazhko RR Lyr stars are given in Column 9 of Table 5. These were computed assuming: (1) the Fernley et al. (1998) M_V values (which lie between the J98 and CC08 values); (2) the ASAS $\langle V\rangle$ values (given in Column 3 of Table 5) for the nine stars having ASAS V, I photometry, and for the other stars the $\langle Kp\rangle$-magnitudes brightened by 0.15 mag (the observed average V–Kp offset for FN Lyr and AW Dra); and (3) the visual extinctions given in Column 7 of Table 5. With uncertainties of $\sim$0.15 mag for M_V, $\sim$0.08 mag for the V–Kp offset, and $\sim$0.03 mag for A_V, these distances are quite uncertain. Taken at face value the nearest of the stars have distances $\sim$3 kpc, and the most distant star is V349 Lyr at $\sim$23 kpc. These estimates will be considerably improved when calibrated *BVRI* photometry becomes available.

6.6 Surface gravities

Mean surface gravities were calculated using equation (15) from J98, and equation (12) from KW99. The J98 formula, which is accurate to $\pm$ 0.004, depends only on the period and is given by

$$\log g = 2.473 - 1.226\log P. \quad (16)$$

The KW99 formula depends on period, mass and effective temperature:

$$\log g = 2.938 + 0.230\log\mathcal{M} - 0.110\log T_{\rm eff} - 1.219\log P. \quad (17)$$

Both estimates are given in Column 4 of Table 6 and the results are in good agreement.

6.7 Pulsational luminosities and masses

Following on from the basic equation of stellar pulsation given by the Ritter (1879) relation, $P\sqrt{\rho} = Q$ (where ρ is the mean density in cgs units and Q is the pulsation constant), van Albada & Baker (1971, 1973) derived an equation relating the pulsation period to mass, luminosity and $T_{\rm eff}$. When this equation and similar more recent equations that include a dependence on metal abundance are used to derive the mass and luminosity for an RR Lyr star such quantities are referred to as pulsational mass $\mathcal{M}$(puls) and pulsational luminosity L(puls). Both are expressed here in solar units.

Pulsational luminosities were calculated with two different formulae given by J98 and are reported in Column 5 of Table 6. In

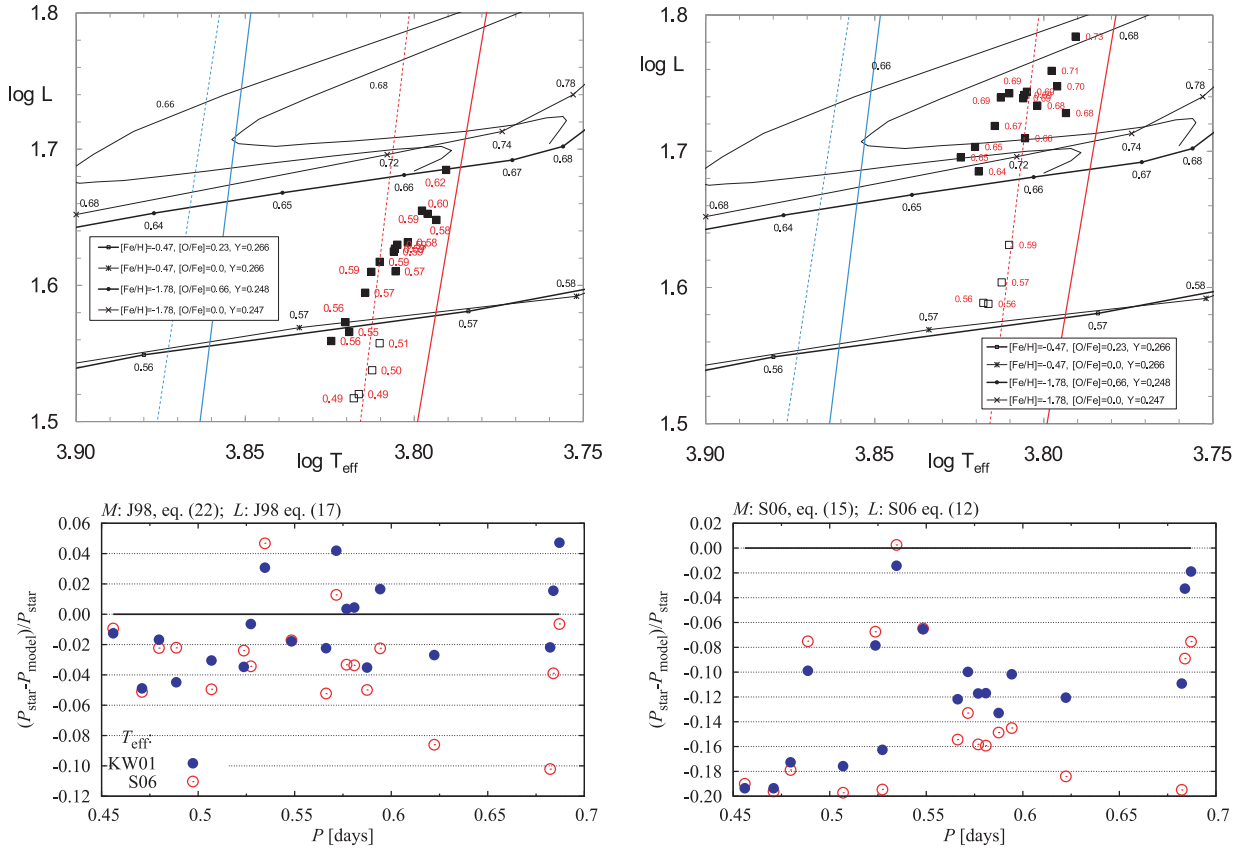

Figure 13. Top panels: HR-diagrams showing the locations of the *Kepler* non-Blazhko RR Lyr stars compared with two sets of HB models (low- and high-metallicity) from Dorman (1992). In both graphs the four metal-rich RR Lyr stars have been plotted with open squares and the metal-poor stars with filled squares; the black numbers next to the ZAHB symbols and the two evolutionary tracks are the assumed masses for the individual stellar evolution models. For the non-Blazhko RR Lyr stars in the top-left panel the L(puls) were calculated with equation (17) of J98 and labelled (in red) with the $\mathcal{M}$(puls) calculated with equation (22) of J98; in the top-right panel the L(evol) were calculated with equation (12) of S06 and labelled (in red) with the $\mathcal{M}$(evol) calculated with equation (15) of S06. Both panels (left and right) show the blue and red edges for the IS computed using the Warsaw pulsation code; the fundamental mode edges are plotted as solid lines, and first-overtone mode edges as dashed lines. Bottom panels: graphs comparing the observed pulsation periods and the pulsation periods derived with the Warsaw pulsation code. The assumed masses and luminosities are the values given in the top panels. For each star two points are plotted, computed assuming the $T_{\rm eff}$ from equation (11) of KW01 (blue dots) and from equation (18) of S06 (red circles). The best agreement is seen in the left-hand panel, with the KW01 temperatures favoured over the S06 values. In both panels, the largest differences are seen for the longest period stars, with no metallicity dependence.

the first case (her equation 16) the luminosity depends only on the metallicity:

$$\log L = 1.464 - 0.106\,[{\rm Fe/H}]_{\rm CG}. \qquad (18)$$

The second formula (her equation 17) also takes into account $T_{\rm eff}$:

$$\log L = 10.260 - 0.062\,[{\rm Fe/H}]_{\rm CG} - 2.294\,\log T_{\rm eff}. \qquad (19)$$

In both cases the lower metallicity stars have the higher luminosities. In the second equation the KW01 effective temperatures (Table 6, Column 2) were used for the calculations. With both equations one sees in the HR diagram two approximately parallel lines, one for the metal-rich stars and one for the metal-poor stars, each with the luminosity increasing as $T_{\rm eff}$ decreases (see the top-left panel of Fig. 13). At a given $T_{\rm eff}$ the luminosity difference between the metal-rich and metal-poor stars is greater with equation (16) than it is with equation (17).

Column 7 of Table 6 contains $\mathcal{M}$(puls) values computed using equations (14) and (22) of J98. The former is given by

$$\log\mathcal{M} = 1.477\,\log L - 1.754\,\log P - 6.272\,\log T_{\rm eff} + 0.037\,[{\rm Fe/H}]_{\rm CG} + 20.884, \qquad (20)$$

and the latter by

$$\log\mathcal{M} = -0.328 - 0.062\,[{\rm Fe/H}]_{\rm CG}. \qquad (21)$$

In both cases the adopted [Fe/H] values given in Table 4 (transformed to the CG system) were used, and in the first equation we used the $\log L$ from J98 equation (17) and the $\log T_{\rm eff}$ from equation (11) of KW01. The average mass for the four metal-rich stars is $\sim$0.50 $\mathcal{M}_{\odot}$ compared with the average mass for the metal-poor stars of $\sim$0.60 $\mathcal{M}_{\odot}$.

6.8 L and $\mathcal{M}$ from stellar evolution models

A ZAHB stellar evolution model takes as its input the mass, $\mathcal{M}$(evol), and chemical composition (X, Y, Z). A subsequent evolutionary track for a given mass and composition gives the luminosity L(evol) and effective temperature as a function of time. Examples of such models are those by Dorman (1992), Bono et al. (1997) and VandenBerg et al. (2000). Based on three different sets of stellar evolution models S6 gives formulae for L(evol) as a function of [Fe/H]. His equation (8), which follows from the models of Caputo

et al. (2000), is given by

$$\log L = 1.245 - 0.451\,[\mathrm{Fe/H}] - 0.097\,[\mathrm{Fe/H}]^2. \quad (22)$$

His equation (10), which is based on the alpha-enhanced ZAHB models of Catelan, Pritzl & Smith (2004), is given by

$$\log L = 1.404 - 0.243\,[\mathrm{Fe/H}] - 0.043\,[\mathrm{Fe/H}]^2. \quad (23)$$

Both of these equations, like the BCD7 absolute magnitude formula discussed above, assume a quadratic dependence on [Fe/H]. This is not the case for equation (12) which is derived from the models of Clementini et al. (2003) and is given by

$$\log L = 1.538 - 1.110\,[\mathrm{Fe/H}]. \quad (24)$$

Luminosities computed with these three formulae are given in Column 6 of Table 6. For the metal-poor stars all three L(evol) are systematically larger than the L(puls) values given in Column 5. For the four metal-rich stars the agreement is better but there is a wide range of L(evol) owing to the linear or non-linear [Fe/H] dependencies. Regardless of which formula was used the most luminous stars have the lowest metallicities and there is internal consistency (as was the case for the J98 luminosities). It is not clear whether the L(puls) or L(evol) are correct. Further comparison of the derived luminosities is given in Section 6.9 (after masses are discussed).

A mass equation with $\mathcal{M}$ varying linearly with [Fe/H] is also given by S06 (his equation 15):

$$\log \mathcal{M} = -0.283 - 0.066\,[\mathrm{Fe/H}]_{\mathrm{ZW}}. \quad (25)$$

Since this equation was derived from the Bono et al. (1997) HB models it gives evolutionary masses. The $\mathcal{M}$(evol) derived with this equation are given in Column 8 of Table 6. A more recent mass formula by BCD7, their equation (7), which is based on the Pietrinferni et al. (2004,2006) HB models, is given by

$$\log \mathcal{M} = -0.2675 - 0.063\,[\mathrm{Fe/H}]. \quad (26)$$

This formula is very similar to the S06 equation. The masses computed with this formula are given in Column 8 of Table 6 and are seen to agree to within 0.01 $\mathcal{M}_\odot$ with the S06 masses. As was the case for the luminosities, the $\mathcal{M}$(evol) are all larger than the corresponding $\mathcal{M}$(puls) values.

6.9 Comparison with evolutionary models

Having computed $\mathcal{M}$, L and T_{eff} values for the non-Blazhko RR Lyr stars from observed Fourier parameters using equations that derive from both pulsation and stellar evolution theory it is of interest to compare the results with the locations of model ZAHBs and evolutionary tracks.

The top two panels of Fig. 13 show HR diagrams with $\log T_{\mathrm{eff}}$ as abscissa and $\log L$ as ordinate, and two sets of ZAHB loci from Dorman (1992) computed for different masses along the ZAHB. The more luminous HB assumes [Fe/H] = −1.78 dex, and the less luminous branch [Fe/H] = −0.47 dex. The numbers next to the symbols are the masses for the individual models, which are seen to be higher for the low-[Fe/H] tracks than for the high-[Fe/H] tracks. For both assumed metallicities oxygen-enhanced and non-enhanced ZAHBs have been plotted – the effect of increasing the oxygen to iron ratio from [O/Fe] = 0 to 0.66 for the low-metallicity ZAHBs is to lower the luminosity and reduce the mass at a given temperature. For the high-metallicity tracks an oxygen enhancement from [O/Fe] = 0 to 0.23 has little effect on the derived L or $\mathcal{M}$. Also plotted in the low-[Fe/H] case are the evolutionary paths away from the ZAHB for two masses, 0.66 and 0.68 $\mathcal{M}_\odot$. In both panels the non-Blazhko RR Lyr stars with low metallicities are represented by large black squares, the four high-metallicity stars are plotted with open squares, and the T_{eff} are the average of the KW01 and S06 values (Column 2 of Table 6).

In the top-left panel of Fig. 13 the luminosities and masses (labelled in red) of the *Kepler* RR Lyr stars were calculated with equations (17) and (22) of J98 and thus are based on pulsation theory. The L(puls) and $\mathcal{M}$(puls) are seen to be systematically smaller than values derived from the ZAHB tracks (for the appropriate metal abundance). The reddest non-Blazhko RR Lyr stars lie close to the fundamental mode red-edge and have the smallest amplitudes. This graph also shows blue and red edges of the IS for the fundamental mode (red and blue solid lines) and first-overtone mode (red and blue dashed lines). The edges were calculated with the Warsaw pulsation code (see Section 7) assuming a mass of 0.65 $\mathcal{M}_\odot$. The *Kepler* non-Blazhko stars all lie in the fundamental mode region of the variability strip, and the smallest amplitude RR Lyr stars (the four metal-rich stars, KIC 7030715 and NR Lyr) have locations near the fundamental red edge (FRE) of the IS. As expected, all the stars near the FRE have low R_{31} values.

In the top-right panel of Fig. 13 the luminosities were calculated with equation (12) of S06, and the masses (labelled in red) with equation (15) of S06; thus they are evolutionary L and $\mathcal{M}$ values. In this case there is very good agreement with the stellar evolution models, as one expects since they are based on stellar evolution models. Enhancing the oxygen to iron ratio by the plotted amounts makes little difference.

It is unclear which are correct, the L(puls) and $\mathcal{M}$(puls), or the L(evol) and $\mathcal{M}$(evol)? The mass and luminosity discrepancies go in the same direction as seen for Cepheids. Pietrzynski et al. (2010) recently derived a dynamical mass $\mathcal{M}$(dynam) for a classical Cepheid in a well-detached, double-lined eclipsing binary in the LMC. The mass they derive is very accurate and favours $\mathcal{M}$(puls). The reason for the discrepancies may be the same, as suggested by Pietrzynski et al. – not enough mass loss has been taken into account in the evolution models. For further guidance on these questions we turn to pulsation models.

7 HYDRODYNAMIC MODELS

Smolec & Moskalik (2008) recently have developed the Warsaw convective pulsation programs for studying stellar pulsation. The codes, both linear and non-linear, are one dimensional and use a single equation to describe the generation of turbulent energy; this is done according to the model proposed by Kuhfuß (1986, see also Wuchterl & Feuchtinger 1998). Even though a simple diffusion approximation is used to describe the radiation field the models are able to reproduce quite well the dynamics of RR Lyrae pulsations.

The most recent application of these programs (Smolec et al. 2011) has been to construct hydrodynamic models for the purpose of testing Stothers' (2006) proposed explanation of the Blazhko phenomenon that is observed in about half of all RR Lyr stars. In these models the strength of the turbulent convection was modulated and the resulting models were compared in detail with the Fourier descriptions of the *Kepler* observations of the RR Lyr stars (Kolenberg et al. 2011).

The initial unmodulated models of the Smolec et al. (2011) study are also applicable for the non-Blazhko stars considered here. The predicted bolometric light curves were transformed to V-band light curves by applying to each pulsation phase a bolometric correction derived from Kurucz (2005).

7.1 Pulsational or evolutionary L, $\mathcal{M}$?

As a check on the luminosities and masses derived from stellar pulsation theory and from the HB models the Warsaw pulsation code was used to calculate pulsation periods. Such periods are very robust and depend very weakly on the assumed convective parameters. The calculations assumed the metallicities given in Table 4, the L(puls) and $\mathcal{M}$(puls) values (calculated with the J98 equations) given in the top-left panel of Fig. 13, and the L(evol) and $\mathcal{M}$(evol) values (from the S06 equations) given in the top-right panel of Fig. 13. The results, summarized in 'per cent difference' diagrams comparing the observed pulsation periods and the model pulsation periods, are shown in the bottom panels of Fig. 13. Because the assumed effective temperatures are important, in both panels two points are plotted for each star, one computed assuming the $T_{\rm eff}$ from equation (11) of KW01 (blue dots), and the other assuming the $T_{\rm eff}$ from equation (18) of S06 (red circles). For the pulsational values (left-hand panel) the best formulae seem to be those in J98, and the KW01 temperatures (blue dots) seem to be preferred over the S06 temperatures (red circles) – in this case the observed and calculated periods always agree to within 5 per cent and ∼half the stars are within 2 per cent. On the other hand, the L and $\mathcal{M}$ values from the stellar evolution models (right-hand panel) result in model periods systematically too large by as much as 20 per cent, with almost no agreement. In both panels the largest differences between the KW01 and S06 temperatures are seen for the longest period stars. The four metal-rich stars all have periods shorter than 0.55 d and there is no systematic metallicity dependence.

7.2 Predicted Fourier parameters

Three sets of models were computed with the Warsaw code, varying L while holding the other variables constant, then $\mathcal{M}$, then [Fe/H]. The resulting Fourier parameters were plotted in diagrams such as those found in Figs 2 and 6–8. In Fig. 14 the luminosity was varied ($\rm L/L_\odot = 40$, 50, 60) while the metallicity was held constant at [Fe/H] $= -1.30$ dex ($Z = 0.001$) with the hydrogen fraction fixed at $X = 0.76$. Two masses were considered, $\mathcal{M}/\mathcal{M}_\odot = 0.65$ (solid lines) and 0.55 (dashed lines). In Fig. 15 the metallicity was varied from [Fe/H] $= -0.24$ dex ($Z = 0.01$), to -1.24 dex ($Z = 0.001$), to -1.93 dex ($Z = 0.0002$)[9] while keeping the other variables constant at $L/L_\odot = 50$, $\mathcal{M}/\mathcal{M}_\odot = 0.65$ and $X = 0.76$.

The A_1 versus $A_{\rm tot}$ diagrams (top-left panels of Figs. 14–15) show very good agreement with the estimates for the non-Blazhko stars (right-hand panel of Fig. 2). The approximately linear trend seems to be independent of luminosity or mass or metallicity variations. However, the fit is not exact and the observed non-linearities (which are small) appear to go in opposite directions to the model predictions.

The ϕ^s_{21} versus A_1 graphs (middle-left panels of Figs 14–15) appear to be quite sensitive to L, $\mathcal{M}$ and metallicity effects (see the lower left panels of Figs 6–7). A star of given mass and composition will move up and to the right as its luminosity increases. Alternatively, a star of given L and composition will move up and to the right if the mass decreases. Moreover, if L, $\mathcal{M}$ and X are kept constant metal-rich stars ought to occupy the high A_1, high ϕ_{21} region of the diagram.

[9] When transforming between Z and [Fe/H] we used [Fe/H] $= \log Z - \log Z_\odot = \log Z + 1.765$, where the solar metallicity was assumed to be $Z_\odot = 0.017\,16$ (Sweigart & Catelan 1998).

To attempt an application, consider the stars AW Dra and V784 Cyg, both of which are seen in Fig. 6 with higher than average ϕ^s_{21} values at a given A_1. If the models are indicative, then the two stars with the largest luminosities might be expected to be AW Dra and V784 Cyg. According to Column 5 of Table 6 AW Dra is one of the most luminous stars in the sample, but V784 Cyg is not – it has one of the lowest luminosities. On the other hand, V784 Cyg is one of the four metal-rich stars, suspected of having low L and low mass. The high location in Fig. 6 of V784 Cyg (and the other high metallicity stars) might be explained by its low mass, whereas the location of AW Dra would seem to be due primarily to its high luminosity (either as a low-[Fe/H] star near the ZAHB or as a more metal rich star in an advanced evolutionary state). The highest L (and highest $\mathcal{M}$) star in the sample, NR Lyr (see Table 6), also has the lowest metallicity (see Table 4), even lower than that of AW Dra; for it the lower [Fe/H] would seem to cancel out the higher L, thus explaining its smaller amplitude and smaller ϕ_{21} than AW Dra.

The top-right and middle-right diagrams of Figs 14–15 are somewhat noisy. The top-right panel of Fig. 14 suggests that the lowest L stars have the smallest R_{21} values (note that the scale matches that shown in the upper-right panel of Fig. 6, but is much reduced from that shown in Fig. 7 for GC stars). Basically, R_{21} and R_{31} have to be small very close to the red edge of the IS. At the red edge the amplitude goes to zero, as do R_{21} and R_{31}. The middle-right panels of Fig. 14 suggest that the lowest-L stars are not expected to have high ϕ_{21} values. This is to be compared with the *Kepler* data shown in the lower-right panel of Fig. 6 that suggest that there is a nearly linear relationship between ϕ_{21} and ϕ_{31} – this is not seen in the models.

The bottom-left panels of Figs 14–15 show that at a given ϕ_{31} a shift to the right can be caused by a luminosity increase or a higher mass. The bottom-left panel of Fig. 14 shows the traditional result that at a given ϕ_{31} metallicity decreases as period increases; but it also seems to be suggesting that at a given period ϕ_{31} increases with decreasing metallicity.

Finally, the bottom-right panel in Fig. 14 shows that at a given $A_{\rm tot}$ and metal abundance stars of higher L for a given mass, or of lower mass for a given L, have longer periods; this is as expected, and similar results are seen in fig. 6 of Dall'Ora et al. (2003). The bottom-right panel of Fig. 14 shows that for a given L and $\mathcal{M}$ varying the metallicity has a relatively small effect on the period. Taken together these two panels suggest that the main factor shifting the periods to longer values in the Bailey diagram (or any of its surrogate diagrams – see Fig. 9) seems to be higher luminosities (which can be caused either by higher ZAHB mass or by advanced HB evolution) and not lower metallicities.

Obviously more work needs to be done to optimize the estimation of the physical variables in these observational planes, but the potential seems high.

8 SUMMARY

The main results of this paper are as follows.

(1) Fourier decomposition has been performed on the 19 least modulated ab-type RR Lyr stars observed with the *Kepler* space telescope at LC (every 30 min) and SC (every 1 min) during the first 417 d of its operation (Q0–Q5).

(2) While none of the RRab stars shows the recently discovered 'period-doubling' effect seen in Blazhko variables, the star KIC 7021124 was discovered to pulsate in the fundamental and second

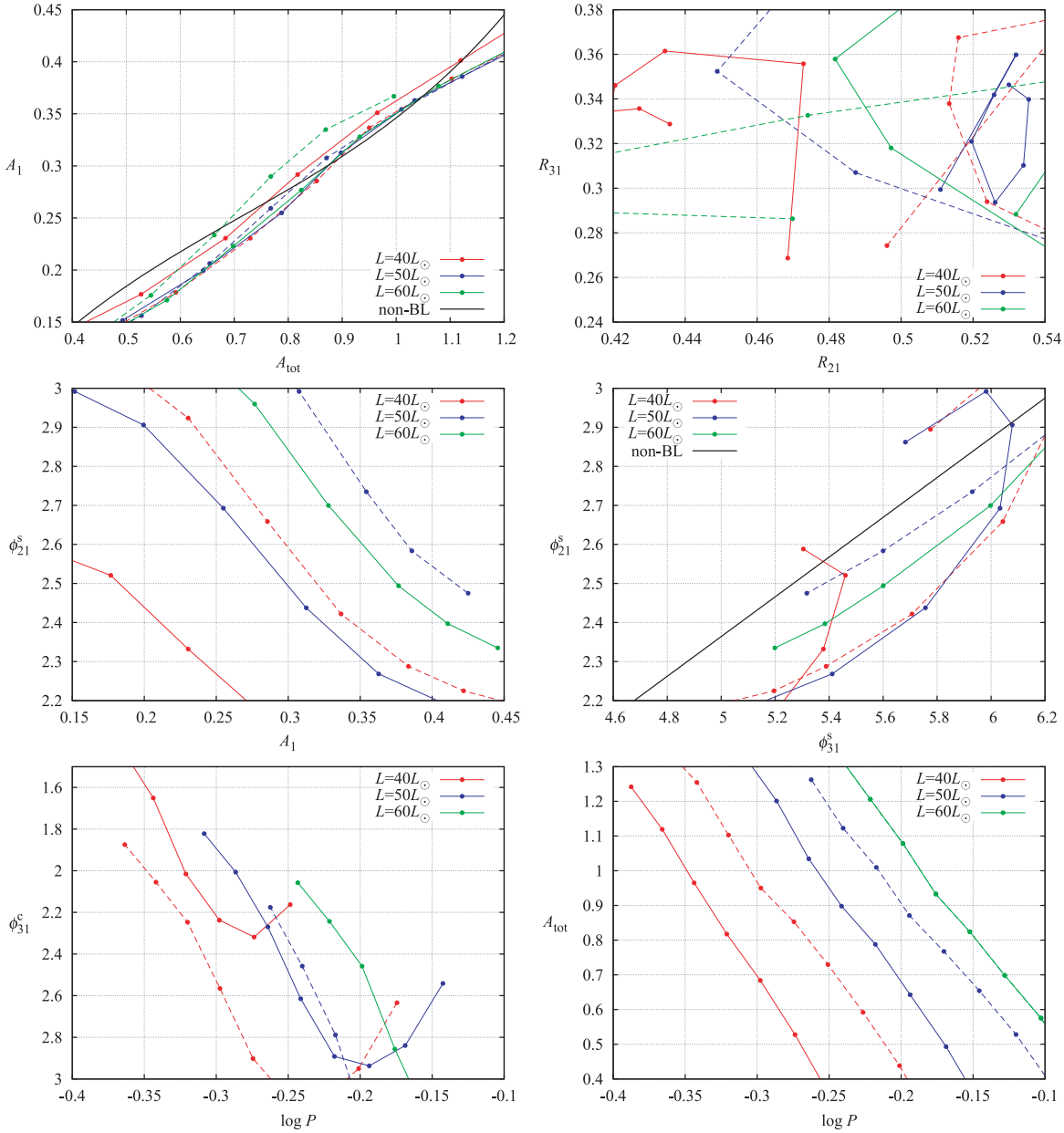

Figure 14. Graphs showing the effect on the pulsation-model Fourier parameters of varying the L, and varying $\mathcal{M}$, while keeping the composition constant at $(X, Z) = (0.76, 0.001)$, i.e. [Fe/H] $= -1.2$ dex. The different colours represent luminosities 40, 50 and 60 $L_\odot$. The solid lines are for $\mathcal{M} = 0.65\mathcal{M}_\odot$ and the dashed lines are for $\mathcal{M} = 0.55\mathcal{M}_\odot$. All ordinates are for the V passband.

overtone modes with a period ratio $P_2/P_0 = 0.593\,05$ and to have properties similar to those of V350 Lyr.

(3) Period change rates and improved periods have been derived from O − C diagrams for several of the stars that have historical data. For AW Dra, data from the last 12 years suggest that its period is increasing at the rate $\mathrm{d}P/\mathrm{d}t = 3.79\,\mathrm{d\,Myr^{-1}}$, while data spanning the last 100 years suggest a slower rate, $\mathrm{d}P/\mathrm{d}t = 0.32\,\mathrm{d\,Myr^{-1}}$. FN Lyr appears to have a very slowly increasing period, and the periods of NR Lyr and NQ Lyr appear to be constant.

(4) Because the differences between the *Kp* and *V* Fourier parameters for three stars (AW Dra, FN Lyr an NR Lyr) are found to be small and systematically different we were able to use extant *V*-band correlations (with small modifications) to derive underlying physical characteristics for the *Kepler* stars. This procedure seems to be validated through comparisons of the *Kepler* stars with other Galactic and LMC field RR Lyr stars and with RR Lyr stars in Galactic and LMC GCs.

(5) Preliminary metal abundances have been derived for all the non-Blazhko RR Lyr stars. 13 of the stars appear to be similar to those found in intermediate metallicity globular clusters (i.e. $[\mathrm{Fe/H}]_{\mathrm{C9}} \sim -1.6$ dex); the most metal-deficient star appears to be NR Lyr with $[\mathrm{Fe/H}]_{\mathrm{C9}} = -2.3$ dex, and the four lowest amplitude stars (KIC 6100702, KIC 9947026, V782 Cyg and V784 Cyg) appear to be metal-rich with $[\mathrm{Fe/H}]_{\mathrm{C9}}$ between -0.55 and $+0.07$ dex.

(6) In general, the luminosities of the metal-rich RR Lyr stars are found to be lower than those of the metal-poor stars; however, the luminosities derived from stellar evolution models are systematically higher than those derived from stellar pulsation models. It is not clear which are correct.

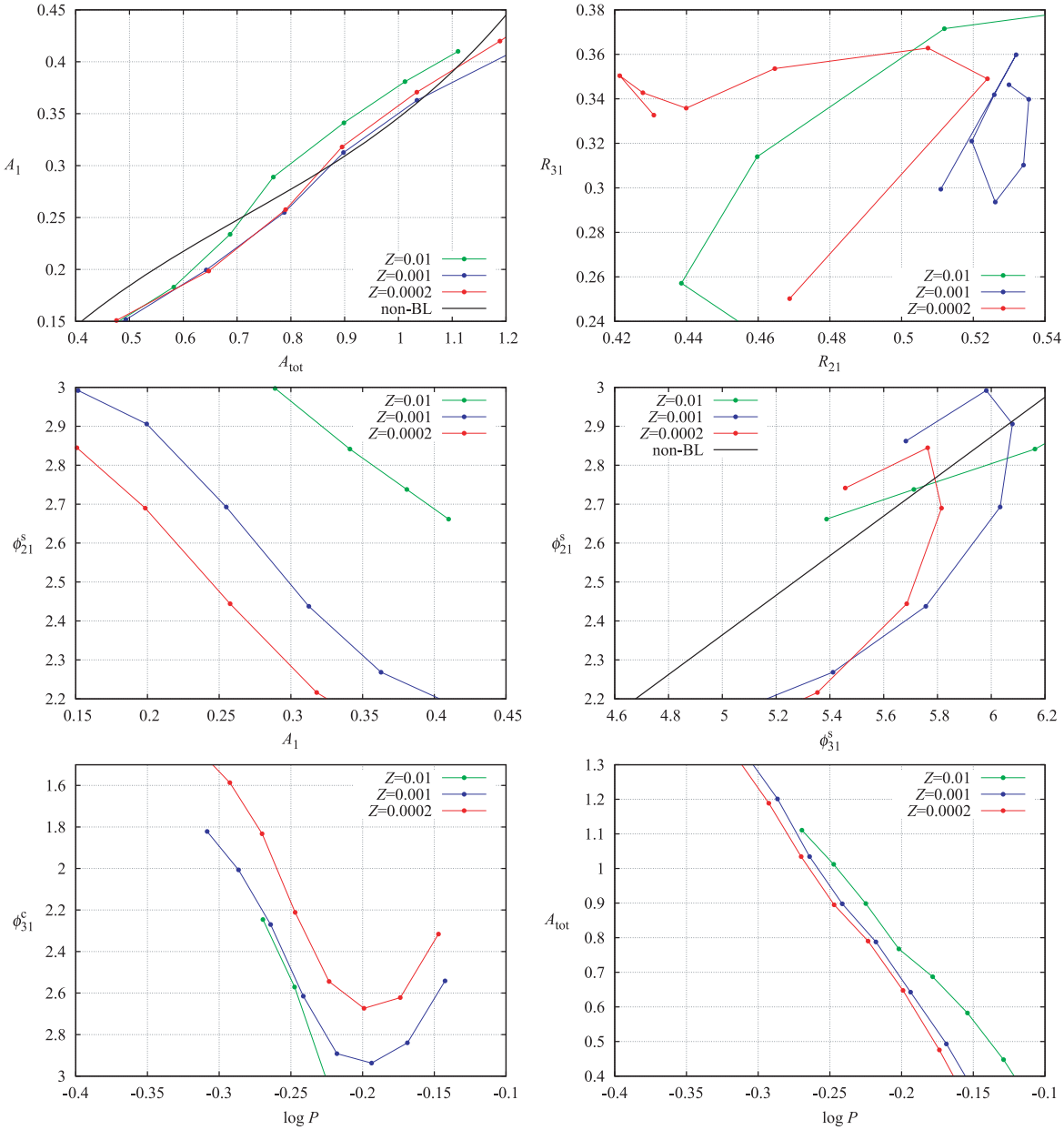

Figure 15. Graphs showing the effect on the Fourier parameters derived with the Warsaw convective pulsation code of varying [Fe/H] from −0.24 dex ($Z = 0.01$, green), to −1.24 dex ($Z = 0.001$, blue), to −1.93 dex ($Z = 0.0002$, red), while keeping the mass, luminosity and hydrogen content constant at $0.65\mathcal{M}_{\odot}$, 50 $L_{\odot}$ and $X = 0.76$. All ordinates are for the V passband.

(7) The three stars with the longest periods, AW Dra, NR Lyr and KIC 7030715 (all with periods ∼0.68 d), also are the reddest and coolest stars. We suspect that AW Dra may be in an evolved state. In general, the stars with the lowest amplitudes are found to be located nearest the red edge of the IS.

(8) The mass range for the entire sample (approximate) is from 0.50 to 0.65 $\mathcal{M}_{\odot}$ if based on pulsation theory, or from 0.56 to 0.72 if based on HB evolution models.

(9) Finally, the Fourier parameters of the stars have been compared with values newly computed with the Warsaw convective pulsation codes. We find that in the *P–A* diagram varying the metallicity for a given L and $\mathcal{M}$ has a relatively small effect on the period-shift at a given amplitude (in fact, the small shift is towards shorter periods for more metal poor stars), and that the main factors causing the period shifts must be L and $\mathcal{M}$.

ACKNOWLEDGMENTS

Funding for this Discovery mission is provided by NASA's Science Mission Directorate. The authors acknowledge the entire *Kepler* team, whose outstanding efforts have made these results possible. JMN gratefully acknowledges Dr. Amanda F. Linnell Nemec (International Statistics & Research Corporation) for a critical reading of the paper, and the Camosun College Faculty Association for funding his attendance at the 3rd KASC Workshop held in Aarhus, Denmark, in 2010 June; he also thanks Dr. Geza Kovács for his software and discussions on Fourier methods, and Dr. Dorota Szczygiel for discussions on the ASAS data. Also, we thank Dr. K. Mighell for sending us his Guest Observer LC:Q2–Q4 data for FN Lyr, and the anonymous referee for a very thoughtful, knowledgeable and helpful report. KK, EG and RSm acknowledge support from the Austrian Fonds zur Förderung der wissenschaftlichen Forschung,

project numbers AP 21205-N16 (RSm), T359-N16 and P19962 (KK and EG). RSz and JB are supported by the Lendület program of the Hungarian Academy of Sciences (HAS) and OTKA Grants K76816 and K83790 and MB08C 81013. RSz acknowledges support of the János Bolyai Research Scholarship of the HAS. The research leading to these results has received funding from the European Community's Seventh Framework Programme (FP7/2007-2013) under grant agreement no. 269194. Finally, as this paper was nearing completion we learned of the death of Dr. Allan Sandage – this paper is dedicated to his memory.

REFERENCES

Alcock C. et al., 2000, ApJ, 542, 257
Alves D. R., Bond H. E., Onken C., 2001, AJ, 121, 318
Arp H. C., 1955, AJ, 60, 317
Baranowski R. et al., 2009, MNRAS, 396, 2194
Benkő J. M. et al., 2010, MNRAS, 409, 1585 (B10)
Blazhko S., 1907, Astron. Nachr., 175, 325
Bono G., Caputo F., Cassisi S., Incerpi R., Marconi M., 1997, ApJ, 483, 811
Bono G., Castellani V., Marconi M., 2000, ApJ, 532, L129
Bono G., Caputo F., Di Criscienzo M., 2007, A&A, 476, 779 (BCD7)
Bookmeyer B. B., Fitch W. S., Lee T. A., Wisiewski W. Z., Johnson H. L., 1977, Rev. Mex. Astron. Astrofis., 2, 235
Burstein D., Heiles C., 1982, AJ, 87, 1165
Busso G. et al., 2007, A&A, 474, 105
Cacciari C., Corwin T. M., Carney B. W., 2005, AJ, 129, 267 (CCC5)
Caputo F., Castellani V., Marconi M., Ripepi V., 2000, MNRAS, 316, 819
Cardelli J. A., Clayton G. C., Mathis J. S., 1989, ApJ, 345, 245
Carney B. W., Storm J., Jones R. V., 1992, ApJ 386, 663
Carretta E., Gratton R. G., 1997, A&AS, 121, 95 (CG)
Carretta E., Bragaglia A., Gratton R., D'Orazi V., Lucatello S., 2009, A&A, 508, 695 (C9)
Cassisi S., Castellani M., Caputo F., Castellani V., 2004, A&A, 426, 641
Castellani V., Di Paolantonio A., Piersimoni A. M., Ripepi V., 1998, A&A, 333, 918
Catelan M., 2004, ApJ, 600, 409
Catelan M., 2009, Ap&SS, 320, 261
Catelan M., Pritzl, B., Smith H. A., 2004, ApJS, 76, 633
Catelan M., Stetson P. B., Pritzl B. J., Smith H. A., Kinemuchi K., Layden A. C., Sweigart A. V., Rich R. M., 2006, ApJ, 651, L133
Catelan M., Cortes C., 2008, ApJ, 676, L135
Christy R. F., 1966, ApJ, 144, 108
Clement C. M., Shelton I., 1999, ApJ, 515, L85
Clementini G., Gratton R., Bragaglia A., Carretta E., Di Fabrizio L., Maio M., 2003, AJ, 125, 1309
Dall'Ora M. et al., 2003, AJ, 126, 197
Demarque P., Zinn R., Lee Y.-W., Yi S., 2000, AJ, 119, 1398 (D00)
Di Criscienzo M., Marconi M., Caputo F., 2004, ApJ, 612, 1092
Dorman B., 1992, ApJS, 81, 221
Dotter A., Chaboyer B., Jevremovic D., Baron E., Ferguson J. W., Sarajedini A., Anderson J., 2007, ApJ, 666, 403
Dotter A. et al., 2010, ApJ, 708, 698
Faulkner J., 1966, ApJ, 144, 978
Faulkner J., Iben I., Jr, 1966, ApJ, 144, 995
Fernley J., Barnes T. G., Skillen I., Hawley S. L., Hanley C. J., Evans D. W., Solano E., Garrido R., 1998, A&A, 330, 515
Gilliland R. L. et al., 2010, ApJ, 713, L160
Harris W. E., 1996, AJ, 112, 1487
Hartwick F. D. A., 1968, ApJ, 154, 475
Hartwick F. D. A., Härm R., Schwarzschild M., 1968, ApJ, 151, 389
Iben I., Jr, 1971, PASP, 83, 697
Iben I., Jr, Faulkner J., 1968, ApJ, 153, 101
Iben I., Jr, Road R. T., 1970, ApJ, 161, 587
Jenkins J. M. et al., 2010a, ApJ, 713, L87
Jenkins J. M. et al., 2010b, ApJ, 713, L120
Jurcsik J., 1995, Acta Astron., 45, 653
Jurcsik J., 1998, A&A, 333, 571 (J98)
Jurcsik J., Kovács G., 1995, in Stobie R. S., Whitelock P. A., eds, ASP Conf. Ser. Vol. 83, Astrophys. App. of Stell. Pulsa., IAU Colloquium 155. Astron. Soc. Pac., San Francisco, p. 385
Jurcsik J., Kovács G., 1996, A&A, 312, 111
Jurcsik J., Benkö J. M., Bakos G. Á., Szeidl B., Szabó R., 2003, ApJ, 597, L49 (J03)
Jurcsik J. et al., 2009, MNRAS, 400, 1006
Kaluzny J., Hilditch R. W., Clement C., Rucinski S. M., 1998, MNRAS, 296, 347
Kaluzny J., Olech A., Thompson I., Pych W., Krzeminski W., Schwarzenberg-Czerny A., 2000, A&A, 143, 215
Koch D. G. et al., 2010, ApJ, 713, L79
Kolenberg K. et al., 2010, ApJ, 713, L198
Kolenberg K. et al., 2011, MNRAS, 411, 878
Kolláth Z., Molnar L., Szábo R., 2011, MNRAS, 414, 1111
Kovács G., 2005, A&A, 438, 227
Kovács G., Jurcsik J., 1996, ApJ, 466, L17 (KJ96)
Kovács G., Jurcsik J., 1997, A&A, 322, 218 (KJ97)
Kovács G., Kanbur S. M., 1998, MNRAS, 295, 834
Kovács G., Kupi G., 2007, A&A, 462, 1007
Kovács G., Walker A. R., 1999, ApJ, 512, 271
Kovács G., Walker A. R., 2001, A&A, 371, 589 (KW01)
Kovács G., Zsoldos E., 1995, A&A, 293, L57
Kraft R. P., Ivans I. I., 2003, PASP, 115, 143
Kuhfuß R., 1986, A&A, 160, 116
Kunder A., Chaboyer B., 2009, AJ, 138, 1284
Kunder A. et al., 2011, AJ, 141, 15
Kurucz R. L., 2005, http://kurucz.harvard.edu/
Layden A., 1994, AJ, 108, 1016
Le Borgne J. F. et al., 2007, A&A, 476, 307
Lee J.-W., Carney B. W., 1999, AJ, 118, 1373
Lee Y.-W., 1989, PhD thesis, Yale University
Lee Y.-W., 1990, ApJ, 363, 159
Lee Y.-W., Demarque P., Zinn R., 1990, ApJ, 350, 155 (LDZ90)
Lee Y.-W., Demarque P., Zinn R., 1994, ApJ, 423, 248 (LDZ94)
Lee Y.-W., Yoon S.-J., Lee H.-C., Woo J.-H., 1999, in Hubeny I., Heap S. R., Cornett R. H., eds, ASP Conf. Ser. Vol. 192, Spectrophotom. Dating of Stars and Galaxies. Astron. Soc. Pac., San Francisco, p. 185
Lee Y.-W., Gim H. B., Casetti-Dinescu D. I., 2007, ApJ, 661, L49
Lenz P., Breger M., 2005, Commun. Asteroseis., 146, 53
Marconi M., Clementini G., 2005, AJ, 129, 2257
Marconi M., Caputo M., Di Criscienzo M., Castellani M., 2003, ApJ, 596, 299
Marconi M., Degl'Innocenti S., 2007, A&A, 474, 557
Miller W. J. (S. J.), 1953, Ricerche Astron., 3, 1
Miller W. J. (S. J.), 1956, Ricerche Astron., 3, 381
Morgan S. M., Simet M., Bargenquast S., 1998, Acta Astron., 48, 341
Nemec A. F. L., Nemec J. M., 1985, AJ, 90, 2317
Nemec J. M., 2004, AJ, 127, 2185
Nemec J. M., Walker A. R., Jeon Y.-B., 2009, AJ, 138, 1310
Oosterhoff P. Th., 1939, Observatory, 62, 104
Oosterhoff P. Th., 1944, Bull. of the Astron. Inst. of the Neth., 10, 55
Pietrinferni A., Cassisi S., Salaris M., Castelli F., 2004, ApJ, 612, 168
Pietrinferni A., Cassisi S., Salaris M., Castelli F., 2006, ApJ, 642, 797
Pietrinferni A., Cassisi S., Salaris M., Percival S., Ferguson J. W., 2009, ApJ, 697, 275
Pietrzynski G. et al., 2010, Nat, 468, 542
Pigulski A., Pojmanski G., Pilecki B., Szczygiel D. M., 2009, Acta Astron., 59, 33
Preston G. W., 1959, ApJ, 130, 507
Pritzl B., Smith H. A., Catelan M., Sweigart A. V., 2000, ApJ, 530, L41
Pritzl B., Smith H. A., Catelan M., Sweigart A. V., 2001, AJ, 122, 2600
Pritzl B., Smith H. A., Catelan M., Sweigart A. V., 2002, AJ, 124, 949
Renzini A., 1983, Mem. S.A.It., 54, 335
Rey S.-C., Yoon S.-J., Lee Y.-W., Chaboyer B., Sarajedini A., 2001, AJ, 122, 3219

Ritter A., 1879, Ann. der Phys, 244, 157
Roederer I. U., Sneden C., 2011, AJ, 142, 22
Rood R. T., Iben I., Jr, 1968, ApJ, 154, 215
Sandage A. R., 1958, in O'Connell D., ed., Stellar Populations. Ricerche Astr. Specola Vaticana, Vol. 5, p. 41
Sandage A., 1981a, ApJ, 244, L23 (S81a)
Sandage A., 1981b, ApJ, 248, 161 (S81b)
Sandage A., 1990, ApJ, 350, 603 (S90)
Sandage A., 1993, AJ, 106, 687 (S93)
Sandage A., 2004, AJ, 128, 858 (S04)
Sandage A., 2006, AJ, 131, 1750 (S06)
Sandage A., 2010, ApJ, 722, 79 (S10)
Sandage A., Tammann G. A., 2006, ARA&A, 44, 93 (ST6)
Sandage A., Tammann G. A., 2008, ApJ, 686, 779 (ST8)
Sandage A. R., Wallerstein G., 1960, ApJ, 131, 598
Sandage A. R., Wildey R. L., 1967, ApJ, 150, 469
Sandage A., Katem B., Sandage M., 1981, ApJS, 46, 41 (SKS)
Sandquist E. L., Gordon M., Levine D., Bolte M., 2010, AJ, 139, 2374
Schlegel D. J., Finkbeiner D. P., Davis M., 1998, 500, 525
Simon N., 1988, ApJ, 328, 747
Simon N., Clement C., 1993, ApJ, 410, 526
Simon N., Lee A. S., 1981, ApJ, 248, 291
Simon N., Teays T. J., 1982, ApJ, 261, 586
Smith H. A., 1995, RR Lyrae Stars. Cambridge Univ. Press, Cambridge
Smolec R., Moskalik P., 2008, Acta Astron., 58, 193
Smolec R., Moskalik P., Kolenberg K., Bryson S., Cote M. T., Morris R. L., 2011, MNRAS, 414, 2950
Sobeck J. S. et al., 2011, AJ, 141, 175
Sodor A., Jurcsik J., Szeidl B., 2009, MNRAS, 394, 261
Soszynski I. et al., 2009, Acta Astron., 59, 1
Storm J., Nordstrom B., Carney B. W., Andersen J., 1994, A&A, 291, 121
Stothers R. B., 2006, ApJ, 652, 643
Sweigart A. V., Catelan M., 1998 ApJ, 501, L63
Sweigart A. V., Gross P. G., 1976, ApJS, 32, 367
Szabó R. et al., 2010, MNRAS, 409, 1244
Szczygiel D. M., Pojmanski G., Pilecki B., 2009, Acta Astron., 59, 137
Tammann G. A., Sandage A., Reindl B., 2008, ApJ, 679, 52 (TSR8)
Valcarce A. A. R., Catelan M., 2008, A&A, 487, 185
van Albada T. S., Baker N., 1971, ApJ, 169, 311
van Albada T. S., Baker N., 1973, ApJ, 185, 477
van den Bergh S., 1967, PASP, 79, 460
VandenBerg D. A., Swenson F. J., Rogers F. J., Iglesias C. A., Alexander D. R., 2000, ApJ, 532, 430
Walker A. R. et al., 2011, MNRAS, 415, 643
Wuchterl G., Feuchtinger M. U., 1998, A&A, 340, 419
Zinn R., West M. J., 1984, ApJS, 55, 45 (ZW)

APPENDIX A: KIC 7021124

During the course of our analyses the star KIC 7021124 was discovered to be a doubly periodic RR Lyr star, similar to V350 Lyr (see B10). From an analysis of the Q1 data (1626 LC observations made over a 30-d period) its period was found to be $P_0 = 0.622\,4925(7)$ d, corresponding to the frequency $f_0 = 1.606\,445(2)\,\mathrm{d}^{-1}$. A light curve phased with this period is plotted in the upper panel of Fig. A1. The bottom panel shows the Fourier transform after prewhitening with f_0 and its harmonics. In addition to residual power seen at the location of the removed primary frequency and its harmonics, we also see a family of at least six additional peaks (labelled with arrows). Adopting the feature at $2.7088\,\mathrm{d}^{-1}$ as the independent frequency f_2, the other frequencies correspond to $f_2 \pm kf_0$, where k is an integer. With this assumption the period ratio is $P_2/P_0 = 0.593\,05$, which is almost identical to that derived by B10 for V350 Lyr ($P_2/P_0 = 0.592$). The two stars also are similar in their fundamental periods, in their Fourier characteristics (see Figs 6, 9, 10), and in their masses and luminosities (see Table 5).

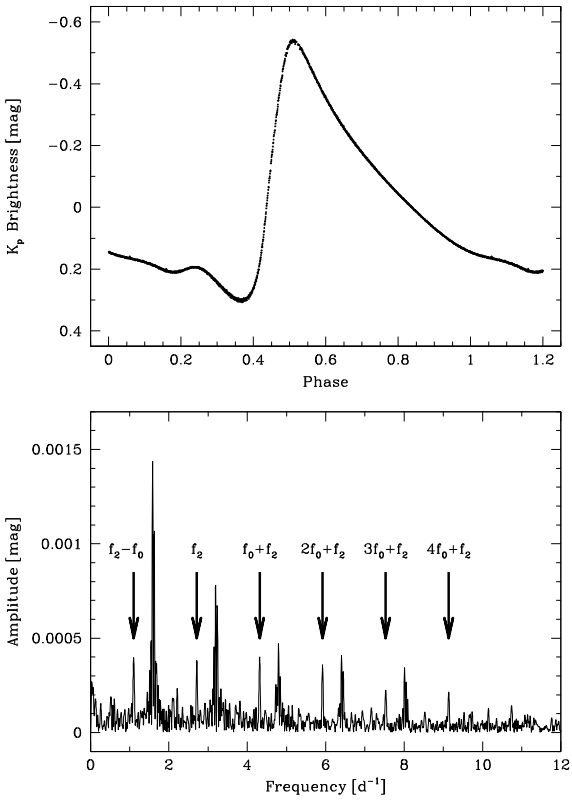

Figure A1. Top: light curve for KIC 7021124, phased with the period 0.622 4925(7) d and $t0 = 549\,53.0$ (the mean *Kp* magnitude, 13.550, has not been added to the ordinate). Bottom: Fourier amplitude spectrum of the detrended Q1 LC data, after prewhitening with the above period. The pattern seen here is similar to that seen for V350 Lyr in fig. 7 of Benkő et al. (2010).

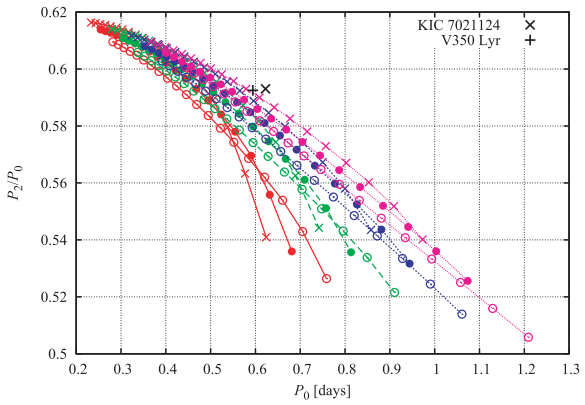

Figure A2. KIC 7021124 (and V350 Lyr) in the Petersen (P_2/P_0 *versus* P_0) diagram. The mass inferred from this diagram is ~0.75 $\mathcal{M}_\odot$, higher than both $\mathcal{M}$(puls) and $\mathcal{M}$(evol).

Fig. A2 shows KIC 7021124 (and V350 Lyr) plotted in the P_2/P_0 *versus* P_0 'Petersen' diagram. The curves were computed with the Warsaw pulsation hydrocode including turbulent convection. The periods and period ratios do not depend strongly on the convective parameters entering the model (which in this case were set C, adopted in Baranowski et al. 2009). Other model parameters are: $Z = 0.0001$ (or [Fe/H] = −2.2); $X = 0.76$ (latest opacities, with new solar mixture); three masses – $0.55\mathcal{M}_\odot$ (open circles), $0.65\mathcal{M}_\odot$ (filled circles), $0.75\mathcal{M}_\odot$ (crosses); and four luminosities: $40\,\mathrm{L}_\odot$ (red), $50\,\mathrm{L}_\odot$ (green), $60\,\mathrm{L}_\odot$ (blue), $70\,\mathrm{L}_\odot$ (purple). The best

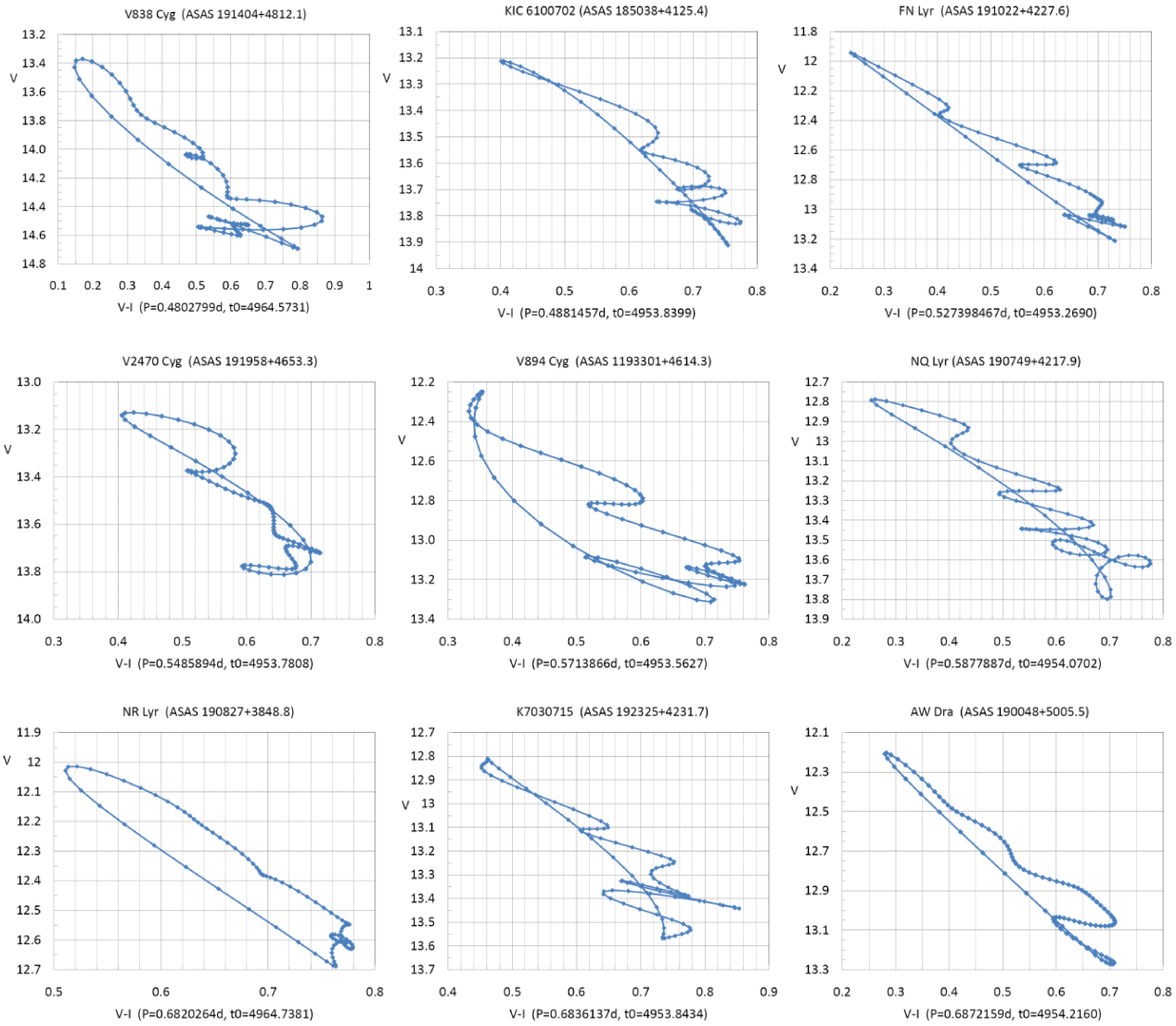

Figure B1. Looping behaviour in the HR diagram for the nine *Kepler* non-Blazhko RR Lyr stars with V, I photometric data in the ASAS-North catalogue. The stars are ordered according to increasing period, and the points along the mean light curves occur at every 1/100th of the phase. Total RTs, V amplitudes, $\langle V \rangle$ magnitudes and $\langle V - I \rangle$ colours for each star are given in the last four columns of Table 2.

agreement for KIC 7021124 (and V350 Lyr) is obtained for a high luminosity and a high mass: $L/L_{\odot} = 70$ and $\mathcal{M}/\mathcal{M}_{\odot} = 0.75$. In Table 6 both stars are among the highest L and $\mathcal{M}$ stars in our sample. The high values inferred from the Petersen diagram are more in accordance with the evolutionary values than the pulsation values.

APPENDIX B: ASAS *V*, *I* PHOTOMETRY

Very little colour information is available for the non-Blazhko RR Lyr stars. Fortunately the ASAS-North survey (see Pigulski et al. 2009) includes calibrated V and I photometry for nine of the brightest *Kepler* non-Blazhko stars (see Section 4.5). Fig. B1 shows the cyclic magnitude and colour behaviour of the nine stars in the $(V - I, V)$ diagram. In every case one observes the well-known trend of bluest colour when the star is brightest (i.e. when phase equals 0.0). The largest colour range is for NQ Lyr and V894 Cyg (the faintest ASAS star in the sample), and the smallest colour range is for the brightest star in the sample, NR Lyr. The apparent red mean colour for NR Lyr probably is due to its relatively large reddening (see Column 5 of Table 5). The 'wiggles' are artificial, a result of noise and imperfect fitting of the mean light curves; nevertheless, the mean trends, magnitudes and colours should be significant.

SUPPORTING INFORMATION

Additional Supporting Information may be found in the online version of this article:

Animations. To illustrate the constancy of the pulsations of the stars studied here, 'animated gifs' have been prepared for all the stars.

Data files. Data files are also available.

Please note: Wiley-Blackwell are not responsible for the content or functionality of any supporting materials supplied by the authors. Any queries (other than missing material) should be directed to the corresponding author for the article.

This paper has been typeset from a TEX/LATEX file prepared by the author.